A Variational Transport Theory Method for Two-Dimensional Reactor Core Calculations

A Thesis
Presented to
The Academic Faculty

by

Scott W. Mosher

In Partial Fulfillment
of the Requirements for the Degree
Doctor of Philosophy in Nuclear Engineering
School of Mechanical Engineering

Georgia Institute of Technology
June 2004

A Variational Transport Theory Method for Two-Dimensional Reactor Core Calculations

Approved by:

Dr. Farzad Rahnema, Advisor

Dr. Thomas D. Morley
(Mathematics)

Dr. C.-K. Chris Wang

Dr. Yousry Y. Azmy
(Penn State University)

Dr. Cassiano R. E. de Oliveira

Date Approved: 28 June 2004

ACKNOWLEDGMENTS

A great deal of gratitude is extended to Professor Farzad Rahnema for his instruction and guidance, and for his friendship throughout my many years at Georgia Tech. Meetings and discussions with Dr. Rahnema have always been something to look forward to and never failed to leave me excited about the ideas that were waiting to be explored. I am deeply indebted to his kindness, his confidence in me, and his tireless effort in being an mentor.

My sincere appreciation to Dr. Chris Wang, Dr. Cassiano de Oliveira, Dr. Tom Morley, and Dr. Yousry Azmy for their willingness to serve on my thesis committee, and for all of their effort in reviewing my dissertation work.

Special recognition goes to my parents, David and Carol Mosher, and to my brother Greg and his wife Liz for all of their kind support and understanding, without which none of this would have been possible. I am extremely grateful for Greg's "tech support hotline" where, over the years, I have received thousands of answers to my programming and general computing questions, not to mention the on-site maintenance of several machines.

Many thanks go to Drs. Dan and Germina Ilas for their friendship. Valuable discussions with Dan about his thesis work ensured that this dissertation got off on the right foot.

Many thanks also go to my fellow graduate students: Ben, Giuseppe, Nate, Ryosky, Steve, and Zach. I'll miss the wide-ranging conversations held while playing bar games and drinking beverages.

Finally, I would like to gratefully acknowledge the support of the Department of Energy's Nuclear Engineering Fellowship Program and Nuclear Energy Research Initiative, and Georgia Tech's Presidential Fellowship Program.

TABLE OF CONTENTS

ACKNOWLEDGMENTS . . . . . **iii**

LIST OF TABLES . . . . . **vii**

LIST OF FIGURES . . . . . **viii**

SUMMARY . . . . . **ix**

CHAPTER I INTRODUCTION **1**

1.1 Background 1

1.2 GET/Nodal Methodology 3

1.2.1 Lattice Cell Homogenization 3

1.2.2 Nodal Diffusion Calculations 4

1.2.3 Heterogeneous Flux Reconstruction 4

1.2.4 Limitations 5

1.3 Additional Literature Review 7

1.3.1 Asymptotic Methods 7

1.3.2 Heterogeneous Response Matrix Methods 8

1.3.3 Variational Nodal Methods 8

1.3.4 Variational Heterogeneous Coarse Mesh Methods 9

1.4 Motivations for New Method Development 12

1.5 Dissertation Objectives 14

1.6 Approach 14

1.7 Organization 15

CHAPTER II EIGENVALUE PROBLEM DECOMPOSITION **17**

2.1 Global Problem 17

2.2 Notational Conventions 18

2.3 Equivalent Local Fixed Source Problems 20

2.4 Local Problem Iterations 21

2.5 Power Iteration Approach 22

2.6 Implicit Fission Source Approach 24

2.6.1 Source Normalization 24

2.6.2 Interface Conditions 25
2.6.3 Symmetry Issues 27
2.6.4 Eigenvalue Estimation 28

CHAPTER III INCIDENT FLUX RESPONSE EXPANSION METHOD 29

3.1 Response Function Expansions 29
3.1.1 Green's Function Solutions to Local Problems 29
3.1.2 General Response Formulation 30
3.1.3 Truncated Expansions 31
3.2 Non-Variational Coarse Mesh Method 32
3.2.1 Partial Current Preservation 33
3.2.2 Response Function Interpolation 33
3.2.3 Approximations 34
3.3 Variational Coarse Mesh Method 34
3.3.1 Global Adjoint Problem 35
3.3.2 Adjoint Method 35
3.3.3 Ilas and Rahnema's Variational Principle 37
3.3.4 De-coupled Finite Element Equations 39
3.3.5 Rayleigh Quotient 42

CHAPTER IV DISCRETE ORDINATES COARSE MESH METHOD . 43

4.1 Discrete Response Function Expansions 43
4.1.1 Discrete Legendre Polynomials 44
4.1.2 One-Dimensional Expansion 45
4.1.3 Two-Dimensional Expansion 46
4.1.4 Response Function Shifting 47
4.2 Computer Code Implementation 48
4.2.1 Fine Mesh Codes 49
4.2.2 Response Function Generators 49
4.2.3 Coarse Mesh Codes 50

CHAPTER V NUMERICAL RESULTS 53

5.1 Method Options 54

5.2 One Dimensional Benchmarks 55
5.2.1 Reference Solution 56
5.2.2 Coarse Mesh Results 56
5.2.3 Discussion 57
5.3 Modified Henry-Worley Benchmark 58
5.3.1 Reference Solution 59
5.3.2 Coarse Mesh Results 60
5.3.3 Discussion 62
5.4 CISE Benchmark 66
5.4.1 Reference Solution 67
5.4.2 Coarse Mesh Results 68
5.4.3 Discussion 69
5.5 HAFAS Benchmark 71
5.5.1 Reference Solution 72
5.5.2 Coarse Mesh Results 73
5.5.3 Discussion 74
CHAPTER VI CONCLUSIONS 79
6.1 Overview 79
6.2 Recommendations for Future Work 80
APPENDIX A BENCHMARK PROBLEMS 81
APPENDIX B COMPLETE COARSE MESH RESULTS 92
REFERENCES 97
VITA 100

LIST OF TABLES

Table 1 One-Dimensional Benchmark Reference Calculations 56
Table 2 One-Dimensional Response Function Parameters 57
Table 3 One-Dimensional Benchmark 0^{th} Order Coarse-Mesh Results Summary I 57
Table 4 One-Dimensional Benchmark 0^{th} Order Coarse-Mesh Results Summary II 57
Table 5 Modified Henry Worley (MHW) Reference Calculation 60
Table 6 MHW Reference Calculation Comparison 60
Table 7 MHW Response Function Parameters 61
Table 8 MHW Inner Iteration Limit Study 61
Table 9 MHW Coarse Mesh Results Summary I 63
Table 10 MHW Coarse Mesh Results Summary II 63
Table 11 CISE Reference Calculation Comparison 67
Table 12 CISE $(2, 5)$ Reference Calculation 68
Table 13 CISE Response Function Parameters 68
Table 14 CISE Coarse Mesh Results Summary I 69
Table 15 CISE Coarse Mesh Results Summary II 70
Table 16 HAFAS Reference Calculation Comparison 72
Table 17 HAFAS $(2, 5)$ Reference Calculation 73
Table 18 HAFAS Response Function Parameters 74
Table 19 HAFAS Coarse Mesh Results Summary I 75
Table 20 HAFAS Coarse Mesh Results Summary II 75
Table 21 One-Dimensional Benchmark Cross Sections 81
Table 22 One-Dimensional Benchmark Material Map 81
Table 23 MHW Benchmark Cross Sections 81
Table 24 MHW Benchmark Material Map 82
Table 25 CISE Benchmark Cross Sections 82
Table 26 One-Dimensional Benchmark Material Map 82
Table 27 HAFAS Benchmark Cross Sections 83
Table 28 HAFAS Benchmark Material Map 83

LIST OF FIGURES

Figure 1 Lattice Cell Decomposition 3

Figure 2 Quarter Model of a 17×17 PWR Assembly 11

Figure 3 Coarse Mesh Boundaries 19

Figure 4 Symmetric Ordering of Local Problem Solutions 27

Figure 5 MHW Coarse-Mesh Results 66

Figure 6 CISE Coarse-Mesh Results 71

Figure 7 HAFAS Coarse-Mesh Results I 77

Figure 8 HAFAS Coarse-Mesh Results II 78

Figure 9 One-Dimensional Benchmark Coarse-Mesh Model 84

Figure 10 One-Dimensional Benchmark Core Configurations 85

Figure 11 MHW Coarse-Mesh Model 86

Figure 12 MHW Core Configuration 87

Figure 13 CISE Coarse-Mesh Model 88

Figure 14 CISE Core Configuration 89

Figure 15 HAFAS Coarse-Mesh Model 90

Figure 16 HAFAS Core Configuration 91

Figure 17 Complete 1-D Benchmark Results 93

Figure 18 Complete MHW Coarse-Mesh Results 94

Figure 19 Complete CISE Coarse-Mesh Results 95

Figure 20 Complete HAFAS Coarse-Mesh Results 96

SUMMARY

It seems very likely that the next generation of reactor analysis methods will be based largely on neutron transport theory, at both the assembly and core levels. Significant progress has been made in recent years toward the goal of developing a transport method that is applicable to large, heterogeneous coarse-meshes. Unfortunately, the major obstacle hindering a more widespread application of transport theory to large-scale calculations is still the computational cost.

In this dissertation, a variational heterogeneous coarse-mesh transport method has been extended from one to two-dimensional Cartesian geometry in a practical fashion. A generalization of the angular flux expansion within a coarse-mesh was developed. This allows a far more efficient class of response functions (or basis functions) to be employed within the framework of the original variational principle. New finite element equations were derived that can be used to compute the expansion coefficients for an individual coarse-mesh given the incident fluxes on the boundary. In addition, the non-variational method previously used to converge the expansion coefficients was developed in a new and more thorough manner by considering the implications of the fission source treatment imposed by the response expansion.

The new coarse-mesh method was implemented for both one and two-dimensional problems in the finite-difference, multigroup, discrete ordinates approximation. An efficient set of response functions was generated using orthogonal boundary conditions constructed from the discrete Legendre polynomials. Several one and two-dimensional heterogeneous light water reactor benchmark problems were studied. Relatively low-order response expansions were used to generate highly accurate results for each problem using both the variational and non-variational coarse-mesh methods. The expansion order was found to have a far

more significant impact on the accuracy of the results than the type of method. The variational techniques provide better accuracy, but at substantially higher computational costs. The non-variational method is extremely robust and was shown to achieve accurate results in the two-dimensional problems, as long as the expansion order was not very low.

CHAPTER I

INTRODUCTION

1.1 Background

Modern nuclear reactor analysis relies on computational methods for predicting the steady-state distribution of the free neutron population everywhere within the core. In commercial power applications, an accurate characterization of this distribution is necessary to ensure that: the reactor can be operated at constant power; the fission chain reaction can be quickly shutdown, especially under accident conditions; the power density in localized regions does not exceed the limits of fuel integrity; and the fuel is utilized in a highly efficient manner. In light water reactor (LWR) analysis, the most widely used computational methods for small-scale (*i.e.*, single fuel assembly) calculations are based on neutron transport theory. For large-scale (*i.e.*, whole-core) calculations, the predominant methods are based on diffusion theory.

The neutron transport equation is the most fundamental and exact description of the distribution of neutrons in space, energy, and direction (of motion) and is the starting point for approximate methods. It can be derived from a particle balance on an infinitesimal volume using only a few assumptions that remove unimportant phenomena, such as neutron-neutron interactions, in most applications (*e.g.,* Case and Zweifel, 1967). The diffusion equation can be derived by adding an additional assumption that the angular flux has a linearly anisotropic directional dependence in problems with isotropic sources and scattering (*e.g.,* Duderstadt and Hamilton, 1976). This allows the removal of the directional variables from the neutron density and simplifies the governing equation and associated numerical methods. Naturally, the diffusion assumption is not valid when the true neutron density has a strong directional dependence, as is the case within several mean free paths of strong absorbers, localized sources, and vacuum boundary conditions.

Certainly it is not the case that transport and diffusion theory based numerical methods are restricted to small and large-scale applications, respectively. It is common practice, however, to conceptually divide methods into two classes based on the relative spatial mesh size over which the numerical approximations are valid. For example, finite difference methods (*e.g.,* Lewis and Miller, 1984) are generally restricted to very small spatial meshes in reactor applications – usually on the order of one thermal mean free path in each dimension (typically less than 1cm). In contrast, nodal methods (*e.g.*, Lawrence, 1986) are based on a higher-order (or even analytical) expansion of the solution in the spatial variable and are applied to meshes much larger than a mean free path. In this thesis, methods requiring fine subdivisions of the spatial domain will be referred to as fine-mesh methods, whereas coarse-mesh methods are those appropriate for much larger grids. Monte Carlo methods (*e.g.*, Spanier and Gelbard, 1969), though not based on any spatial discretization scheme, fall into the fine-mesh class due to the precision (and expense) with which the spatial variable is treated. An additional convention will be to refer to the highly detailed calculations to which fine-mesh methods are typically applied, and the large-scale problems for which coarse-mesh methods are preferred, as fine-mesh and coarse-mesh calculations, respectively.

Traditionally, both fine and coarse-mesh methods have been restricted to systems in which a spatial mesh contains a homogeneous material. For fine-mesh methods, it is generally only a minor inconvenience to place spatial grid boundaries at or close to material interfaces. For coarse-mesh methods, the impact is much greater because a single coarse-mesh in a reactor problem may actually contain fuel rods, coolant, and control materials. An entire body of research has been dedicated to the development of homogeneous material properties that support accurate coarse-mesh calculations. However, not all coarse-mesh methods are restricted to homogeneous nodes. For this reason, the literature review that follows is divided into two sections. First, the predominant coarse-mesh methodology used in light water reactor analysis is reviewed, and the limitations of the homogenization technique are discussed. The subsequent section reviews transport theory based coarse-mesh methods that avoid conventional homogenization procedures.

1.2 GET/Nodal Methodology

The steady-state neutronics analysis of both new reactor designs and the reload cores of operating reactors involves a large number of whole-core calculations in order to optimize loading patterns and determine control system parameters. Calculations are performed at several time steps to ensure that operating margins are not exceeded under normal conditions at any time. At the current speed of computational machinery, it is absolutely impractical to perform all of these calculations by applying fine-mesh transport methods to a model containing detail at the level of individual fuel rods, control elements, and coolant regions in an entire reactor core. For this reason, the current generation of core-level neutronics methods is based on a two-phase approach.

1.2.1 Lattice Cell Homogenization

The first phase of a conventional core calculation involves applying computationally expensive transport theory to relatively small sub-regions of the core domain, called lattice cells. The decomposition of a hypothetical pressurized water reactor (PWR) core into lattice cells is illustrated in Figure 1. A lattice cell typically contains a single fuel assembly plus half

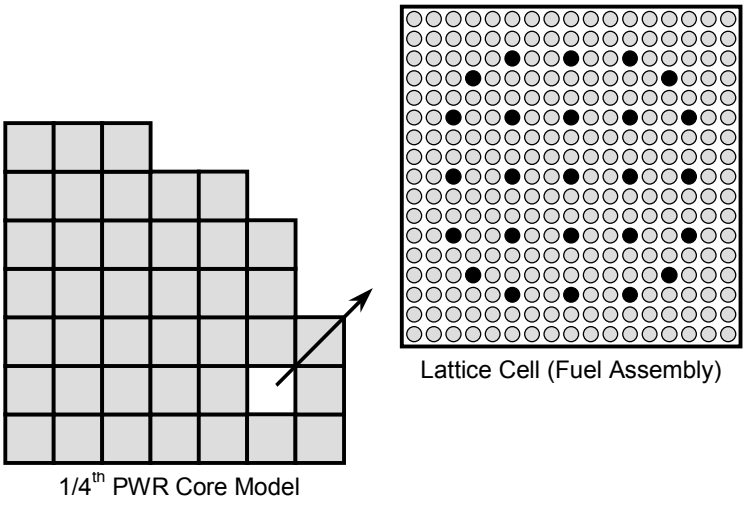

Figure 1: Lattice Cell Decomposition

of the surrounding coolant gap and is precisely modeled in two-dimensional (2-D) geometry with materials characterized by fine-group cross sections. Specular reflective (symmetry)

boundary conditions are used, so that the lattice cell transport problem is equivalent to one involving an infinitely large core composed of a single type of assembly. A transport calculation is performed for each unique lattice cell using discrete ordinates (Carlson and Lathrop, 1968), collision probability (*e.g.*, Stamm'ler and Abbate, 1983), or characteristic (*e.g.*, Sanchez and McCormick, 1982) methods. The neutron flux distribution from these fine-mesh calculations is used to spatially homogenize and condense (with respect to energy) cross sections and generate other physics data using generalized equivalence theory (Smith, 1980; 1986). The homogenized lattice cell data are then used in a simplified core model to which less expensive diffusion theory is applied in the second phase, the coarse-mesh calculations.

1.2.2 Nodal Diffusion Calculations

The current state-of-the-art coarse-mesh computational methods are based on nodal diffusion theory (*e.g.*, Lawrence, 1986). A lattice cell is typically represented by a single coarse-mesh or node (these terms will be used interchangeably). The nodal approach involves a high-order or analytical expansion of the intra-nodal flux shape in order to achieve a higher degree of accuracy, for a given node size, than the conventional finite difference approach to discretizing the spatial variable. A transverse integration procedure is often employed to reduce the multi-dimensional equations to a set of coupled one-dimensional equations. The resulting system is then solved on a three-dimensional core model consisting of homogeneous nodes characterized by the generalized equivalence theory (GET) constants generated in the first phase. This overall approach will hereafter be referred to as the GET/nodal methodology.

1.2.3 Heterogeneous Flux Reconstruction

After solving the nodal diffusion equations, it is necessary to estimate the power generated in individual fuel rods. The rod powers are used to ensure that operating parameters, such as linear heat generation rate and minimum critical power ratio, do not exceed prespecified limits. Since the nodal solution only attempts to preserve node-integrated leakage and reaction rates, it does not contain enough detail to accurately estimate the fluxes in

localized regions within the nodes. The detailed, or heterogeneous, flux distribution can be approximated by modulating the smooth nodal solution with the fine-mesh transport solutions using a variety of techniques (*e.g.*, Koebke and Hetzelt, 1985). This procedure is commonly referred to as flux reconstruction or de-homogenization.

1.2.4 Limitations

It is well known that the accuracy of the GET/nodal methodology tends to deteriorate as the core-level heterogeneity increases (*e.g.*, Rahnema and Nichita, 1997). At first, it may seem that this limitation is a result of the approximations inherent in diffusion theory, which was applied in the nodal calculation. Diffusion theory is certainly valid within each homogeneous lattice cell. At the interface between lattice cells, generalized equivalence theory employs discontinuity factors (DFs) generated by the transport calculations in order to correct the inter-nodal fluxes and currents. In fact, the DFs render the node-homogenized diffusion coefficients, which otherwise control the accuracy of the diffusion approximation, arbitrary. Smith (1980) showed that a nodal diffusion calculation will exactly reproduce the node-integrated reaction rates, interface-integrated currents, and the reactor eigenvalue associated with a whole-core fine-mesh diffusion calculation when the reference lattice cell constants are used. So the GET/nodal method's limitations in highly heterogeneous problems do not stem from the application of diffusion theory. As it turns out, the actual culprits are the approximations made in the homogenization and de-homogenization procedures that are necessary to support the application of homogeneous coarse-mesh methods to practical problems.

In generalized equivalence theory, the ideal homogenized macroscopic cross section associated with an arbitrary reaction x is calculated by weighting the heterogeneous, fine-group cross section with the intra-nodal flux from a whole-core fine-mesh diffusion calculation

$$\hat{\Sigma}_{xh} \equiv \frac{\sum_{g \in h} \int_V \Sigma_{xg}(\tilde{\mathbf{r}}) \Phi_g(\tilde{\mathbf{r}}) dV}{\sum_{g \in h} \int_V \hat{\Phi}_g(\tilde{\mathbf{r}}) dV}, \tag{1}$$

where $\Phi_g(\tilde{\mathbf{r}})$ denotes the heterogeneous scalar flux at location $\tilde{\mathbf{r}}$ in fine-group g, h denotes a

broad (collapsed) group to be used in the nodal calculation, V denotes the spatial domain of the lattice cell, and a caret ($\hat{}$) is used to distinguish homogenized quantities from heterogeneous ones. In the case of group-to-group scattering cross sections a slightly different formula is used, however this is not important in the current discussion. Naturally, if the heterogeneous fine-mesh solution were known there would generally be no reason to perform a nodal calculation. So in practice, the scalar flux from the lattice cell transport calculation, denoted ϕ, is used for homogenization

$$\hat{\Sigma}_{xh} \approx \frac{\sum_{g\in h} \int_V \Sigma_{xg}(\tilde{\mathbf{r}})\phi_g(\tilde{\mathbf{r}})dV}{\sum_{g\in h} \int_V \phi_g(\tilde{\mathbf{r}})dV}. \tag{2}$$

The ideal discontinuity factor (DF), denoted f, associated with a single coarse-mesh interface, S, is defined as the ratio of interface-averaged scalar fluxes from the heterogeneous and nodal solutions

$$f_h \equiv \frac{\sum_{g\in h} \int_S \Phi_g(\tilde{\mathbf{r}})dS}{\sum_{g\in h} \int_S \varphi_g(\tilde{\mathbf{r}})dS}. \tag{3}$$

The nodal solution, φ, depends on the discontinuity factors, and the heterogeneous solution is not known anyway, so in practice the DFs are estimated as the ratio of the surface-averaged to volume-averaged lattice cell transport fluxes

$$f_h \approx \frac{\sum_{g\in h} \int_S \phi_g(\tilde{\mathbf{r}})\frac{dS}{s}}{\sum_{g\in h} \int_V \phi_g(\tilde{\mathbf{r}})\frac{dV}{v}}, \tag{4}$$

where s denotes the surface area of S, and v denotes the volume of V.

The limitation associated with calculating approximate lattice cell constants via Eqs. (2) and (4) is that ϕ has the spatial shape and energy spectrum associated with the infinite-medium problem and therefore lacks the effects of spatial and spectral interactions with adjacent lattice cells of different types. For assemblies at the center of relatively homogeneous reactor cores, ϕ will likely be a very good approximation of the heterogeneous flux, Φ.

Near the core periphery or between assemblies with vastly different material properties (*e.g.*, between controlled and fresh assemblies) significant inter-nodal flux gradients will generally exist, and the infinite-medium solution will likely be a poor approximation of the heterogeneous solution. Inaccuracies in the lattice cell transport flux impact the homogenized constants, the nodal solution, and also the detailed heterogeneous flux used to estimate rod fission densities. This is the consequence of the approximations made in computationally de-coupling a highly coupled sub-region of the reactor core.

1.3 Additional Literature Review

In this section, publicly available literature describing core-level transport theory methods that do not rely on generalized equivalence theory for homogenizing lattice cells is reviewed. It is convenient to classify the literature into four areas: asymptotic methods, heterogeneous response matrix methods, variational nodal methods, and variational heterogeneous coarse-mesh methods. Work in the last category will be reviewed in detail, since it is particularly relevant to this thesis, for reasons given in a later section.

1.3.1 Asymptotic Methods

Zhang, Rizwan-uddin, and Dorning (1995; 1997) developed a multiple-scale asymptotic expansion method starting from either the diffusion or transport equation, which results in a systematic homogenization theory and a self-consistent local flux reconstruction procedure. The two spatial scales employed are similar to those previously used by Larsen (1975; 1976) in an asymptotic approach for heterogeneous media comprised of exactly periodic pin-cells. The method developed by Zhang *et al.* is based on the assumption that the core is an array of near-periodic fuel assemblies. The results presented in (Zhang, Rizwan-uddin, and Dorning, 1997) show significant improvement over generalized equivalence theory in two quarter-core 2-D PWR benchmark problems.

Despite the encouraging results, there are two significant drawbacks to the asymptotic method as described in (Zhang, Rizwan-uddin, and Dorning, 1997). First, the authors

state that the iterative solution procedure will diverge without very tight convergence criteria (10^{-10} to 10^{-12}) for the forward and adjoint eigenvalue and auxiliary fixed source calculations. Second, the method is restricted to the one-group approximation, which is not appropriate for modern reactor analysis.

1.3.2 Heterogeneous Response Matrix Methods

Villarino and Stamm'ler (1984) developed a heterogeneous coarse-mesh method based on pre-computed, invariant quantities associated with individual coarse-meshes, which they called the heterogeneous response method. Specifically, a lattice cell is characterized by the fluxes (responses) caused by in-volume sources and incident currents, which were computed using collision probability techniques. The coarse-meshes were coupled by cosine interface currents in slab geometry, and accurate results were produced. The extension of the method to two and three-dimensional geometries was discussed, however additional work on this particular method was not found in the literature.

Rathkopf and Martin (1986) developed a similar formulation of the coarse-mesh response to both incident currents and in-volume sources. However, the responses were computed by the finite element method in space and direction. Though the authors reported an implementation of the method in 2-D geometry, only results for 1-D problems were published. No additional publications on this topic were found.

1.3.3 Variational Nodal Methods

The variational nodal method has traditionally required homogeneous nodes (Dilber and Lewis, 1985). In the past few years, progress has been made toward refining the finite element discretization of the spatial domain into so-called finite subelements that allow the treatment of heterogeneous nodes (Lewis, Palmiotti, and Taiwo, 1999; Smith *et al.*, 2000).

The first paper (Lewis, Palmiotti, and Taiwo, 1999) describes a variational nodal formulation intended for systems with assembly-sized nodes containing a finite subelement for each pin-cell (one fuel rod plus some surrounding coolant). The spatial dependence of the flux within each subelement is expanded in four bilinear trial functions. This technique

avoids assembly, but not pin-cell homogenization, which may lead to errors in locally heterogeneous regions of a lattice cell (*e.g.*, near a gadolinium absorber rod). More importantly, the number of unique pin-cells in an operating reactor is much larger than the number of unique fuel assemblies, due to non-uniform depletion effects. The authors present accurate results for a set of 2-D benchmark problems defined in terms of homogeneous, two-group pin-cell cross sections.

The second paper (Smith *et al.*, 2000) describes progress toward a further refinement in which the node size is reduced to that of a pin-cell with triangular subelements corresponding to truly homogeneous regions within the pin-cell. This method avoids the errors associated with homogenization altogether. On the other hand, this particular method seems to merely involve the application of the previous method to the fine-mesh level, along with the associated increase in computational expense. The authors present accurate results for a quarter-core 2-D PWR problem composed of a reflector and four fuel assemblies with seven unique pin-cells.

1.3.4 Variational Heterogeneous Coarse Mesh Methods

Recent work at Georgia Tech by Nichita and Rahnema (2003) and Ilas and Rahnema (2001; 2003) concerned the development of finite element methods based on diffusion and transport theory, respectively. In both methods, the neutron flux within a heterogeneous coarse-mesh was expanded in solutions of the governing equation, instead of polynomials or other simple basis functions. With this technique, arbitrarily heterogeneous coarse-meshes of any size can be treated with a high degree of accuracy.

In Ilas and Rahnema's method, unique lattice cell types are characterized by surface Green's functions (SGFs), defined to be the solution of fixed source transport equations that include a fission source term. Traditionally, the response caused by in-volume fission sources is not included in the SGFs, but is considered separately using volume Green's functions (*e.g.*, Case and Zweifel, 1967). In either case, all of the surface Green's functions that characterize a unique coarse-mesh type satisfy the same transport equation, but different boundary conditions. To be more specific, consider the discrete ordinates approximation of

the multigroup transport equation in 1-D slab geometry with isotropic scattering. Ilas and Rahnema considered a single surface Green's function, denoted S, to be the solution to

$$\left[\mu_n \frac{d}{dx} + \sigma_g(x)\right] S_{gn}(x) = \frac{1}{2} \sum_{g'=1}^{G} \left[\left(\sigma_{g' \to g}(x) + \frac{1}{k} \chi_g(x) \nu \sigma_{fg'}(x) \right) \sum_{n'=1}^{N} w_{n'} S_{g'n'}(x) \right] \quad (5)$$

where: n and $n' = 1, ..., N$ are ordinate indices; μ_n and w_n are the ordinate direction cosines and weights, respectively; g and $g' = 1, ..., G$ are energy group indices; and k is a fixed estimate of the eigenvalue of the larger system in which the coarse-mesh belongs. The spatial variable x is restricted to the coarse-mesh domain, say $x_\ell \leq x \leq x_r$. Note that the finite difference form of Eq. (5) was used in numerical calculations, however the continuous form shown here allows a less cumbersome notation.

Associated with Eq. (5) is a known incident flux boundary condition that is nearly identical to a vacuum condition, except that a unit angular flux in a single energy group and in a single entering direction is present on one of the coarse-mesh boundaries. For example, the SGFs associated with the left-side boundary are subject to the general boundary condition

$$S_{gn}(x_\ell) = \delta_{hg} \delta_{mn} \quad \text{for } \mu_m > 0 \quad (6)$$

where h is the incident energy group index, m is the incident direction index, and δ is the Kronecker delta. Individual surface Green's functions are identified by the four parameters h, m, x_b, and k, where x_b denotes either x_ℓ or x_r. For a given value of k, there are a total of $G \times N$ of these SGFs that collectively characterize a slab coarse-mesh. Using a notation in which the parameters are explicitly shown, the angular flux, ψ, within a coarse-mesh can be written in terms of the incident flux on the boundaries, ξ, as

$$\psi_{gn}(x) = \sum_b \sum_h \sum_m \xi_{hm}(x_b) S_{hm \to gn}(k; x_b \to x). \quad (7)$$

The summations range over both coarse-mesh boundaries, all incident energy groups, and the entering directions (which depend on the boundary). This relationship holds because of the linearity of the transport equation.

At this point, it should be noted that Ilas and Rahnema's response formulation is rather different than the ones described in (Villarino and Stamm'ler, 1984) and (Rathkopf and

Martin, 1986). In those methods, a node is characterized by solutions to fine-mesh, fixed source problems with no fission source. Consequently, responses to both incident fluxes and in-volume sources (*i.e.*, separate surface and volume Green's functions) are required. This leads to a significantly larger number of response functions that must be computed for a given coarse-mesh type. For example, consider a typical two-dimensional PWR fuel assembly model consisting of a 17×17 array of fuel rods, which is symmetric about 90° rotations of the spatial axes (*i.e.*, quarter-symmetry), as illustrated in Figure 2. The lightly

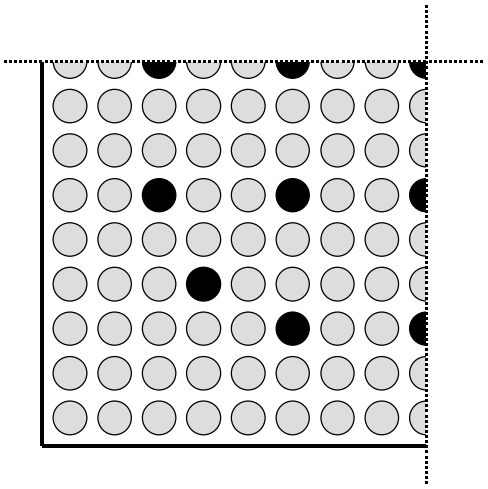

Figure 2: Quarter Model of a 17×17 PWR Assembly

shaded circles represent fuel rods, whereas the dark circles represent control rod guide tubes, which are generally filled with coolant during full-power operation. For low-enriched, fresh fuel without burnable absorbers, it is reasonable to represent the isotropic fission source within each fuel rod as spatially uniform. In this case, $72 \times G_f$ in-volume response functions must be generated per lattice cell type, where G_f denotes the number of energy groups in which the fission spectrum, χ_g, is non-zero. The approach of Ilas and Rahnema avoids these extra computations and the uniform fission source assumption, which is only valid for weakly absorbing fuel. In addition, the coarse-mesh calculations do not involve the explicit convergence of the fission source magnitude in each rod as a function of G_f energy groups. Convergence of the boundary fluxes automatically implies convergence of the fission source distribution when the SGFs from Eq. (5) are employed.

The authors presented two approaches to solving the core-level problem using the expansion in Eq. (7). The first approach was to solve finite element equations (for ξ and k) that were derived by substituting the expansion into a variational principle and taking a functional derivative with respect to the adjoint fluxes on coarse-mesh boundaries. In that case, the surface Green's functions become finite element basis functions. The second approach consisted of an iterative sweeping procedure to converge the global flux solution, similar to that of conventional discrete ordinates methods, and a Rayleigh quotient for estimating k. In the first approach, both ξ and k have second-order accuracy (with respect to the first-order error in the SGF trial functions), whereas only k has second-order accuracy in the second approach. Some difficulties in finding a converged, continuous solution to the finite element equations were encountered, so the application of the second approach was explored more thoroughly.

Though Ilas and Rahnema's method avoids volume Green's functions, the SGFs defined by Eq. (5) depend on global eigenvalue estimates and therefore must be updated whenever a new estimate is obtained. Initially, an iteration between the lattice cell and core-level calculations was natural. When response functions were computed for each new estimate of k determined by the Rayleigh quotient, the procedure was shown to converge exactly to the heterogeneous fine-mesh solution. In a different approach, the authors found that the method could be made much more efficient by initially computing response functions for a set of k values and then using linear interpolation to update the functions as necessary. This makes Ilas and Rahnema's coarse-mesh method a two-phase approach, since the lattice cell computations could be restricted to the first phase. On the other hand, the converged solution produced in this manner contains some residual error from the interpolation process.

1.4 Motivations for New Method Development

The GET/nodal methodology was developed and refined for the currently operating class of light water reactors (Generation II). Until about a decade ago, the reload cores of these reactors were designed with relatively homogeneous distributions of fuel, moderator,

and absorber materials. The current core design trend, however, is toward higher degrees of heterogeneity. In order to lengthen operating cycles (time between refueling outages) and increase fuel utilization, recent cores have been designed with higher amounts of total fissile mass which has necessitated the addition of burnable absorbers to hold down the reactivity at the beginning of core life. The presence of burnable absorbers is accommodated by varying the fuel enrichment of the surrounding pins, which leads to increased heterogeneity at the assembly-level. The presence of reload assemblies with long operating histories and new assemblies, which have substantially different isotopic compositions, leads to increased heterogeneity at the core-level. It is reasonable to expect these, or similar, design features to be present in future light water reactor configurations due to the constant appetite for increases in plant production and reductions in cost.

A neutronics method that is able to characterize the core-wide power distribution more accurately than current methods will more clearly identify the extent to which candidate core configurations meet design goals. It would also support, from an engineering standpoint, the pursuit of maximal increases in fuel utilization and operating cycle length and decreases in spent fuel inventory and operating margins (which must account for computational uncertainties). A neutronics method that is based on less restrictive assumptions than current methods will contribute to these improvements for a wider range of systems. Therefore, it seems very likely that the next generation of reactor analysis methods will be based largely on transport theory, at both the assembly and core-levels, and involve fewer approximations than current methods.

The transport theory based methods reviewed in the previous section show some significant progress toward achieving these goals. Unfortunately, the major obstacle hindering a more widespread application of the methods to large-scale calculations is still the computational cost. With the previously reviewed transport methods that have been extended to 2-D geometry, only applications to a few model problems, which are much smaller than the GET/nodal models used in actual power reactor analysis, have been reported in the literature. Therefore, a relevant line of research is the development of new heterogeneous

coarse-mesh methods or improvements to existing methods with an emphasis on reducing computational cost while maintaining a high degree of accuracy.

1.5 Dissertation Objectives

The objective of this dissertation is to develop a coarse-mesh method that

1) is based solely on transport theory,

2) does not require homogenization or discontinuity factors,

3) contains an accurate and consistent flux reconstruction procedure,

4) does not restrict the size of the coarse-meshes,

5) is formulated to limit the scope of the fine-mesh computations, and

6) can be applied to realistic two-dimensional Cartesian geometry models of light water reactors.

The method will be implemented in a computer code and tested on realistic light water reactor benchmark problems.

1.6 Approach

The heterogeneous coarse-mesh method will be developed by adapting and extending the method of Ilas and Rahnema to two-dimensional Cartesian geometry. A straightforward implementation of the existing method (*i.e.*, one that does not involve any new ideas) will lead to an algorithm that requires an extraordinary amount of computational time to characterize the coarse-meshes in realistic problems. This is entirely due to the enormous number of surface Green's functions associated with coarse-meshes in multi-dimensional geometries.

The total number of surface Green's functions, T, associated with a multigroup, finite difference, discrete ordinates coarse-mesh model in one and two-dimensional Cartesian geometry is, in general,

$$T_{1D} = N \times G \tag{8}$$

and

$$T_{2D} = \frac{1}{4} N(N+2) \times G \times (X+Y)\,, \tag{9}$$

where: X and Y denote the number of spatial fine-meshes spanning the x and y dimensions of the coarse-mesh; N denotes the directional quadrature order (*i.e.*, the N of S_N); G denotes the number of energy groups; and it has been assumed that a level-symmetric quadrature set is used in the two-dimensional model. Coarse-mesh symmetries can be exploited to reduce the number of SGFs that must be computed. However, it is clear that the geometric growth in the size of a complete set of response functions is a problem. For example, a four-group, S_{16} model of a 1-D coarse-mesh can be characterized by 64 SGFs. For a 2-D coarse-mesh with $X = Y = 35$, the number grows to over 20,000!

For the new coarse-mesh method to be practical, it must be able to produce highly accurate results without requiring the generation of a complete set of response functions. In this case, the surface Green's functions are not a good choice in which to expand the intra-nodal angular flux. Simply neglecting individual SGFs will computationally close paths of entry into a coarse-mesh, leading to substantial errors in reactor problems (Mosher and Rahnema, 2003). It is clear that Ilas and Rahnema's method must be reformulated and adapted to achieve the dissertation objectives.

1.7 Organization

The remainder of this thesis is organized as follows. The exact decomposition of an eigenvalue problem into a set of coupled fixed source problems is discussed in Chapter 2. Two general approaches to iteratively solving the coupled problems are described. The first is a conventional power iteration method, which is of a similar character to those used in the heterogeneous response matrix methods reviewed earlier. In the second approach, which was employed in the variational heterogeneous coarse-mesh methods, the fission source is considered implicitly. This second iterative method is developed in a new and more thorough manner by identifying the implications of the source treatment. In Chapter 3, a new coarse-mesh method, called the incident flux response expansion method, which is based on a generalization of the Green's function approach to solving local fixed source problems, is

presented. Both variational and non-variational techniques for converging the coarse-mesh boundary fluxes and global eigenvalue are described. The numerical implementation of the method in the finite difference discrete ordinates setting, based on an efficient discrete response expansion, is discussed in Chapter 4. A comparison of the results generated by the new method and reference fine-mesh calculations for several one and two-dimensional light water reactor benchmark problems is presented in Chapter 5. Conclusions and recommendations for future work can be found in Chapter 6. A description of the benchmark problems and the complete set of coarse-mesh results are provided in Appendices A and B, respectively.

CHAPTER II

EIGENVALUE PROBLEM DECOMPOSITION

In this chapter, the exact decomposition of an eigenvalue problem into a set of coupled fixed source problems is discussed. Two general approaches to iteratively solving the decomposed problem are described. The first is a conventional power iteration method, while the second involves an implicit treatment of the fission source. The latter method is developed in a new and more thorough manner by identifying the implications of the source treatment.

2.1 Global Problem

The fundamental tool used in steady-state analyses of systems with fissionable material is the homogeneous form of the neutron transport equation

$$\mathbf{H}\psi(\tilde{\mathbf{r}},\hat{\mathbf{\Omega}},E)=\frac{1}{k}\mathbf{F}\psi(\tilde{\mathbf{r}},\hat{\mathbf{\Omega}},E), \tag{10}$$

where the operators $\mathbf{H}$ and $\mathbf{F}$ are defined as

$$\mathbf{H}\equiv\hat{\mathbf{\Omega}}\cdot\nabla+\sigma_t(\tilde{\mathbf{r}},E)-\int_0^\infty\int_{4\pi}dE'd\hat{\mathbf{\Omega}}'\sigma_s(\tilde{\mathbf{r}},\hat{\mathbf{\Omega}}',E'\rightarrow\hat{\mathbf{\Omega}},E) \tag{11}$$

and

$$\mathbf{F}\equiv\frac{1}{4\pi}\chi(\tilde{\mathbf{r}},E)\int_0^\infty\int_{4\pi}dE'd\hat{\mathbf{\Omega}}'\nu\sigma_f(\tilde{\mathbf{r}},E'). \tag{12}$$

Equation (10) is applied to the system of interest, V, along with a boundary condition

$$\psi(\tilde{\mathbf{r}},\hat{\mathbf{\Omega}},E)=\mathbf{B}\psi(\tilde{\mathbf{r}}',\hat{\mathbf{\Omega}}',E'),\quad\text{for }\tilde{\mathbf{r}},\,\tilde{\mathbf{r}}'\in\partial V,\;\hat{\mathbf{n}}\cdot\hat{\mathbf{\Omega}}<0,\text{ and }\hat{\mathbf{n}}\cdot\hat{\mathbf{\Omega}}'>0, \tag{13}$$

where $\mathbf{B}$ is a boundary condition operator, ∂V denotes the external boundary of V, and $\hat{\mathbf{n}}$ is the outward normal unit vector on ∂V.

The asymptotic behavior of the system (*i.e.*, that which exists after initial transients die out) is characterized by the solution to Eqs. (10) and (13) associated with the largest real

eigenvalue. In that case, the eigenvalue, k, is the ratio of neutrons in successive generations, and the eigenfunction, $\psi(\tilde{\mathbf{r}}, \hat{\mathbf{\Omega}}, E)$, is the neutron flux distribution in space, direction, and energy. The boundary condition applies to the flux entering the system from the surrounding environment.

2.2 Notational Conventions

Let the spatial domain of the global eigenvalue problem be divided into a set of coarse-meshes, denoted by V_i where $i = 1, ..., I$. The intersection of the coarse-mesh domains is restricted to the coarse-mesh boundaries, denoted by ∂V_i, while the union is subject to the condition

$$\bigcup_{i=1}^{I} V_i = V. \tag{14}$$

In the sections that follow, a shorthand phase-space notation will be used in conjunction with subscripts and superscripts that indicate restrictions on the range of the spatial and angular variables. This convention is intended to provide a concise way to refer to individual coarse-meshes, coarse-mesh boundaries, and the directions leading into and out of a coarse-mesh.

Let the phase-space of the global problem be denoted by the shorthand notation

$$\mathbf{w} \equiv (\tilde{\mathbf{r}}, \hat{\mathbf{\Omega}}, E), \quad \text{for } \tilde{\mathbf{r}} \in V. \tag{15}$$

The addition of a single subscript indicates a restriction of the spatial variable to an individual coarse-mesh, for example

$$\mathbf{w}_i \equiv (\tilde{\mathbf{r}}, \hat{\mathbf{\Omega}}, E), \quad \text{for } \tilde{\mathbf{r}} \in V_i. \tag{16}$$

A double subscript further restricts the spatial variable to a bounding surface of a coarse-mesh.

Sub-regions of a coarse-mesh boundary are divided into two mutually exclusive types. The first is a common boundary between two adjacent coarse-meshes, hereafter referred

to as an interface. In this case, each subscript corresponds to a unique coarse-mesh index (typically denoted by the variable indices i and j), for example

$$\mathbf{w}_{ij} \equiv (\tilde{\mathbf{r}}, \hat{\mathbf{\Omega}}, E), \quad \text{for } \tilde{\mathbf{r}} \in \partial V_i \text{ and } \tilde{\mathbf{r}} \in \partial V_j. \tag{17}$$

The second type of coarse-mesh boundary is one coincident with the external system boundary, hereafter referred to as a boundary segment. In this case, the second subscript corresponds to a unique boundary segment index (typically denoted by the variable index b), for example

$$\mathbf{w}_{ib} \equiv (\tilde{\mathbf{r}}, \hat{\mathbf{\Omega}}, E), \quad \text{for } \tilde{\mathbf{r}} \in \partial V_i \text{ and } \tilde{\mathbf{r}} \in \partial V. \tag{18}$$

In some situations it will be convenient to refer to the coarse-mesh boundary sub-regions without regard to the type. In this case, the variable index s will be used, for example $\mathbf{w}_{is}$. The interaction of different boundaries is illustrated in Figure 3, which represents part of a global system (at the periphery), in which two adjacent coarse-meshes, V_i and V_j, are highlighted.

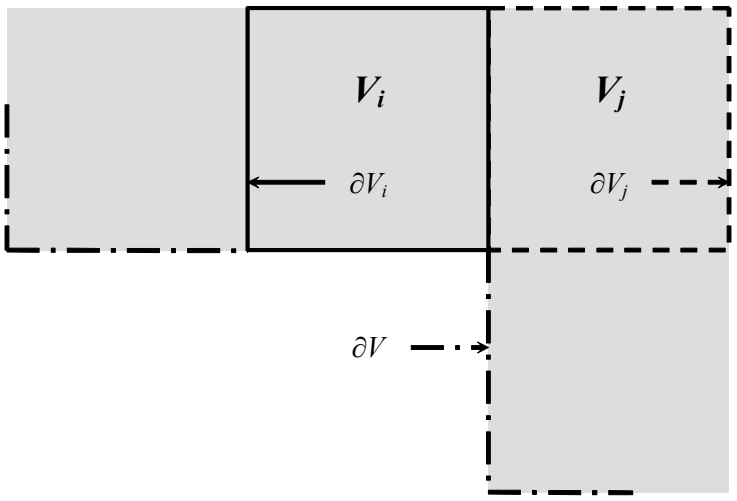

Figure 3: Coarse Mesh Boundaries

Superscript "+" and "–" symbols will be used to indicate angular half-space restrictions for surface quantities (*i.e.*, considering the sign of $\hat{\mathbf{n}} \cdot \hat{\mathbf{\Omega}}$). The outward normal vector $\hat{\mathbf{n}}$, and hence the sign, is defined relative to the coarse-mesh identified by the first or only subscript,

or relative to the global system in the case of no subscripts. This convention is illustrated in the phase-space notation

$$\mathbf{w}_{ij}^{\pm} \equiv (\tilde{\mathbf{r}}, \hat{\mathbf{\Omega}}, E), \quad \text{for } \tilde{\mathbf{r}} \in \partial V_i, \, \tilde{\mathbf{r}} \in \partial V_j, \text{ and } \hat{\mathbf{n}}_i \cdot \hat{\mathbf{\Omega}} \gtrless 0, \tag{19}$$

where $\hat{\mathbf{n}}_i$ denotes the outward normal on ∂V_i. If a single subscript is used with the +/– superscripts, then it indicates a restriction of the spatial variable to the coarse-mesh boundary along with an angular half-space restriction, for example

$$\mathbf{w}_{i}^{\pm} \equiv (\tilde{\mathbf{r}}, \hat{\mathbf{\Omega}}, E), \quad \text{for } \tilde{\mathbf{r}} \in \partial V_i, \text{ and } \hat{\mathbf{n}}_i \cdot \hat{\mathbf{\Omega}} \gtrless 0. \tag{20}$$

This notation is particularly convenient for denoting the fluxes exiting or entering a coarse-mesh.

A final convention concerns the limiting values of functions that are discontinuous across coarse-mesh boundaries. For example, at an interface between coarse-meshes V_i and V_j, let $f(\mathbf{w}_{ij})$ denote the limiting value of the function f as the interface is approached from inside coarse-mesh V_i. The limit of f as the interface is approached from the opposite direction is denoted by $f(\mathbf{w}_{ji})$.

2.3 Equivalent Local Fixed Source Problems

Consider the following local fixed source problem in coarse-mesh V_i

$$\mathbf{H}\varphi(\mathbf{w}_i) = Q(\mathbf{w}_i), \tag{21}$$

which is subject to a general known incident flux boundary condition

$$\varphi(\mathbf{w}_i^-) = \gamma(\mathbf{w}_i^-). \tag{22}$$

Equations (21) and (22) constitute I local fixed source problems with boundary conditions and solutions contained within γ and φ, respectively.

An equation for the difference between ψ, the solution to the global eigenvalue problem, and φ, the mosaic of solutions to the local fixed source problems, denoted δ, can be found by subtracting Eq. (21) from Eq. (10)

$$\mathbf{H}\delta(\mathbf{w}_i) = \frac{1}{k}\mathbf{F}\psi(\mathbf{w}_i) - Q(\mathbf{w}_i), \tag{23}$$

since $\mathbf{H}$ is a linear operator. Equation (23) is a fixed source transport equation with a boundary condition that follows from Eq. (22)

$$\delta(\mathbf{w}_i^-) = \psi(\mathbf{w}_i^-) - \gamma(\mathbf{w}_i^-). \tag{24}$$

Within V_i the distribution δ is driven by an independent source, which is equal to the difference between the fission term from the eigenvalue equation and the fixed source used in the local problem, as well as an incident flux, which is equal to the difference between the global eigenfunction on ∂V_i and the boundary condition of the local problem. Certainly δ will be small whenever the magnitudes of both sources are small.

For the case in which the right-hand sides of Eqs. (23) and (24) vanish, δ is trivially zero and the solution to the local fixed source problem is identical to the eigenfunction of the global problem everywhere within the coarse-mesh. Consequently, an eigenvalue problem in a large, heterogeneous system can be decomposed into a set of smaller, fixed source problems, without approximation. The local problems are governed by the homogeneous transport equation

$$\mathbf{H}\varphi(\mathbf{w}_i) = \frac{1}{k}\mathbf{F}\varphi(\mathbf{w}_i), \tag{25}$$

with the inhomogeneous boundary condition

$$\varphi(\mathbf{w}_i^-) = \psi(\mathbf{w}_i^-). \tag{26}$$

The boundary conditions of an individual local problem are coupled to the fluxes exiting the neighboring coarse-meshes, and, in some cases, also those returning from the external boundary when a reflective global boundary condition has been imposed.

2.4 Local Problem Iterations

The decomposition described so far has no immediate practical value since the local problems are cast in terms of the solution to the global eigenvalue problem. Clearly, an iterative procedure must be developed to accurately estimate both k and $\psi(\mathbf{w}_i^-)$, for all i, while considering only the local problems. When those values are accurately known, the global eigenfunction can be constructed by solving Eqs. (25) and (26) in each coarse-mesh.

Two distinctly different algorithms that can be used to iteratively solve the decomposed global eigenvalue problem are described in the two sections that follow. Both approaches involve iterations on two levels: outer iterations on the global eigenvalue, and inner iterations on the local problem boundary conditions. The eigenvalue iterations will be indexed by $u = 1, ..., U$, and quantities associated with the u^{th} iteration will be denoted by a superscript (u). The inner iterations within eigenvalue iteration u will be indexed by $v = 1, ..., V_u$, and quantities associated with the v^{th} iteration will be denoted by a superscript (u, v).

2.5 Power Iteration Approach

The first approach is characterized by the treatment of the fission neutron source as a fixed distribution during an outer iteration. The procedure is initiated with a guess of the global eigenvalue, $k^{(0)}$, and a normalized guess of the local problem boundary conditions, $\gamma^{(1,1)}$, corresponding to a uniform flux distribution so that for $i = 1, ..., I$

$$\gamma^{(1,1)}(\mathbf{w}_i^-) = \frac{1}{\int d\mathbf{w}\mathbf{F}(1)}. \tag{27}$$

An exception to Eq. (27) is made on coarse-mesh boundary segments where known incident flux boundary conditions have been imposed. A normalized initial guess of the fission source term is also computed

$$Q^{(0)} \equiv \frac{1}{k^{(0)}} \frac{\mathbf{F}(1)}{\int d\mathbf{w}\mathbf{F}(1)}, \tag{28}$$

which is consistent with the initial boundary conditions.

During each inner iteration v within outer iteration u, the following local transport equation is solved in each coarse-mesh

$$\mathbf{H}\varphi^{(u,v)}(\mathbf{w}_i) = Q^{(u-1)}(\mathbf{w}_i), \tag{29}$$

with the boundary condition

$$\varphi^{(u,v)}(\mathbf{w}_i^-) = \gamma^{(u,v)}(\mathbf{w}_i^-). \tag{30}$$

The boundary conditions are updated between inner iterations by

$$\gamma^{(u,v+1)}(\mathbf{w}_{ji}^-) = \varphi^{(u,v)}(\mathbf{w}_{ij}^+) \tag{31}$$

and

$$\gamma^{(u,v+1)}(\mathbf{w}_{ib}^{-}) = \mathbf{B}\varphi^{(u,v)}(\mathbf{w}_{ib}^{+}). \tag{32}$$

That is, the coarse-mesh exiting fluxes computed during the current iteration are used in setting next iteration boundary conditions for neighboring coarse-meshes (on interfaces) and on boundary segments. The inner iterations are continued until the following convergence criterion is satisfied

$$\left| \frac{\gamma^{(u,v+1)}}{\gamma^{(u,v)}} - 1 \right| \leq \epsilon_\gamma \tag{33}$$

pointwise on the coarse-mesh boundaries, as well as in direction and energy, where ϵ_γ is a scalar constant.

At the conclusion of an outer iteration, the last flux estimate,

$$\varphi^{(u)} \equiv \varphi^{(u,V_u)}, \tag{34}$$

is used to update the global eigenvalue by

$$k^{(u)} = \frac{\int d\mathbf{w}\mathbf{F}\varphi^{(u)}}{\int d\mathbf{w}\mathbf{H}\varphi^{(u)}}. \tag{35}$$

Another outer iteration is performed unless the following convergence criterion is satisfied

$$\left| k^{(u)} - k^{(u-1)} \right| \leq \epsilon_k. \tag{36}$$

At the start of the next iteration, the fission source distribution is calculated according to

$$Q^{(u)} = \frac{1}{k^{(u)}} \frac{\mathbf{F}\varphi^{(u)}}{\int d\mathbf{w}\mathbf{F}\varphi^{(u)}}. \tag{37}$$

Apart from the decomposition of the eigenvalue problem, this scheme is just the conventional source or power iteration method traditionally used for solving eigenvalue transport problems (*e.g.*, Lewis and Miller, 1980). The heterogeneous response matrix methods of (Villarino and Stamm'ler, 1984) and (Rathkopf and Martin, 1986) are based on this approach. A different technique, which is the basis of the coarse-mesh method developed in this thesis, is described in the next section.

2.6 Implicit Fission Source Approach

An alternative to the power iteration approach is to treat the fission source distribution implicitly by generating solutions to local fixed source equations that are homogeneous (*i.e.*, lacking an independent source term). To be more specific, consider solving the following transport equation in each coarse-mesh during inner iteration v within outer iteration u

$$\mathbf{H}\varphi^{(u,v)}(\mathbf{w}_i) = \frac{1}{k^{(u-1)}}\mathbf{F}\varphi^{(u,v)}(\mathbf{w}_i), \tag{38}$$

with the boundary condition

$$\varphi^{(u,v)}(\mathbf{w}_i^-) = \gamma^{(u,v)}(\mathbf{w}_i^-). \tag{39}$$

This problem is expected to have a unique, steady-state solution as long as coarse-mesh V_i, with fission cross sections scaled by the factor $1/k^{(u-1)}$, is subcritical in a vacuum (Bell and Glasstone, §1.5d, 1970). The advantage of this approach over the power iteration method, is that a smaller number of Green's functions can be used to generate the local problem solutions, as discussed in Section 1.3.4.

Treating the fission source implicitly creates three important considerations that did not have to be addressed with the power iteration approach. Specifically, the normalization of the source magnitude, the continuity of the global flux estimates, and the estimation of the global eigenvalue are all affected by changing the local transport equation from Eq. (29) to (38). These issues are dealt with in the following sub-sections.

2.6.1 Source Normalization

In the power iteration approach, the independent source distribution in Eq. (37) was consistently normalized and held constant during the inner iterations so that the global flux estimates could converge to a unique limit. In this approach, the intra-nodal flux (and hence the fission source) is a response to the incident fluxes represented by the local problem boundary conditions in Eq. (39). Thus, the magnitude of the boundary conditions must be controlled so that the global flux estimates can again converge to a unique limit. This is accomplished by updating the boundary conditions with normalized fluxes from the

previous iteration (or an initial guess), according to

$$\gamma^{(u,v+1)}(\mathbf{w}_{ji}^{-}) = \frac{1}{N}\varphi^{(u,v)}(\mathbf{w}_{ij}^{+}) \tag{40}$$

and

$$\gamma^{(u,v+1)}(\mathbf{w}_{ib}^{-}) = \frac{1}{N}\mathbf{B}\varphi^{(u,v)}(\mathbf{w}_{ib}^{+}), \tag{41}$$

where

$$N \equiv \int d\mathbf{w}\mathbf{F}\varphi^{(u,v)}. \tag{42}$$

Note that the normalization constant generally varies from inner iteration to inner iteration, however the superscripts have been omitted for brevity.

Using Eqs. (40) and (41), the local boundary conditions in every inner iteration are fluxes that have originated from a global fission source with a magnitude of $1/k^{(u-1)}$. The source caused by the boundary conditions has a magnitude N that depends on the relationship between $k^{(u-1)}$ and the true eigenvalue of the global problem, k, so that generally

$$N < 1, \quad \text{for } k^{(u-1)} > k, \tag{43a}$$

$$N = 1, \quad \text{for } k^{(u-1)} = k, \quad \text{and} \tag{43b}$$

$$N > 1, \quad \text{for } k^{(u-1)} < k. \tag{43c}$$

2.6.2 Interface Conditions

The local transport equations solved in the power iteration and implicit fission source approaches are Eqs. (29) and (38), respectively. At the end of an inner iteration, the mosaic of local problem solutions, φ, satisfies either the global equation

$$\mathbf{H}\varphi^{(u,v)}(\mathbf{w}) = Q^{(u-1)}(\mathbf{w}) \tag{44}$$

or

$$\mathbf{H}\varphi^{(u,v)}(\mathbf{w}) = \frac{1}{k^{(u-1)}}\mathbf{F}\varphi^{(u,v)}(\mathbf{w}), \tag{45}$$

within every coarse-mesh. However, φ may not be continuous (along a given trajectory $\tilde{\mathbf{r}} + \ell\hat{\mathbf{\Omega}}$ at a given energy E) on coarse-mesh interfaces. Consequently, the global equations are not necessarily satisfied at the interfaces, since $\hat{\mathbf{\Omega}} \cdot \nabla\varphi$ may be undefined there. In

addition, φ may not satisfy global boundary conditions that are implicitly defined (*i.e.*, periodic or reflective) and require many iterations to converge.

It is generally possible to find a unique, continuous solution to Eq. (44) with a physically meaningful global boundary condition (*e.g.*, vacuum or symmetry), as long as Q does not contain a delta function representing a highly localized source. It is not possible, however, to find a continuous solution to Eq. (45) unless $k^{(u-1)}$ is exactly an eigenvalue of the global system. This fact is already accounted for in the iterative procedure. If the implicit fission source inner iterations converge according to Eq. (33) with $\epsilon_\gamma << 1$, then the angular flux transmitted between adjacent coarse-meshes will be related by

$$\varphi(\mathbf{w}_{ji}^-) \cong \frac{1}{N}\varphi(\mathbf{w}_{ij}^+), \tag{46}$$

whereas the entering and exiting fluxes at the external system boundary will be related by

$$\varphi(\mathbf{w}_{ib}^-) \cong \frac{1}{N}\mathbf{B}\varphi(\mathbf{w}_{ib}^+). \tag{47}$$

Consequently, discontinuities will be present in the flux estimates whenever $k^{(u-1)}$ is not an eigenvalue of the global system, as must be the case.

When $N \neq 1$, Eq. (46) implies that neutrons are created (for $N < 1$) or destroyed (for $N > 1$) on coarse-mesh boundaries. It is reasonable to expect numerical convergence problems whenever this non-physical phenomenon affects the currents crossing a coarse-mesh interface in opposite directions. In fact, non-convergence of the boundary condition iterations (due to oscillations between two modes) has been observed in several one-dimensional discrete ordinates problems when only Eq. (40) is used to couple adjacent coarse-meshes.

Continuity of the angular flux on coarse-mesh interfaces in 2π half-spaces of directions can be enforced by updating local problem boundary conditions within an inner iteration, wherever possible. The locations where this can be performed depend on the order in which the local problems are solved. For example, at an interface between coarse-meshes V_i and V_j, the following connection can be made before an inner iteration is complete

$$\gamma^{(u,v)}(\mathbf{w}_{ij}^-) = \varphi^{(u,v)}(\mathbf{w}_{ji}^+), \tag{48}$$

if the local problem in V_j is solved before the one in V_i. In the opposite 2π half-space, Eq. (40) must be used. In practice, this avoids the numerical instabilities associated with the presence of angular flux discontinuities in opposite directions across a coarse-mesh interface.

2.6.3 Symmetry Issues

With the updating of local problem boundary conditions on coarse-mesh interfaces using Equations (40) and (48), some consideration has to be given to the orientation of the continuous and discontinuous interface fluxes when the exact global eigenvalue is unknown. The orientation is determined by the order in which the local problems are solved. An arbitrarily chosen order will not generally lead to a symmetric global flux estimate in a symmetric problem.

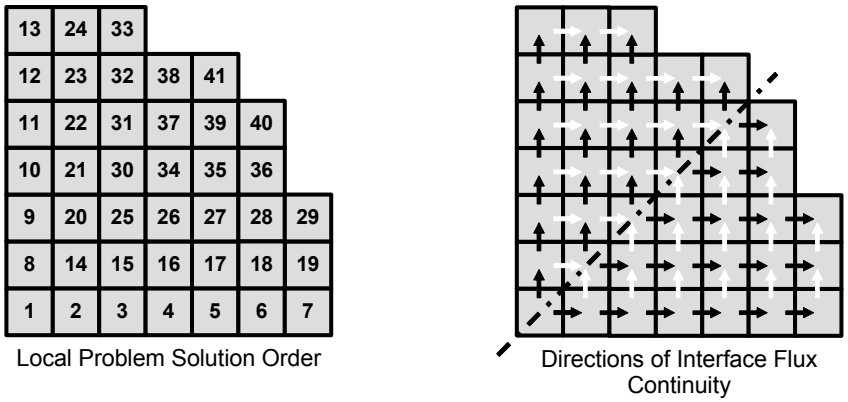

Figure 4: Symmetric Ordering of Local Problem Solutions

As an example, consider Figure 4 above, which represents one-quarter of a PWR core model that has $1/8^{th}$ symmetry. One possible ordering of the local problem solutions is illustrated in the left-side diagram. The resulting orientation of the continuous interface fluxes (in a directional half-space) is illustrated in the right-side diagram. The light and dark shading of the arrows is intended to highlight the fact that this solution order does lead to symmetric global flux estimates.

2.6.4 Eigenvalue Estimation

In the power iteration approach, improved estimates of the eigenvalue were generated as the ratio of gains to losses using Eq. (35). In the implicit fission source approach, a fixed gain-to-loss ratio has been imposed, equal to the $k^{(u-1)}$ value in Eq. (45). Consequently, a direct calculation of the global neutron balance will not lead to any new information, and a different formula must be used to calculate an improved estimate of k.

When $k^{(u-1)}$ is greater than or less than the exact k, neutrons are non-physically gained or lost on the coarse-mesh boundaries, respectively, so that the imposed balance of neutrons is obeyed. In this situation, a reasonable approach to generating improved eigenvalue estimates is to simply ignore the angular flux discontinuities on the coarse-mesh interfaces. The eigenvalue estimate may be then updated by

$$k^{(u)} = \frac{\int d\mathbf{w}\mathbf{F}\varphi^{(u)}}{L + \int d\mathbf{w}\mathbf{A}\varphi^{(u)}}, \tag{49}$$

where the absorption operator is defined as

$$\mathbf{A} \equiv \mathbf{H} - \hat{\mathbf{\Omega}} \cdot \nabla. \tag{50}$$

The quantity

$$L \equiv \int_{\partial V} \int_{4\pi} \int_0^\infty dS\, d\hat{\mathbf{\Omega}}\, dE\, \hat{\mathbf{n}} \cdot \hat{\mathbf{\Omega}} \varphi^{(u)} \tag{51}$$

is the net leakage from the boundary, which is not equal to the net the leakage from the system when angular flux discontinuities are present.

CHAPTER III

INCIDENT FLUX RESPONSE EXPANSION METHOD

In this chapter, a new coarse-mesh method is developed by generalizing the Green's function technique for solving the local fixed source problems in the implicit fission source approach presented in the previous chapter. Both variational and non-variational methods are developed based on the general expansion. The numerical implementation of the method is discussed in Chapter 4.

3.1 Response Function Expansions

It is clear that solving an eigenvalue problem using the implicit fission source approach requires the computation of numerous solutions to the local fixed source problems. However, it is only the boundary conditions of the local problems that vary within an outer iteration. Hence, it is natural to think of using Green's function solutions as a means for increasing the efficiency of this process. This idea was exploited in previous work (Ilas and Rahnema, 2001).

3.1.1 Green's Function Solutions to Local Problems

Consider the following local problem within coarse-mesh V_i

$$\mathbf{H}\varphi(\mathbf{w}_i) = \frac{1}{k}\mathbf{F}\varphi(\mathbf{w}_i), \tag{52}$$

$$\varphi(\mathbf{w}_i^-) = \gamma(\mathbf{w}_i^-). \tag{53}$$

As before, k is a fixed estimate of the eigenvalue of the global system and γ is a known incident flux distribution, so that the above equations represent a fixed source transport problem. The solution to Eqs. (52) and (53) can be expressed as

$$\varphi(\mathbf{w}_i) = \int d\mathbf{w}_i^{-\prime}\gamma(\mathbf{w}_i^{-\prime})G(\mathbf{w}_i^{-\prime} \rightarrow \mathbf{w}_i), \tag{54}$$

where G is Ilas and Rahnema's surface Green's function. This particular Green's function is defined as the solution to the local transport equation

$$\mathbf{H}G(\mathbf{w}_i^{-\prime} \rightarrow \mathbf{w}_i) = \frac{1}{k}\mathbf{F}G(\mathbf{w}_i^{-\prime} \rightarrow \mathbf{w}_i), \tag{55}$$

with a singular boundary condition

$$G(\mathbf{w}_i^{-\prime} \rightarrow \mathbf{w}_i^{-}) = \delta(\mathbf{w}_i^{-} - \mathbf{w}_i^{-\prime}). \tag{56}$$

The shorthand phase-space notation used in the Dirac delta function actually represents a product of delta functions in the scalar phase-space variables (*e.g.*, x, μ, E, *etc.*) so that the principal characteristics are maintained. That is

$$\delta(\mathbf{w}_i^{-} - \mathbf{w}_i^{-\prime}) = 0, \quad \text{for } \mathbf{w}_i^{-} \neq \mathbf{w}_i^{-\prime}, \tag{57}$$

and

$$\int d\mathbf{w}_i^{-} f(\mathbf{w}_i^{-})\delta(\mathbf{w}_i^{-} - \mathbf{w}_i^{-\prime}) = f(\mathbf{w}_i^{-\prime}). \tag{58}$$

The Green's functions provide the capability to quickly generate accurate solutions to the local problems using Eq. (54), during the inner iterations of the implicit fission source approach. Since the k estimate appears in Eq. (55), the Green's functions must be updated at the beginning of each outer iteration. However, SGFs need only be generated for each unique coarse mesh type. In this way, the solution to a large, heterogeneous eigenvalue problem can generally be computed more efficiently using Green's functions than by generating direct solutions to the local problems (in each coarse-mesh during each inner iteration).

3.1.2 General Response Formulation

The Green's functions represent the response of a coarse-mesh to an incident flux entering through a single location, in a single direction, and at a single energy. Individual responses can be superimposed to compute the integrated response of the coarse mesh to an arbitrary incident flux distribution. The Green's functions are not unique in this respect.

Let Γ_m, where $m = 0, 1, ...$, be a set of orthonormal functions on $\mathbf{w}_{is}^-$

$$\int d\mathbf{w}_{is}^- \Gamma_m \Gamma_n = \delta_{mn}, \tag{59}$$

where s indexes the interfaces and boundary segments that comprise the surface of coarse-mesh V_i, and δ is now the Kronecker delta. Let a response function, R, be defined as the solution to the transport equation

$$\mathbf{H} R_{is}^m(\mathbf{w}_i) = \frac{1}{k} \mathbf{F} R_{is}^m(\mathbf{w}_i), \tag{60}$$

with the boundary condition

$$R_{is}^m(\mathbf{w}_i^-) = \begin{cases} \Gamma_m, & \text{for } \mathbf{w}_i^- \bigcap \mathbf{w}_{is}^- \\ 0, & \text{otherwise.} \end{cases} \tag{61}$$

The solution to the local fixed source problem in Eqs. (52) and (53) can be expressed as the response expansion

$$\varphi(\mathbf{w}_i) = \sum_{m=0}^{\infty} \sum_s c_{is}^m R_{is}^m(\mathbf{w}_i), \tag{62}$$

where the coefficients are

$$c_{is}^m \equiv \int d\mathbf{w}_{is}^- \gamma(\mathbf{w}_{is}^-) \Gamma_m(\mathbf{w}_{is}^-). \tag{63}$$

Ilas and Rahnema's surface Green's functions are a specific type of response function, which is associated with delta function boundary conditions and with expansion coefficients that are simply the incident fluxes themselves.

3.1.3 Truncated Expansions

With the intent of developing an efficient coarse-mesh method for multi-dimensional geometries, it is clearly desirable to identify a set of boundary conditions, Γ_m, that would allow the response expansion in Eq. (62) to be truncated,

$$\varphi(\mathbf{w}_i) \cong \sum_{m=0}^{M} \sum_s c_{is}^m R_{is}^m(\mathbf{w}_i), \tag{64}$$

while maintaining an accurate characterization of the integrated coarse-mesh response. Moreover, the boundary conditions that lead to a highly accurate representation of φ with the smallest value of M are the most desirable.

Unfortunately, the surface Green's functions are not an efficient basis in which to represent the coarse-mesh response. Truncating a Green's function expansion computationally closes paths of entry into a coarse-mesh, since a fraction of the incident fluxes must always be set to zero, and leads to poor results in reactor calculations. Certainly a less singular set of boundary conditions would be more amenable to truncation.

Since transport theory response functions for heterogeneous coarse-meshes cannot be generated by analytical techniques, fine-mesh transport methods must be used in practice. The search for an efficient response basis is greatly affected by the form of the numerical phase-space imposed by the fine-mesh method. For example, a response function boundary condition set that is appropriate for discrete ordinates calculations would not fit within the context of a spherical harmonics method, and vice versa. For that reason, the Γ_m's in Eq. (61) will be left unspecified for the remainder of this chapter. In Chapter 4, a numerical method based on a particular choice of boundary conditions (and fine-mesh method) is presented.

3.2 Non-Variational Coarse Mesh Method

Using the truncated response expansion in Eq. (64) within the implicit fission source approach is conceptually straightforward. At the beginning of an outer iteration, a set of response functions for each unique coarse-mesh type are computed according to Eqs. (60) and (61) with the most recent global eigenvalue estimate. During the inner iterations, local problems are solved by computing expansion coefficients according to Eq. (63) and constructing the flux estimate within the coarse-mesh using Eq. (64). The remainder of the implicit fission source method remains essentially unchanged.

There are two improvements, however, that can be made to the non-variational method just described. The first relates to the coarse-mesh coupling, while the second is an alternative technique for updating the response functions with new eigenvalue estimates.

3.2.1 Partial Current Preservation

With a truncated response expansion, the distribution of the angular fluxes transmitted across coarse-mesh interfaces will be distorted due to the incomplete response set. This is also true of the angular fluxes returning from implicit boundary conditions (*i.e.*, reflective or periodic). Flux discontinuities will generally be present in every direction across an interface, as opposed to the half-range continuity obtained by solving the local problems directly or using a full expansion (discussed in Section 2.6.3). With low-order expansions, substantial discontinuities in the partial currents may exist, which affects the system neutron balance.

The loss of information in the angular flux transmitted between coarse-meshes can only be repaired by increasing the response expansion order, M, in Eq. (64). On the other hand, the partial current integrated over an interface or boundary segment can be preserved. For example, if coarse-mesh V_j is treated before its neighbor V_i, then the coefficients from Eq. (63), denoted c_{ij}^m $(m = 0, 1, ..., M)$, can be adjusted to preserve the total number of neutrons transmitted from V_j to V_i, by

$$\tilde{c}_{ij}^m = r c_{ij}^m, \tag{65}$$

where the adjustment ratio is

$$r \equiv \frac{\int d\mathbf{w}_{ji}^+ \, \hat{\mathbf{n}}_j \cdot \hat{\mathbf{\Omega}} \, \varphi(\mathbf{w}_{ji}^+)}{\sum\limits_{m'} \int d\mathbf{w}_{ij}^- \left| \hat{\mathbf{n}}_i \cdot \hat{\mathbf{\Omega}} \right| c_{ij}^{m'} \Gamma_{m'}(\mathbf{w}_{ij}^-)}. \tag{66}$$

This procedure can always be used, since the difference between the adjusted and unadjusted coefficients will asymptotically approach zero as the expansion order increases.

3.2.2 Response Function Interpolation

Ilas and Rahnema (2001) used a linear interpolation procedure to update the response functions between outer iterations with the most recent estimate of the global eigenvalue. Since the response functions for fixed k values can be pre-computed (*i.e.*, generated prior to the start of a coarse-mesh calculation), this technique greatly increases the efficiency of the method by avoiding expensive iterations between the coarse and fine-mesh calculations.

That interpolation scheme will be employed in both the non-variational and variational (discussed later) coarse-mesh methods developed in this thesis.

Let a series of pre-determined values, k_n, be used to compute a series of response functions, R_n, according to Eqs. (60) and (61), where $n = 1, 2, ...$ When a new eigenvalue estimate, k, is generated during the coarse-mesh calculations, so that

$$k_n \leq k \leq k_{n+1}, \tag{67}$$

the response functions are updated according to

$$R = aR_n + (1 - a) R_{n+1}, \tag{68}$$

where the linear interpolation coefficient is

$$a \equiv \frac{\frac{1}{k} - \frac{1}{k_{n+1}}}{\frac{1}{k_n} - \frac{1}{k_{n+1}}}. \tag{69}$$

3.2.3 Approximations

At this point, it is clear that there are two approximations made in the coarse-mesh method that will cause the results to deviate from a reference fine-mesh calculation. The first is the truncation of the response expansion in Eq. (62). The second is the linear interpolation procedure used to update the response functions between outer iterations. The extent of these approximations can be controlled by varying the expansion order, M, in Eq. (64), and by varying the density of the eigenvalue estimates, k_n, over which the interpolation is performed.

3.3 Variational Coarse Mesh Method

The eigenvalue problem decomposition, implicit fission source approach, and response expansion technique have, so far, been presented only as a means for solving the neutron transport equation presented in Section 2.1, hereafter referred to as the forward mode equation. In fact, the ideas have a straightforward application to the solution of equations that are mathematically adjoint to Eqs. (10) and (13). The utility of the adjoint application is that a variational method can be developed by considering both the forward and adjoint

mode transport of neutrons in a global eigenvalue problem. In principle, higher-order accuracy can be obtained by using the adjoint solution as an importance (or weighting) function in the computation of quantities of interest. Such a variational method is developed in this section.

3.3.1 Global Adjoint Problem

The homogeneous adjoint transport equation is

$$\mathbf{H}^{\dagger}\psi^{\dagger}(\tilde{\mathbf{r}},\hat{\mathbf{\Omega}},E)=\frac{1}{k}\mathbf{F}^{\dagger}\psi^{\dagger}(\tilde{\mathbf{r}},\hat{\mathbf{\Omega}},E), \tag{70}$$

where the operators $\mathbf{H}^{\dagger}$ and $\mathbf{F}^{\dagger}$ are defined as

$$\mathbf{H}^{\dagger}\equiv-\hat{\mathbf{\Omega}}\cdot\nabla+\sigma_t(\tilde{\mathbf{r}},E)-\int_0^{\infty}\int_{4\pi}dE'd\hat{\mathbf{\Omega}}'\sigma_s(\tilde{\mathbf{r}},\hat{\mathbf{\Omega}},E\rightarrow\hat{\mathbf{\Omega}}',E') \tag{71}$$

and

$$\mathbf{F}^{\dagger}\equiv\frac{1}{4\pi}\nu\sigma_f(\tilde{\mathbf{r}},E)\int_0^{\infty}\int_{4\pi}dE'd\hat{\mathbf{\Omega}}'\chi(\tilde{\mathbf{r}},E'). \tag{72}$$

The adjoint equation differs from the forward one in that the neutron motion is in the $-\hat{\mathbf{\Omega}}$ direction, and that the initial and final energy states are reversed in the scattering and fission terms. Associated with Eq. (70) is a boundary condition

$$\psi^{\dagger}(\tilde{\mathbf{r}},\hat{\mathbf{\Omega}},E)=\mathbf{B}^{\dagger}\psi^{\dagger}(\tilde{\mathbf{r}}',\hat{\mathbf{\Omega}}',E'),\quad\text{for }\tilde{\mathbf{r}},\,\tilde{\mathbf{r}}'\in\partial V,\,\hat{\mathbf{n}}\cdot\hat{\mathbf{\Omega}}>0,\text{ and }\hat{\mathbf{n}}\cdot\hat{\mathbf{\Omega}}'<0, \tag{73}$$

where $\mathbf{B}^{\dagger}$ is an adjoint boundary condition operator. For a given system and boundary condition, the largest real adjoint eigenvalue is identical to that from the forward equation.

3.3.2 Adjoint Method

The fundamental difference in the application of the implicit fission source approach to a global adjoint problem, is that the local problems are posed in terms of a fixed source adjoint equation

$$\mathbf{H}^{\dagger}\varphi^{\dagger}(\mathbf{w}_i)=\frac{1}{k}\mathbf{F}^{\dagger}\varphi^{\dagger}(\mathbf{w}_i), \tag{74}$$

with the boundary condition

$$\varphi^{\dagger}(\mathbf{w}_i^{+})=\gamma^{\dagger}(\mathbf{w}_i^{+}). \tag{75}$$

As before, the adjoint fluxes exiting a coarse-mesh are used to update the adjoint boundary conditions of neighboring coarse-meshes. However, "exiting" and "entering" adjoint fluxes are defined in opposite 2π directional half-spaces from their forward counterparts. In addition, the constant used to normalize boundary conditions between inner iterations may be redefined in terms of the adjoint fission operator $\mathbf{F}^\dagger$. This is optional however, since the normalization is arbitrary.

In the incident flux response expansion method, adjoint response functions are naturally defined as the solution to

$$\mathbf{H}^\dagger R_{it}^{\dagger n}(\mathbf{w}_i) = \frac{1}{k}\mathbf{F}^\dagger R_{it}^{\dagger n}(\mathbf{w}_i), \tag{76}$$

with the boundary condition

$$R_{it}^{\dagger n}(\mathbf{w}_i^+) = \begin{cases} \Gamma_n^\dagger, & \text{for } \mathbf{w}_i^+ \bigcap \mathbf{w}_{it}^+ \\ 0, & \text{otherwise} \end{cases} \tag{77}$$

where n denotes the adjoint expansion order index and t denotes the surface index. In the adjoint case, the functions $\Gamma_n^\dagger$ must be orthonormal on $\mathbf{w}_{it}^+$, as opposed to $\mathbf{w}_{is}^-$ in the forward case. The adjoint angular flux within coarse-mesh V_i is expanded as

$$\varphi^\dagger(\mathbf{w}_i) \cong \sum_{n=0}^{N} \sum_t c_{it}^{\dagger n} R_{it}^{\dagger n}(\mathbf{w}_i), \tag{78}$$

where the adjoint coefficients are defined as

$$c_{it}^{\dagger m} \equiv \int d\mathbf{w}_{it}^+ \gamma^\dagger(\mathbf{w}_{it}^+) \Gamma_n^\dagger(\mathbf{w}_{it}^+). \tag{79}$$

The calculation of the eigenvalue must, of course, be based on the adjoint operators

$$k^{(u)} = \frac{\int d\mathbf{w} \mathbf{F}^\dagger \varphi^{\dagger(u)}}{L^\dagger + \int d\mathbf{w} \mathbf{A}^\dagger \varphi^{\dagger(u)}}, \tag{80}$$

where

$$\mathbf{A}^\dagger \equiv \mathbf{H}^\dagger + \hat{\mathbf{\Omega}} \cdot \nabla. \tag{81}$$

The adjoint net leakage term has an opposite sign from the forward one

$$L^\dagger \equiv -\int_{\partial V} \int_{4\pi} \int_0^\infty dS \, d\hat{\mathbf{\Omega}} \, dE \; \hat{\mathbf{n}} \cdot \hat{\mathbf{\Omega}} \varphi^{\dagger(u)}. \tag{82}$$

3.3.3 Ilas and Rahnema's Variational Principle

The variational principle developed by Ilas and Rahnema (2001; 2003) serves as a starting point for the development of a variational algorithm incorporating all of the previously presented ideas. In this sub-section, the principle is described in detail and its previous application to coarse-mesh transport problems is briefly reviewed. In the sub-sections that follow, two new techniques for applying the principle to coarse-mesh transport problems are developed.

Ilas and Rahnema's principle admits forward and adjoint angular flux trial functions that may be discontinuous on coarse-mesh interfaces and also may not satisfy the global boundary condition. The general form of the principle for a system comprised of I coarse-meshes is

$$\mathbb{F}\left[\varphi,\varphi^{\dagger};\lambda\right]=\sum_{i=1}^{I}\mathbb{F}_{i}\left[\varphi(\mathbf{w}_{i}),\varphi^{\dagger}(\mathbf{w}_{i});\lambda\right], \tag{83}$$

where the coarse-mesh functionals are defined as

$$\begin{aligned}\mathbb{F}_{i} \equiv\ & \mathbb{G}_{i}\left[\varphi(\mathbf{w}_{i})\right]+\left\langle\mathbf{H}\varphi(\mathbf{w}_{i}),\varphi^{\dagger}(\mathbf{w}_{i})\right\rangle-\lambda\left\langle\mathbf{F}\varphi(\mathbf{w}_{i}),\varphi^{\dagger}(\mathbf{w}_{i})\right\rangle-\left\langle q(\mathbf{w}_{i}),\varphi^{\dagger}(\mathbf{w}_{i})\right\rangle \\ & -\sum_{j\rightarrow i}\left\langle\varphi(\mathbf{w}_{ij}^{-})-\varphi(\mathbf{w}_{ji}^{+}),\hat{\mathbf{n}}_{i}\cdot\hat{\mathbf{\Omega}}\left[\alpha\varphi^{\dagger}(\mathbf{w}_{ij}^{-})+(1-\alpha)\,\varphi^{\dagger}(\mathbf{w}_{ji}^{+})\right]\right\rangle_{ij}^{-} \\ & -\sum_{b\rightarrow i}\left\langle\varphi(\mathbf{w}_{ib}^{-})-\mathbf{B}\varphi(\mathbf{w}_{ib}^{+}),\hat{\mathbf{n}}_{i}\cdot\hat{\mathbf{\Omega}}\varphi^{\dagger}(\mathbf{w}_{ib}^{-})\right\rangle_{ib}^{-}.\end{aligned} \tag{84}$$

A conventional inner product notation has been used to denote, for example,

$$\left\langle f,g^{\dagger}\right\rangle\equiv\int d\mathbf{w}\,f\,g^{\dagger}. \tag{85}$$

The subscripts and superscripts attached to the angle brackets denote spatial and angular restrictions as described in Section 2.2.

The first term in the principle is the functional $\mathbb{G}_i$, an arbitrary quantity of interest that depends only on the forward trial function, such as a reaction rate. The second and third terms correspond to the left and right-hand sides of the transport equation, respectively. In the third term, λ is parameter that corresponds to a trial estimate of $1/k$. The fourth term contains a fixed source distribution, q. This makes the principle applicable

to both the fixed source and eigenvalue forms of the transport equation. The fifth term accounts for discontinuities in the trial functions on coarse-mesh interfaces, and contains a free parameter α that can be chosen in the range $0 \leq \alpha \leq 1$. The notation "$j \rightarrow i$" denotes that the summation is performed over all interfaces between coarse-mesh V_i and its neighbors (indexed by j). The last term accounts for trial functions that do not exactly satisfy the global boundary condition, and the summation is performed over the boundary segments of V_i (if any).

The Euler-Lagrange equations of the variational principle are the exact forward and adjoint transport equations, interface continuity conditions, and boundary conditions. Specifically,

$$\mathbf{H}\psi = \Lambda\mathbf{F}\psi + q, \tag{86}$$

$$\psi(\mathbf{w}_{ij}) = \psi(\mathbf{w}_{ji}), \quad \text{for all } i \text{ and } j \rightarrow i, \tag{87}$$

$$\psi(\mathbf{w}_{ib}^{-}) = \mathbf{B}\psi(\mathbf{w}_{ib}^{+}), \quad \text{for all } i \text{ and } b \rightarrow i, \tag{88}$$

$$\mathbf{H}^{\dagger}\psi^{\dagger} = \frac{1}{k}\mathbf{F}^{\dagger}\psi^{\dagger} - \mathbb{G}'\left[\psi\right], \tag{89}$$

$$\psi^{\dagger}(\mathbf{w}_{ij}) = \psi^{\dagger}(\mathbf{w}_{ji}), \quad \text{for all } i \text{ and } j, \tag{90}$$

$$\psi^{\dagger}(\mathbf{w}_{ib}^{+}) = \mathbf{B}^{\dagger}\psi^{\dagger}(\mathbf{w}_{ib}^{-}), \quad \text{for all } i \text{ and } b \rightarrow i, \tag{91}$$

$$\delta\lambda = 0, \tag{92}$$

where ψ and $\psi^{\dagger}$ are the exact forward and adjoint angular flux solutions, Λ is the inverse of the exact k, $\mathbb{G}'$ is the functional derivative of $\mathbb{G}$ (Volterra, 1959), and $\delta\lambda$ is the first-order error in λ. The proof that $\mathbb{F}$ is indeed stationary about the exact solutions was shown in (Ilas and Rahnema, 2003) and independently verified by the author.

The principle was originally used to derive finite element equations based on a complete forward and adjoint surface Green's function response expansion (*i.e.*, not truncated). In this case, the expansion coefficients are just the angular fluxes on the coarse-mesh boundaries. By substituting the expansions into the principle and taking a functional derivative with respect to the adjoint coefficients, linear algebraic equations of the form

$$\hat{\mathbf{H}}\xi = \lambda\hat{\mathbf{F}}\xi + Q, \tag{93}$$

were obtained in the 1-D, multigroup, discrete ordinates approximation. The $\hat{\mathbf{F}}$ matrix originates from the fission term of the principle, while the $\hat{\mathbf{H}}$ matrix incorporates all of the other terms except the fixed source term. The ξ vector contains the forward angular fluxes (expansion coefficients) on all coarse-mesh boundaries in the system, while the Q vector is an inner product of the fixed source distribution and the adjoint response functions. Note that the adjoint coefficients were removed from the system by the functional derivative step. Alternatively, an equation for the adjoint coefficients can be derived by taking a different functional derivative to remove the forward coefficients.

The algebraic finite element equations were found to be ill-conditioned and difficult to solve numerically. Large angular flux discontinuities on the coarse-mesh interfaces were present in apparently converged solutions. An auxiliary technique was developed to fix-up the boundary fluxes, however a non-variational procedure was eventually favored for estimating ξ. The procedure consisted of a straightforward right-to-left sweep through the coarse-meshes in the system, and was used in conjunction with the following Rayleigh quotient for variationally updating the eigenvalue estimates

$$k = \frac{\xi^{\intercal}\hat{\mathbf{F}}\xi}{\xi^{\intercal}\hat{\mathbf{H}}\xi}, \tag{94}$$

where $\xi^{\intercal}$ denotes the transpose of ξ. This Rayleigh quotient requires the generation of both forward and adjoint response functions, but does not require the solution of a global adjoint problem.

3.3.4 De-coupled Finite Element Equations

In Ilas and Rahnema's finite element equations, the relationship between the expansion coefficients in adjacent coarse-meshes is governed by the interface term of the coarse-mesh functional

$$\mathbb{I}_i \equiv \sum_{j \to i} \left\langle \varphi(\mathbf{w}_{ij}^-) - \varphi(\mathbf{w}_{ji}^+), \hat{\mathbf{n}}_i \cdot \hat{\mathbf{\Omega}} \left[\alpha \varphi^\dagger(\mathbf{w}_{ij}^-) + (1-\alpha)\, \varphi^\dagger(\mathbf{w}_{ji}^+) \right] \right\rangle_{ij}^{-}. \tag{95}$$

In the derivation, the forward trial flux incident upon coarse-mesh V_i at its interface with V_j, namely $\varphi(\mathbf{w}_{ji}^+)$, is expanded in terms of the coefficients and response functions from V_j.

Consequently, the V_i coefficients at this interface are coupled to all of the V_j coefficients, and the V_j coefficients at the interface are coupled to all of the V_i coefficients. It is reasonable to expect that this extensive coupling is at least partly responsible for the numerical difficulties previously encountered in solving these equations. In this sub-section, a new set of finite element equations will be derived while avoiding the type of coupling just described.

With the intention of applying the variational principle to eigenvalue problems, the substitutions $\mathbb{G}_i = \mathbf{0}$ and $q = 0$ are immediately apparent. In addition, a choice for the parameter α will be made at the outset. In the interface term $\mathbb{I}_i$, the discontinuity in the forward trial flux entering coarse-mesh V_i is weighted by a linear combination of the adjoint trial fluxes exiting the coarse mesh. Since a truncated response expansion leads to some distortion of the fluxes transmitted between coarse-meshes, it is expected that $\varphi^\dagger(\mathbf{w}_{ij}^-)$ generally has better information content than $\varphi^\dagger(\mathbf{w}_{ji}^+)$. Consequently, the choice $\alpha = 1$ is natural. The simplified coarse-mesh functional resulting from these three substitutions, $\tilde{\mathbb{F}}_i$, is conveniently expressed as a sum of a volume and surface term

$$\tilde{\mathbb{F}}_i = \mathbb{V}_i + \mathbb{S}_i, \tag{96}$$

where

$$\mathbb{V}_i \equiv \left\langle (\mathbf{H} - \lambda \mathbf{F})\, \varphi(\mathbf{w}_i), \varphi^\dagger(\mathbf{w}_i) \right\rangle. \tag{97}$$

A surface index s that combines both the interface and boundary segment indices allows the surface term to be conveniently expressed as

$$\mathbb{S}_i \equiv \sum_s \left\langle \varphi(\mathbf{w}_{si}^+) - \varphi(\mathbf{w}_{is}^-), \hat{\mathbf{n}}_i \cdot \hat{\mathbf{\Omega}} \varphi^\dagger(\mathbf{w}_{is}^-) \right\rangle_{is}^-, \tag{98}$$

where

$$\varphi(\mathbf{w}_{si}^+) \equiv \begin{cases} \varphi(\mathbf{w}_{ji}^+), & \text{when } s = j \text{ (an interface)}, \\ \mathbf{B}\varphi(\mathbf{w}_{ib}^+), & \text{when } s = b \text{ (a boundary segment)}. \end{cases} \tag{99}$$

The next step is to expand the trial functions in Eqs. (97) and (98) using Eqs. (64) and (78) to arrive at

$$\mathbb{V}_i = \sum_{n=0}^{N} \sum_t c_{it}^{\dagger n} \left\{ \sum_{m=0}^{M} \sum_s c_{is}^m \left\langle (\mathbf{H} - \lambda \mathbf{F})\, R_{is}^m(\mathbf{w}_i), R_{it}^{\dagger n}(\mathbf{w}_i) \right\rangle \right\} \tag{100}$$

and

$$\mathbb{S}_i = \sum_{n=0}^{N} \sum_t c_{it}^{\dagger n} \left\{ \sum_s \left\langle \varphi(\mathbf{w}_{si}^+) - \sum_{m=0}^{M} c_{is}^m R_{is}^m(\mathbf{w}_{is}^-), \hat{\mathbf{n}}_i \cdot \hat{\mathbf{\Omega}} R_{it}^{\dagger n}(\mathbf{w}_{is}^-) \right\rangle_{is}^{-} \right\} \tag{101}$$

Note that the forward angular trial fluxes exiting the neighboring coarse-meshes and returning from boundary segments have not been expanded. That is, the fluxes $\varphi(\mathbf{w}_{si}^+)$ are now assumed to be known quantities. As an intended consequence, the direct coupling between the expansion coefficients in neighboring coarse-meshes has been broken.

A set of equations for the forward expansion coefficients is obtained by setting to zero the functional derivative of $\tilde{\mathbb{F}}_i$ with respect to each adjoint coefficient

$$\sum_{m=0}^{M} \sum_s A_{ist}^{mn} c_{is}^m = b_{it}^n, \text{ for all } n \text{ and } t \tag{102}$$

where

$$A_{ist}^{mn} \equiv \left\langle (\mathbf{H} - \lambda \mathbf{F}) R_{is}^m(\mathbf{w}_i), R_{it}^{\dagger n}(\mathbf{w}_i) \right\rangle + \left\langle \hat{\mathbf{n}}_s \cdot \hat{\mathbf{\Omega}} R_{is}^m(\mathbf{w}_{is}^-), R_{it}^{\dagger n}(\mathbf{w}_{is}^-) \right\rangle_{is}^{-} \tag{103}$$

and

$$b_{it}^n \equiv \sum_s \left\langle \hat{\mathbf{n}}_s \cdot \hat{\mathbf{\Omega}} \varphi(\mathbf{w}_{si}^+), R_{it}^{\dagger n}(\mathbf{w}_{is}^-) \right\rangle_{is}^{-}, \tag{104}$$

while $\hat{\mathbf{n}}_s$ is the inward normal on $\mathbf{w}_{is}$. The finite element coefficients, A_{ist}^{mn}, depend only on the forward and adjoint response functions and λ, the trial estimate of $1/k$. The constants b_{it}^n are computed by integrating an adjoint-weighted incident partial current over all of the coarse-mesh surfaces.

By combining the forward expansion order m and surface index s into a column index, and by combining the adjoint order n and surface index t into a row index, A_{ist}^{mn} can be represented by a matrix $\hat{\mathbf{A}}$. Similarly, c_{is}^m and b_{it}^n can be represented by the vectors $\hat{\mathbf{x}}$ and $\hat{\mathbf{b}}$ to arrive at the simple matrix equation $\hat{\mathbf{A}} \cdot \hat{\mathbf{x}} = \hat{\mathbf{b}}$. If the maximum forward and adjoint expansion orders, M and N respectively, are identical, $\hat{\mathbf{A}}$ will be a square matrix. Otherwise, the system will be underdetermined when $M > N$ and overdetermined when $M < N$. Hereafter, it will be assumed that $M = N$.

Since the fluxes $\varphi(\mathbf{w}_{si}^+)$ have been regarded as known quantities, an iterative procedure will be necessary to apply these finite element equations in practice. The implicit fission

source approach is ideal for this purpose. These equations can be solved to estimate the expansion coefficients during the inner iterations, while λ is considered fixed. There is a unique $\hat{\mathbf{A}}$ matrix for each unique coarse-mesh type, which must be updated only at the beginning of each outer iteration (when λ is updated). The $\hat{\mathbf{b}}$ vector is constructed and the equations are solved in each coarse-mesh during each inner iteration. This finite element approach is a variational alternative to the non-variational procedure of computing the coefficients by a straightforward expansion of $\varphi(\mathbf{w}_{si}^{+})$.

3.3.5 Rayleigh Quotient

The functional

$$\tilde{\mathbb{F}}\left[\varphi, \varphi^{\dagger}; \lambda\right] = \sum_{i=1}^{I} \tilde{\mathbb{F}}_i, \tag{105}$$

where $\tilde{\mathbb{F}}_i$ is the coarse-mesh functional from Eq. (96), is stationary about zero. Consequently, a new Rayleigh quotient can be developed by a trivial rearrangement of the terms in $\tilde{\mathbb{F}}$ to obtain

$$\mathbb{R}\left[\varphi, \varphi^{\dagger}\right] \equiv \left\langle \mathbf{F}\varphi(\mathbf{w}_i), \varphi^{\dagger}(\mathbf{w}_i) \right\rangle \Big/ \left\{ \left\langle \mathbf{H}\varphi(\mathbf{w}_i), \varphi^{\dagger}(\mathbf{w}_i) \right\rangle - \sum_{i=1}^{I} \mathbb{S}_i \right\}, \tag{106}$$

where $\mathbb{S}_i$ is the surface term defined by Eq. (98).

The above Rayleigh quotient requires both forward and adjoint trial functions, hence it can only be used when both forward and adjoint global problems are solved. In this sense, it is less efficient than Ilas and Rahnema's quotient, which does not require an adjoint solution (but does require both forward and adjoint response functions). On the other hand, given that an adjoint trial function is available, Eq. (106) can be computed much more efficiently than Eq. (94). This is due to the fact that the response expansion of φ and $\varphi^{\dagger}$ leads to a greater number of terms in the quotient, and that the volume terms involve the application of the transport operators to the forward mode response function value in each spatial fine-mesh, direction, and energy group. All numerical experience with Eq. (106), indicates that eigenvalue estimates with a substantially higher degree of accuracy than the non-variational estimate from Eq. (49) are obtained for a wide range of problems, regardless of the expansion order. Such numerical evidence is presented in Chapter 5.

CHAPTER IV

DISCRETE ORDINATES COARSE MESH METHOD

In this chapter, the numerical implementation of the incident flux response expansion method is discussed. The multigroup, finite-difference, discrete ordinates approximation will be used for computing coarse-mesh response functions. The discrete ordinates method was favored for this work because of its speed, simplicity, and wide-spread application. At this point, it is worth noting that the accuracy of the implemented coarse-mesh method is ultimately limited by the accuracy of the fine-mesh method – especially with respect to the numerical parameters (*i.e.*, spatial mesh size, number of directions, *etc.*) chosen when computing response functions.

Having selected a fine-mesh method, the principal focus of this chapter is to identify an efficient set of discrete ordinates boundary conditions with which to generate forward and adjoint response functions. Following that, a brief description of the computer codes that were developed to perform actual transport calculations is presented. A comparison of the coarse-mesh results to reference fine-mesh calculations on several one and two-dimensional benchmark problems is the subject of Chapter 5.

4.1 Discrete Response Function Expansions

Since response functions are fine-mesh solutions in practice, the expansions presented in Chapter 3 hold only if the response function boundary conditions are orthonormal within the context of the numerical phase-space imposed by the fine-mesh method. In the multigroup, finite-difference, discrete ordinates approximation, the phase-space is characterized by a discrete spatial, angular, and energy mesh. Boundary conditions, in this case, could be constructed using functions that are orthogonal on a discrete set of points (or intervals).

4.1.1 Discrete Legendre Polynomials

There is a discrete analog of the continuous Legendre polynomials – the so-called discrete Legendre polynomials (DLPs). A thorough exploration of the properties of the DLPs, as well as an algorithm for generating the polynomials, was published by Neuman and Schonbach (1974). The authors briefly mention using the polynomials in curve-fitting and weighted residual method work. Numerous articles can be found regarding the application of DLPs in the fields of signal processing and control system analysis. However, a previous application of the polynomials in the nuclear engineering literature was not found.

The discrete Legendre polynomials are a set of orthogonal functions on uniform intervals $i = 1, 2, ..., M+1$. Let the m^{th} order polynomial be denoted by $P_m(i; M)$, where the parameter M denotes the maximum polynomial order in the set. The normalized polynomials satisfy the orthogonality relation

$$\left\langle P_\ell, P_m \right\rangle \equiv \sum_{i=1}^{M+1} P_\ell(i;M) P_m(i;M) = \delta_{\ell m} \tag{107}$$

For example, the unnormalized DLPs (denoted by $\tilde{P}$) corresponding to $M = 5$, are

$$\begin{aligned}
\tilde{P}_0(i,5) &= 1 \\
\tilde{P}_1(i,5) &= 1 - \frac{2}{5}i \\
\tilde{P}_2(i,5) &= 1 - \frac{6}{5}i + \frac{3}{10}i^{(2)} \\
\tilde{P}_3(i,5) &= 1 - \frac{12}{5}i + \frac{3}{2}i^{(2)} - \frac{1}{3}i^{(3)} \\
\tilde{P}_4(i,5) &= 1 - 4i + \frac{9}{2}i^{(2)} - \frac{7}{3}i^{(3)} + \frac{7}{12}i^{(4)} \\
\tilde{P}_5(i,5) &= 1 - 6i + \frac{21}{2}i^{(2)} - \frac{28}{3}i^{(3)} + \frac{21}{4}i^{(4)} - \frac{21}{10}i^{(5)}
\end{aligned} \tag{108}$$

where

$$i^{(k)} \equiv i(i-1)...(i-k+1) \tag{109}$$

is the k^{th} fading factorial of i. The actual values of the normalized polynomials for this case

are shown below in vector notation (to four significant digits)

$$\begin{aligned}
P_0 &= [0.4082, \quad 0.4082, \quad 0.4082, \quad 0.4082, \quad 0.4082, \quad 0.4082] \\
P_1 &= [0.5976, \quad 0.3586, \quad 0.1195, \quad -0.1195, \quad -0.3586, \quad -0.5976] \\
P_2 &= [0.5455, \quad -0.1091, \quad -0.4364, \quad -0.4364, \quad -0.1091, \quad 0.5455] \\
P_3 &= [0.3727, \quad -0.5217, \quad -0.2981, \quad 0.2981, \quad 0.5217, \quad -0.3727] \\
P_4 &= [0.1890, \quad -0.5669, \quad 0.3780, \quad 0.3780, \quad -0.5669, \quad 0.1890] \\
P_5 &= [0.0630, \quad -0.3150, \quad 0.6299, \quad -0.6299, \quad 0.3150, \quad -0.0630]
\end{aligned} \tag{110}$$

In the sub-sections that follow, these discrete Legendre polynomials will be used to construct response function boundary conditions for discrete ordinates calculations.

4.1.2 One-Dimensional Expansion

In one-dimensional Cartesian (slab) geometry, a forward mode response function is the solution to the following fixed source discrete ordinates transport equation

$$\frac{\mu_n}{\Delta_i}\Big[R(i_r,g,n) - R(i_\ell,g,n)\Big] + \sigma_g^i R(i,g,n) = \frac{1}{2}\sum_{g'=1}^{G}\left[\left(\sigma_{g'\to g}^i + \frac{1}{k}\chi_g \nu\sigma_{fg'}^i\right)\sum_{n'=1}^{N} w_{n'} R(i,g',n')\right] \tag{111}$$

where isotropic scattering has been shown for simplicity. In the above equation: n and $n' = 1, ..., N$ are ordinate indices; μ_n and w_n are the ordinate direction cosines and weights, respectively; g and $g' = 1, ..., G$ are energy group indices; $i = 1, ..., I$ is the spatial fine-mesh index, while i_r, i_ℓ, and Δ_i denote the right and left node edges and node width; and k is a fixed estimate of the eigenvalue of the larger system in which the coarse-mesh belongs.

Note than an auxiliary relationship (*e.g.*, diamond difference model) is used with the above equation, in practice.

Response functions can be computed using the following set of orthonormal boundary conditions

$$\Gamma_\ell^{hm}(g,n) = \delta_{gh} P_m(n - \tfrac{N}{2}; \tfrac{N}{2} - 1), \tag{112}$$

$$\Gamma_r^{hm}(g,n) = \delta_{gh} P_m(n; \tfrac{N}{2} - 1), \tag{113}$$

given that the quadrature set has the same number of directions with positive and negative μ, and that the ordinates are ordered by increasing μ value. The angular dependence of the boundary conditions is governed by the discrete Legendre polynomials, while the energy groups are treated independently. Adjoint response functions can be computed in a completely straightforward fashion, by setting

$$\Gamma_{\ell}^{\dagger hm} \equiv \Gamma_{r}^{hm}, \tag{114}$$

and

$$\Gamma_{r}^{\dagger hm} \equiv \Gamma_{\ell}^{hm}. \tag{115}$$

A set of coarse-mesh calculations based on this response function set is presented in Section 5.1.

4.1.3 Two-Dimensional Expansion

In two-dimensional Cartesian (x, y) geometry, a forward mode response function is the solution to the following fixed source discrete ordinates transport equation

$$\frac{\mu_n}{\Delta_i}\Big[R(i_E,j,g,n) - R(i_W,j,g,n)\Big] + \frac{\eta_n}{\Delta_j}\Big[R(i,j_N,g,n) - R(i,j_S,g,n)\Big] + \sigma_g^{ij} R(i,j,g,n) = \frac{1}{2}\sum_{g'=1}^{G}\left[\left(\sigma_{g'\to g}^{ij} + \frac{1}{k}\chi_g \nu\sigma_{fg'}^{ij}\right)\sum_{n'=1}^{N} w_{n'} R(i,j,g',n')\right] \tag{116}$$

where isotropic scattering has been again shown for simplicity. In the above equation: $i = 1, ..., I$ and $j = 1, ..., J$ are the spatial fine-mesh intervals in the x and y dimensions, respectively; i_E, i_W, j_N, j_S, denote the east, west, north, and south node edges; Δ_i and Δ_j are the x and y dimension interval widths; and η is the direction cosine with the y axis.

With a product quadrature set in (x, y) geometry (*e.g.*, Abu-Shumays, 1979), the directions within an octant of the unit sphere are formed by a Cartesian product of a set of azimuthal and polar angles. Let this be informally denoted as

$$\left\{\hat{\mathbf{\Omega}}_n;\ n = 1, ..., N_\theta \cdot N_\phi\right\} = \left\{\theta_p;\ p = 1, ..., N_\theta\right\} \times \left\{\phi_q;\ q = 1, ..., N_\phi\right\}, \tag{117}$$

where the polar angles, $\theta_p \in (0, \frac{\pi}{2})$, are defined with respect to the z axis, and the azimuthal angles, $\phi_q \in (0, \frac{\pi}{2})$, are defined with respect to the x axis. The directions are formally

constructed by

$$\hat{\mathbf{\Omega}}_n = \sin\theta_p \cos\phi_q \hat{\mathbf{x}} + \sin\theta_p \sin\phi_q \hat{\mathbf{y}} + \cos\theta_p \hat{\mathbf{z}}, \tag{118}$$

where $\hat{\mathbf{x}}$, $\hat{\mathbf{y}}$, and $\hat{\mathbf{z}}$ are unit vectors in the direction of the Cartesian spatial axes. In addition, the quadrature weights are just a product of the individual polar and azimuthal weights, that is

$$w_n = w_p w_a. \tag{119}$$

Response functions can be computed using boundary conditions that contain a product of discrete Legendre polynomials in the spatial, azimuthal, and polar dimensions. For example, for the southern coarse-mesh boundary

$$\Gamma_S^{hk\ell m}(i,g,n) = \delta_{gh} P_k(i; I-1) P_\ell(q'; 2N_\phi - 1) P_m(p'; N_\theta - 1), \tag{120}$$

where p' and q' denote angular indices that are, for example, ordered by decreasing θ and increasing $\phi \in (0, \pi)$, respectively. Response functions associated with the other coarse-mesh boundaries, as well as adjoint mode response functions, can be formed in a completely analogous fashion. Coarse-mesh calculations based on this response function set are presented in Sections 5.2 to 5.5.

4.1.4 Response Function Shifting

Like the continuous Legendre polynomials, the discrete Legendre polynomials have negative values for orders greater than zero. In principle, the transport equation is linear regardless of the positivity of the boundary conditions. However, it is unconventional to perform fine-mesh calculations with negative-valued boundary conditions, and some codes may not even allow such conditions. In addition, the negative fluxes and sources that are characteristic of the higher-order response functions may disrupt acceleration algorithms. The straightforward solution to this problem is to use the zeroth-order boundary condition to shift the higher-order conditions to every positive values.

For example, on the left boundary of a one-dimensional coarse-mesh, the m^{th} order boundary condition is adjusted to

$$\tilde{\Gamma}_{\ell}^{hm} = \Gamma_{\ell}^{hm} + c\Gamma_{\ell}^{h0}, \tag{121}$$

where $m > 0$ and c is a scalar constant chosen so that $\tilde{\Gamma}_{\ell}^{hm} \geq 0$. From this boundary condition, the response function $\tilde{R}_{\ell}^{hm}$ is generated, where

$$\tilde{R}_{\ell}^{hm} = R_{\ell}^{hm} + cR_{\ell}^{h0}, \tag{122}$$

and the actual m^{th} order response function, R_{ℓ}^{hm}, is computed by subtraction.

4.2 Computer Code Implementation

The implementation of the incident flux response expansion method involves three computational components. First, a fine-mesh code must be employed to compute the response functions as solutions to individual fixed source transport problems. For this dissertation work, the fine-mesh code also serves to generate reference solutions to the benchmark eigenvalue problems so that the accuracy of the new method can be determined. Second, it is convenient to develop a response function generator to automate the process of constructing the response function boundary conditions, executing the fine-mesh code, performing response function shifting, and storing the response data in a convenient format for subsequent calculations. Finally, and most importantly, a new coarse-mesh code must be developed.

The new method was initially implemented for one-dimensional problems. The subsequent application of the method to large, two-dimensional problems necessitated the use and development of separate 2-D codes that were designed to maximize computational speed while keeping memory requirements feasible for execution on desktop PCs (*i.e.*, peak allocation less than 1GB). All codes that were used to perform the numerical calculations presented in Chapter 5 were compiled using Compaq Visual Fortran Professional Edition 6.6.B (commercially available software) on the Microsoft Windows XP Professional operating system. Additional details of the computational components are provided in the following sub-sections.

4.2.1 Fine Mesh Codes

For the purpose of solving one-dimensional fine-mesh discrete ordinates problems, a new code was developed, called SLATE. Though this capability is provided by several existing codes, for example ANISN (Engle, 1967), it was found to be extremely convenient to have a simple and straightforward fine-mesh module during the early stages of development. SLATE solves fixed source and eigenvalue problems using the finite-difference, multigroup, discrete ordinates approximation in one-dimensional slab geometry. No acceleration schemes were implemented, due to the speed with which one-dimensional problems can be solved on modern processors. SLATE was verified by comparing results to those from the ANISN code on three heterogeneous eigenvalue problems (Azmy, 2003), as well as analytical solutions on several pure-absorber and infinite-medium fixed source problems.

For two-dimensional fine-mesh calculations, the discrete ordinates code DORT (Rhoades and Childs, 1988) was used. The version corresponds to that distributed with the DOORS 3.2 package (Radiation Safety Information Computational Center, 1998). The source code was provided by Penn State University (Azmy, 2003), as part of a collaborative NERI project, and contains a minor modification to the original source that corrects an error in the angular flux output. The GIP code (Rhoades and Emmett, 1982), which prepares cross section data for DORT, was also compiled and installed. The DORT test problems included in the DOORS 3.2 package were executed, and the output was verified against original output files.

4.2.2 Response Function Generators

The RFGEN code was developed to generate response functions for one-dimensional problems by driving the SLATE fine mesh code. Gauss-Legendre quadrature constants and the diamond difference flux extrapolation model were used for all response function (as well as reference eigenvalue calculations) presented in Section 5.1. No response function shifting is performed by RFGEN, since SLATE does not use negative flux fix-up or acceleration techniques. The convergence of the fine-mesh calculations was not found to be impeded by negative-valued boundary conditions. The SLATE code contains an option to store

solutions (*e.g.*, response function data) in binary files for subsequent use. Consequently, it not necessary for RFGEN to post-process any computational results.

The RFGEN2 code was developed to drive GIP and DORT to generate response functions for two-dimensional problems. The scaling of the fission source term in Eq. (60) is accomplished by adjusting the neutron production cross sections ($\nu\sigma_f$) that are input to GIP, based on user-input k values. For all response function and reference eigenvalue calculations presented in Sections 5.2 to 5.5, the diamond difference scheme was used. In addition, the product quadrature constants recently published by Abu-Shumays (2001) for two-dimensional (x, y) geometry problems were used, instead of the level-symmetric quadratures distributed with the DORT code. Response function shifting is performed, so that only positive-valued boundary conditions are specified in the DORT calculations. The angular flux binary files output by DORT are post-processed into a more convenient format for the coarse-mesh calculations. The format of the DORT binary files, as well as program code to read the files, were supplied by Penn State (Azmy, 2003).

Default values of all DORT computational options were used, with the following exception. A fission rescaling algorithm is activated by default for fixed source problems containing fissionable material. Since the response function calculations involve a system driven by a source incident on the boundary, fission rescaling tends to largely inhibit convergence. Consequently, this feature was defeated for all response function calculations by setting the input parameter SORMIN to a value of -1.

4.2.3 Coarse Mesh Codes

The REXTRAN and REXTRAN2 codes were developed to solve large, heterogeneous eigenvalue problems using the incident flux response expansion method in one and two-dimensional geometries, respectively. Both variational and non-variational inner and outer iteration algorithms were implemented. The codes also contain a feature to compare the final solution to one stored in a binary file (*e.g.*, a reference solution) so that accuracy of the coarse-mesh results can be obtained in a consistent way. The solution comparison output was verified to be correct (by inspection) for several calculations.

The truncation of the response function expansion is controlled by setting a maximum expansion order in the polar dimension (1-D) or the spatial, angular, and polar dimensions (2-D). Response functions for all possible combinations of the expansion orders less than the maximum order(s) are used. For example, let $R^{k\ell m}$ denote the response function computed using the $\Gamma^{k\ell m}$ boundary condition, as in Eq. (120), associated with one surface of a coarse-mesh in a one-group problem. A forward mode REXTRAN2 calculation with maximum spatial, azimuthal, and polar orders of 2, 1, and 0, respectively, will use the following set of response functions: $\left\{R^{000}, R^{010}, R^{100}, R^{110}, R^{200}, R^{210}\right\}$.

In both coarse-mesh codes, the inner and outer iterations are controlled by conventional iteration limits and convergence criteria. The outer iterations are terminated when the iteration limit is reached or when the eigenvalue estimates satisfy the following convergence criteria

$$\left|k^{(u)} - k^{(u-1)}\right| \leq \epsilon_k, \tag{123}$$

where u is the outer iteration index, and ϵ_k is a user-defined scalar constant. In REXTRAN, the inner iterations are terminated when the limit is reached or (hopefully) when the angular flux estimates satisfy the following convergence criteria

$$\max_{i,g,n} \left| \frac{\psi^{(v)}(i,g,n)}{\psi^{(v-1)}(i,g,n)} - 1 \right| \leq \epsilon_\psi, \tag{124}$$

where: v is the inner iteration index; i, g, and n denote the spatial fine-mesh, group, and ordinate indices, respectively; and ψ represents the node-average angular flux everywhere in the global problem. In two-dimensional problems, this type of convergence criteria is extremely expensive to evaluate, so convergence is defined directly in terms of the expansion coefficients in REXTRAN2, as

$$\max_{i,s,g,m} \frac{\left|c_{is}^{gm(v)} - c_{is}^{gm(v-1)}\right|}{\sqrt{\sum_m \left(c_{is}^{gm(v-1)}\right)^2}} \leq \epsilon_c, \tag{125}$$

where i, s, g, and m denote the coarse-mesh, coarse-mesh boundary, group, and expansion order indices, respectively. This convergence measure has been defined so that a change in a coefficient is scaled proportionately to its contribution to the within-group flux incident

on the coarse-mesh boundary. This prevents large changes in very small coefficients, which have little impact on the solution, from thwarting convergence. For the problems studied in Sections 5.2 to 5.5, it has been verified that reducing ϵ_c from 1×10^{-5} to a lower value results in differences in the eigenvalue and edit region fission densities of less than 0.001%.

The coarse-mesh codes use routines from the IMSL Math library, distributed with Compaq Visual Fortran Professional Edition 6.6.B, to solve the finite element equations. In particular, the LFCRG routine is used to compute the LU decomposition of the finite element matrices for each coarse-mesh type. This routine also produces an estimated inverse condition number and issues a warning if the matrix is singular or near-singular (*i.e.*, the inverse condition number is less than or close to the machine precision). A solution to the equations is generated by passing the decomposed matrix and right-hand side vector to the LFSRG routine, which directly solves the equations without iterative refinement. All computations are performed in single-precision (32-bit) arithmetic for speed.

CHAPTER V

NUMERICAL RESULTS

In this chapter, the implemented incident flux response expansion method is tested on several one and two-dimensional reactor benchmark problems. The accuracy of the new method is determined through comparisons to fine-mesh eigenvalue solutions that have been generated by the same codes used to compute the response functions. An important question to be answered by the numerical studies in this chapter is: how should the computational parameters be chosen to achieve accurate results in the least amount of time? Naturally, it is an extremely difficult (if not impossible) task to find a general answer to this question. However, an extensive study of the coarse-mesh results versus maximum response expansion orders and method options has been performed with each problem presented in this Chapter. The complete coarse-mesh results are tabulated in Appendix B.

The quantities of interest in the numerical calculations are the eigenvalues and edit region fission rates. An edit region is defined as a set of fine-meshes within a coarse-mesh that contain a fissionable material. The fission rate within an edit region k is calculated by

$$F_k \equiv \sum_{i,j \in k} \sum_g V_{ij} \sigma_{fg}^{ij} \phi(i,j,g), \tag{126}$$

where: V_{ij} denotes the volume of the spatial fine-mesh in the i^{th} and j^{th} x and y-dimension intervals, respectively; σ_{fg} is the fission cross section in group g; and ϕ is the scalar flux density. The summations are performed over the spatial fine-meshes within the edit region and all energy groups. The average fission rate fractional difference over a collection of edit regions is hereafter defined as

$$\text{Avg. FD} \equiv \frac{1}{K} \sum_k \frac{\left| F_k^{CM} - F_k^{FM} \right|}{F_k^{FM}}, \tag{127}$$

where K denotes the number of edit regions, and superscripts "CM" and "FM" denote the coarse-mesh and reference fine-mesh fission rates, respectively. A maximum fission rate

fractional difference is also defined as

$$\text{Max. FD} \equiv \max_k \left(\frac{F_k^{CM} - F_k^{FM}}{F_k^{FM}} \right). \tag{128}$$

The average and maximum differences will correspond to all of the edit regions in the problem being studied, unless otherwise specified. For the two-dimensional problems, the average and maximum values will also be shown for each coarse-mesh in a map of the system.

For a given benchmark problem, the same quadrature set and spatial fine-mesh (per coarse-mesh type) were used in the reference eigenvalue and response function calculations. All fine and coarse-mesh eigenvalue calculations were initiated with a guess of $k = 1$, as well as a uniform flux distribution or uniform expansion coefficients, along with an eigenvalue convergence criteria of 1×10^{-6}. The fixed source response function calculations were initiated with zero flux guesses, and a user-specified fission source scaling factor. In the 1-D calculations, a flux convergence criteria of 1×10^{-6} was used, whereas the 2-D calculations were based on a criteria of 1×10^{-5} for the flux, fission source, and expansion coefficient convergence. A limit of 4 inner iterations per group per outer iteration was used in all DORT fine-mesh calculations. For the coarse-mesh calculations, the optimal inner iteration limit varies significantly with the method option (discussed in the following section) as well as problem size. Consequently, different limits were used in different problems.

All calculations described in the chapter were performed on a desktop PC with an AMD Athlon XP 2800+ (2.08GHz) processor with 1GB of DDR400 RAM under the Microsoft Windows XP Professional operating system.

5.1 Method Options

To determine the relative worth of the variational and non-variational techniques that were developed in this dissertation work, the benchmark problems are solved using three method options. Each option is given an abbreviation, for convenience. The options considered are:

NV: non-variational iterations. Coefficients are computed by a straightforward expansion of the fluxes incident from neighboring coarse-meshes, and the eigenvalue is computed according to Eq. (49). Only the forward mode problem is solved.

RQ: non-variational inner iterations with variational outer iterations. Both forward and adjoint inner iterations are performed, and the eigenvalue is computed using the Rayleigh quotient in Eq. (106).

V: variational iterations. Since the solution of the finite element equations is computationally expensive, non-varational forward and adjoint inner iterations are performed until the Rayleigh quotient has converged (as in the **RQ** option). At that point, one additional set of inner iterations is performed by solving the finite element equations. No additional update of the eigenvalue is performed, since this has been found to lead to only negligible differences from the converged Rayleigh quotient.

A concise notational convention will also be used to denote the product quadrature orders and the maximum response expansion orders used in the two-dimensional calculations. The doublet notation (N_ϕ, N_θ) will be used to denote a product quadrature set from (Abu-Shumays, 2001) with N_ϕ and N_θ azimuthal and polar directions, respectively, per octant of the unit sphere. A total of $4 \cdot N_\phi \cdot N_\theta$ directions are treated in a two-dimensional calculation, due to the symmetry about the z-axis. The triplet notation $(M_{xy}, M_\phi, M_\theta)$ will be used to denote a coarse-mesh calculation with maximum spatial, azimuthal, and polar expansion orders of M_{xy}, M_ϕ, and M_θ, respectively. Note that all possible combinations of the response orders less than the maximum orders are used, so that a $(M_{xy}, M_\phi, M_\theta)$ calculation uses $(M_{xy}+1)\cdot(M_\phi+1)\cdot(M_\theta+1)$ response functions per group per coarse-mesh boundary per coarse-mesh type. The inherent symmetries of a coarse-mesh geometry are fully exploited to reduce the total number of response function calculations.

5.2 One Dimensional Benchmarks

The new coarse-mesh method was initially evaluated on the set of one-dimensional benchmark problems published in (Ilas and Rahnema, 2003). A total of four coarse-mesh

types, each containing six material regions are used to construct three core configurations with varying degrees of heterogeneity. Four materials characterized by two-group cross sections are used in the problems. Each configuration is composed of seven fuel assemblies of two unique types arranged in an alternating pattern. The coarse-mesh model and core configurations are shown in Figures 9 and 10 in Appendix A.

5.2.1 Reference Solution

The spatial fine-mesh was chosen so that each water and fuel region was divided into two and four meshes, with uniform widths of 0.579cm and 0.83205cm, respectively. Therefore, each coarse-mesh model and core configuration contains 20 and 140 spatial fine-meshes. Four edit regions per coarse-mesh were considered, corresponding to the four 3.321cm width fuel regions. A S_{32} Gauss-Legendre quadrature set was used to generate SLATE reference solutions. The details of the reference calculations are shown in the table below.

Table 1: One-Dimensional Benchmark Reference Calculations

	Core 1	Core 2	Core 3
Eigenvalue	1.258247	1.007066	0.805372
Total Inner / Outer Iterations	1825 / 57	1943 / 58	2424 / 74
Actual Flux / k Convergence	9.4E-7 / 0.0E+0	9.8E-7 / 0.0E+0	9.4E-7 / 1.2E-7
Computational Time (sec)	0.44	0.47	0.58

Since SLATE contains no acceleration techniques, a large number of inner and outer iterations were performed to converge the solutions. A limit of 20 inner iterations per group per outer iteration was used. The optimal limits were not studied, due to the speed with the calculations converge in real time.

5.2.2 Coarse Mesh Results

Forward and adjoint mode response functions were computed for each of the four coarse-mesh types with the parameters shown in Table 2. A study of the coarse-mesh results versus expansion order and method for each of the three configurations was conducted.

The complete results are shown in Figure 17 in Appendix B. The results for a 0^{th} order polar expansion versus method option are shown in Tables 3 and 4. An additional study was performed with the **RQ** method to determine if the accuracy of the results is significantly affected by the quadrature order used to solve the problem. Fine and coarse-mesh results were generated for the S_{16}, S_{64} , and S_{128} quadrature sets. It was found that the quadrature order had a negligible effect on the coarse-mesh eigenvalue and fission rate results.

Table 2: One-Dimensional Response Function Parameters

Maximum Polar Order	5^{th}
k Grid	0.7, 0.8, 0.9, 1.0, 1.1, 1.2, 1.3
Total Response Functions	672
Total Computational Time (sec)	126.8

Table 3: One-Dimensional Benchmark 0^{th} Order Coarse-Mesh Results Summary I

	NV Method		
Core	k Diff.	Avg. FD	Max. FD
1	0.113%	0.610%	-1.843%
2	0.247%	1.071%	-2.499%
3	0.422%	1.807%	-3.872%

Table 4: One-Dimensional Benchmark 0^{th} Order Coarse-Mesh Results Summary II

	RQ Method			**V** Method	
Core	k Diff.	Avg. FD	Max. FD	Avg. FD	Max. FD
1	0.001%	0.648%	-1.861%	0.357%	-1.296%
2	-0.004%	1.142%	-2.529%	0.458%	-1.091%
3	-0.019%	2.134%	-4.187%	0.796%	-2.129%

5.2.3 Discussion

The heterogeneity of the problems increases significantly from core configuration 1 to configuration 3. Nonetheless, it is clear that a first-order expansion provides excellent

accuracy for all three problems, regardless of the method option used. Increasing the expansion order improves the results to an asymptotic limit that is non-zero because of the interpolation error in the response functions. In each case, the residual interpolation error is much less than 1%.

The **RQ** method substantially improves the eigenvalue accuracy in the 0^{th} and 1^{st} order expansions. Beyond 1^{st} order, the eigenvalue errors are very small, regardless of the method used. Relatively small changes in the fission rate accuracy occur with the **RQ** method versus the **NV** method. Since the non-variational inner iteration technique is used in both cases, this is entirely a result of changing the eigenvalue estimate with which the response functions are computed. However, improving the eigenvalue does not guarantee improvements in the fission rates, and in many cases the fission rate accuracy is slightly worsened.

The **V** method improves the average and maximum fission rate errors for every expansion order, except 1^{st} order. The reasons for this behavior are not obvious. However, the asymptotic fission rate errors (approached as the expansion order is increased) are an order of magnitude smaller with the **V** method. It is interesting to note that the conditioning of the finite element matrices degrades as the expansion order increases (see Figure 17). As a result, the actual convergence of the inner iterations deteriorates with increasing expansion order. In any case, the finite element method is very stable about the exact solution, for each of the three one-dimensional problems.

5.3 Modified Henry-Worley Benchmark

The first two-dimensional problem to be studied is a slight variation of the Henry-Worley BWR benchmark problem presented in (Smith, 1980). The problem is a quarter-core configuration containing three coarse-mesh types. Each coarse-mesh type contains two material regions, and a total of three materials (fuel, coolant, and control material) are used in the problem. The coarse-mesh model and its dimensions are illustrated in Figure 11 in Appendix A. The materials in the original problem were characterized by two-group diffusion theory cross sections. The benchmark is easily converted to a transport problem

by defining the total cross section as

$$\sigma_{tg} \equiv \frac{1}{3D_g}, \tag{129}$$

where D_g is the diffusion coefficient in group g. In addition, zero flux and zero net current boundary conditions are replaced by vacuum and specular reflective conditions.

The original problem was modified by expanding the full core from a 7×7 to an 8×8 system of coarse-meshes. In other words, the modified quarter-core problem does not contain any half or quarter coarse-meshes, leading to fewer coarse-mesh types that must be considered. The core configuration of the modified problem is presented in Figure 12. The homogeneous fuel material within each coarse-mesh is divided into four equal-volume edit regions, as illustrated by the dashed lines in Figure 11.

This benchmark problem serves as an excellent starting point for evaluating the two-dimensional method, due to its simple composition. With the material interfaces well separated from the coarse-mesh boundaries (except at the core-reflector interface), it is expected that a relatively low-order response function expansion should lead to accurate results. On the other hand, the configuration is quite small (32×32 cm), so the flux shape is dominated by neutron leakage from the core (*i.e.*, substantial flux gradients exist).

5.3.1 Reference Solution

Since the thermal mean free path is roughly 1cm in this problem, a spatial mesh with a uniform node size of 0.5cm $\times$ 0.5cm was used to model the core. Each coarse-mesh contains a 16×16 fine-mesh, and the overall problem is represented on a 64×64 spatial grid. A $(2, 4)$ quadrature set was used to generate a reference DORT solution to this problem. The details of the reference calculation are shown in the table below.

A comparison was made with an additional reference calculation using a $(4, 9)$ quadrature in order to demonstrate that the $(2, 4)$ solution is reasonably close to that asymptotically approached by increasing the number of directions. The comparison is summarized in the table below.

Table 5: Modified Henry Worley (MHW) Reference Calculation

Eigenvalue	0.821647
Total Inner / Outer Iterations	81 / 17
Actual Flux / k Convergence	7.7E-6 / 0.0E+0
Computational Time (sec)	2.0

Table 6: MHW Reference Calculation Comparison

Eigenvalue Difference	0.002 %
Average FR Difference	0.012 %
Maximum FR Difference	0.049 %

It is worth noting that the eigenvalue for the (unmodified) Henry-Worley diffusion problem, as calculated by the QUANDRY nodal code using a 6×6 non-uniform spatial fine-mesh per coarse-mesh, was reported to be 0.80399 (Smith, 1980). The eigenvalue for the unmodified problem is lower than that of the modified one, which is expected due to its smaller size.

5.3.2 Coarse Mesh Results

Forward and adjoint mode response functions were computed for each of the three coarse-mesh types with the parameters shown in Table 7. Since coarse-mesh type W (water node) does not contain any fissionable material, the fission source scaling factor is irrelevant, and only 72 response functions were generated (compared to 288 for coarse-mesh types A and B). Note that the total computational time shown in the table below includes not only the calculation of the responses by DORT, but also the time required to post-process the results into a more convenient and consolidated binary format.

The inner iteration limit used in fine-mesh discrete ordinates codes has a significant impact on the overall computational efficiency of a calculation. Performing too many inner iterations while the eigenvalue and fission source distribution are far from converged is wasteful. It is expected that this is also the case for the coarse-mesh method. However, the implicit fission source approach is quite difference from the conventional power iteration

Table 7: MHW Response Function Parameters

Maximum Spatial Order	2^{nd}
Maximum Azimuthal Order	2^{nd}
Maximum Polar Order	1^{st}
k Grid	0.7, 0.8, 0.9, 1.0
Total Response Functions	648
Total Computational Time (sec)	86.2

method for solving eigenvalue problems. A study of the total number of iterations and computational time required to solve the modified Henry-Worley problem as a function of the inner iteration limit (per outer iteration) was conducted using a (0,0,0) expansion. The results, which are shown in Table 8, were not found to be significantly affected by the response expansion order. For the **RQ** method, only the number of forward mode inner iterations are shown, however the computational time includes the solution of the global adjoint problem.

Table 8: MHW Inner Iteration Limit Study

	NV Method		**RQ** Method	
Limit	Inner / Outer Itns.	Time (sec)	Inner / Outer Itns.	Time (sec)
15	130 / 15	0.11	48 / 4	1.34
10	96 / 15	0.11	**38 / 4**	**1.31**
5	**57 / 15**	**0.11**	42 / 9	2.94
4	57 / 18	0.11	42 / 11	3.62
3	54 / 20	0.11	-	-

It is not surprising that the optimal inner iteration limit depends on the method type. The computation of the variational estimate of k is far more expensive than the non-variational estimate. Consequently, the relative cost of an inner versus an outer iteration is significantly different with the **RQ** method. Also, the Rayleigh quotient requires far fewer outer iterations to converge than the **NV** method, as expected. The **V** method was not included in this study, since the finite element inner iterations are initiated with converged

RQ method results. The limit on the finite element iterations is set high so that convergence is achieved without spending any time updating the eigenvalue. All **NV** and **RQ** method results shown in the remainder of this sub-section are based on a limit of 5 and 10 inner iterations, respectively.

A thorough study of the coarse-mesh results versus expansion order and method was conducted. Calculations with eighteen different maximum expansion order combinations, covering the range from $(0, 0, 0)$ to $(2, 2, 1)$, were performed with each of the methods. The complete comparison of the coarse-mesh and reference fine-mesh results is shown in Figure 18 in Appendix B.

5.3.3 Discussion

A quick examination of Figure 18 indicates that increasing the number of response functions does not guarantee improved estimates of the quantities of interest, as was generally the case with the one-dimensional problems. In fact, this is characteristic of nearly all of the two-dimensional problems studied in this dissertation work. It should be the case the representation of the angular flux entering the coarse-mesh is improved (or at least not worsened) by increasing the maximum expansion orders. However, each dimension has a different relative importance in different regions of the problem. Moreover, there is no guarantee that reducing errors in the incident fluxes reduces the errors in the quantities of interest. Low order expansions may benefit from fortuitous error cancellations, especially when the edit regions are relatively large.

To examine the impact of varying the maximum expansion order in an individual dimension an average was calculated of the differences associated with all of the calculations shown in Figure 18 having a given maximum expansion order in a given dimension. The results are shown in Tables 9 and 10.

For all method options, the eigenvalue accuracy is strongly dependent on the maximum spatial expansion order. This is not unexpected, since neutron leakage has a large impact

Table 9: MHW Coarse Mesh Results Summary I

		NV Method		
Dimension	Max. Order	k Diff.	Avg. FD	Max. FD
Spatial	0	2.38%	1.60%	4.27%
	1	1.72%	0.61%	2.16%
	2	1.66%	0.79%	2.62%
Azimuthal	0	2.61%	1.44%	4.86%
	1	1.65%	0.81%	2.23%
	2	1.50%	0.75%	1.97%
Polar	0	2.06%	1.04%	3.21%
	1	1.78%	0.96%	2.83%

Table 10: MHW Coarse Mesh Results Summary II

		RQ Method			**V** Method	
Dimension	Max. Order	k Diff.	Avg. FD	Max. FD	Avg. FD	Max. FD
Spatial	0	0.61%	1.66%	4.73%	0.99%	3.58%
	1	0.04%	0.57%	1.90%	0.41%	1.19%
	2	0.06%	0.70%	2.41%	0.38%	1.41%
Azimuthal	0	0.22%	1.40%	4.59%	0.65%	2.43%
	1	0.23%	0.78%	2.38%	0.81%	2.55%
	2	0.26%	0.75%	2.08%	0.19%	0.62%
Polar	0	0.23%	1.01%	3.19%	0.51%	1.67%
	1	0.24%	0.95%	2.84%	0.79%	2.95%

on the neutron balance in a small configuration, and causes large flux gradients that are not well represented by a constant or linear spatial shape along the coarse-mesh boundaries. For the **NV** method, the eigenvalue accuracy is also strongly dependent on the azimuthal expansion order.

As expected, the Rayleigh quotient substantially improves the eigenvalue accuracy over the **NV** method in every calculation. The most dramatic example is the $(1, 0, 0)$ calculation, in which the eigenvalue error is reduced from 3.64% to 0.10%. On the average, the **RQ** method does not substantially influence the fission rate accuracy. In cases where the **NV** method eigenvalue errors are large, the **RQ** method has a greater impact on the fission rates. However, improving the eigenvalue estimate at which the response functions are computed, does not guarantee improvements in the fission rates.

The spatial and azimuthal dimensions have a significant impact on the fission rate accuracy. Increasing the maximum expansion order in either of these dimensions from 0^{th} to 1^{st} order, significantly improves the fission rate results, on the average. However, it is interesting to note that increasing the maximum spatial order from 1^{st} to 2^{nd} order reduces fission rate accuracy, on the average. The (2,0,0) and (2,0,1) calculations are the main contributors to this effect. The remaining 2^{nd} spatial order cases performed much better.

In 10 of the 18 cases, the **V** method significantly improves the fission rate accuracy. In one case the fission rate accuracy was slightly reduced, and in seven cases the method failed to converge to the correct solution. Consequently, the **V** method results are not as complete as the other methods, so the average differences in Tables 9 and 10 above were computed over a smaller number of calculations. The root cause of the non-convergence of the method was not isolated. It does not seem likely that the accuracy of individual response functions is the culprit. For example, the **V** method converges as expected in the $(1, 0, 0)$ and $(0, 1, 0)$ cases, but does not converge in the $(1, 1, 0)$ case, which contains a combination of only the response functions used in cases that did converge. In addition, the $(1, 2, 0)$, $(2, 1, 0)$, and $(2, 2, 0)$ calculations converged, which contain all of the response functions used in the $(1, 1, 0)$ case.

The singular values of the finite element coefficient matrices were computed for the unconverged cases, and it was determined that matrices were neither numerically singular nor close to singular. Using double-precision (64-bit) arrays to store the finite element matrix, and using double-precision IMSL routines to solve the equations had absolutely no impact on the solution. This may, however, be due to the fact that the DORT code computes response functions in single-precision arithmetic. An additional attempt to achieve a converged solution in these cases was made by implementing an iterative refinement technique as follows. Since the **V** method is initiated with a converged eigenvalue and expansion coefficients from the **RQ** method, the variational coefficients can be computed as a correction to the non-variational coefficients in the first iteration. Let $\hat{\mathbf{A}}$ be the finite element coefficient matrix for a given coarse-mesh type, let $\hat{\mathbf{x}}$ be the vector of the expansion coefficients to be determined, and let $\hat{\mathbf{b}}$ be the right-hand side vector. The non-variational coefficients $(\hat{\mathbf{x}} + \boldsymbol{\delta}\hat{\mathbf{x}})$ satisfy the equation

$$\hat{\mathbf{A}}(\hat{\mathbf{x}} + \boldsymbol{\delta}\hat{\mathbf{x}}) = \hat{\mathbf{b}} + \boldsymbol{\delta}\hat{\mathbf{b}}. \tag{130}$$

Since $\hat{\mathbf{A}}$, $(\hat{\mathbf{x}} + \boldsymbol{\delta}\hat{\mathbf{x}})$, and $\hat{\mathbf{b}}$ are known quantities, it is straightforward to calculate the residual

$$\boldsymbol{\delta}\hat{\mathbf{b}} = \hat{\mathbf{A}}(\hat{\mathbf{x}} + \boldsymbol{\delta}\hat{\mathbf{x}}) - \hat{\mathbf{b}}, \tag{131}$$

and compute the first-order correction to the non-variational coefficients by solving

$$\hat{\mathbf{A}}\boldsymbol{\delta}\hat{\mathbf{x}} = \boldsymbol{\delta}\hat{\mathbf{b}} \tag{132}$$

for $\boldsymbol{\delta}\hat{\mathbf{x}}$. It was hoped that the non-variational coefficients would be close enough to the true solution of the finite element equations (variational coefficients) that this procedure would find the correct solution. Unfortunately, this technique was found to have exactly the same behavior as encountered before.

Figure 5 shows the average and maximum edit region fission rate errors within each coarse-mesh (as arranged in Figure 12) for the $(0, 0, 0)$ and $(2, 2, 1)$ **NV** method calculations. The normalized reference fission rates are also shown. The shaded blocks represent the controlled assemblies. It can be seen that the errors increase with increasing distance from the center of the core, as expected.

		0.627 3.295% (5.334%) 0.231% (0.254%)
	0.947 1.986% (3.683%) 0.194% (0.197%)	**0.926** 1.971% (3.439%) 0.206% (0.269%)
1.184[a] 1.279% (2.162%)[b] 0.043% (0.077%)[c]	**1.317** 1.367% (2.649%) 0.083% (0.115%)	**0.878** 1.843% (3.214%) 0.233% (0.297%)

[a] normalized reference fission rate
[b] (0,0,0) calculation: Avg. FD (Max. FD)
[c] (2,2,1) calculation: Avg. FD (Max. FD)

Figure 5: MHW Coarse-Mesh Results

5.4 CISE Benchmark

The CISE BWR benchmark problem presented in (Smith, 1980) is a large quarter-core problem containing five coarse-mesh types. Each coarse-mesh contains three material regions, and a total of four materials (fresh fuel, depleted fuel, coolant, and control material) with two-group cross sections are used in the problem. The coarse-mesh model and core configuration are illustrated in Figures 13 and 14 in Appendix A. This benchmark was converted to a transport problem in same way as the modified Henry-Worley problem discussed in the previous section.

This benchmark problem represents a significant challenge, due to its large size and the presence of several control blades. Moreover, the blades run along the coarse-mesh boundaries, causing a large, localized perturbation to the flux shape. This is precisely the location at which the approximations in the incident flux response expansion method come into play.

5.4.1 Reference Solution

In this problem, the thermal mean free path is roughly 1cm, except in the control material where it is only 0.45cm. Consequently, a non-uniform spatial mesh was used in this problem. In the water gap and blade regions, a mesh width of 0.25cm was used in the transverse direction, whereas mesh-widths of 0.25 and 0.5cm were used in the opposite spatial dimension. To be more specific, the fine-mesh widths in each dimension were chosen as $\{6 \times 0.25\text{cm}, 24 \times 0.5\text{cm}, 6 \times 0.25\text{cm}\}$, so that each coarse-mesh contains a non-uniform 36×36 spatial fine mesh. The homogeneous fuel material within each coarse-mesh was assigned a single edit region.

The CISE problem is defined so that the outer boundary of the system approximates an overall circular shape. The REXTRAN2 code, however, was written to solve coarse-mesh problems that are an overall rectangular shape. As a result, an additional coarse mesh type (X) was added. Naturally X contains no material, so this is equivalent to extending the vacuum boundary condition. Since response functions for a vacuum node can be computed very quickly, the scope of the problem is not significantly affected. In this case, the overall problem is a 9×9 array of coarse-meshes, and a 324×324 array of fine-meshes.

Five quadrature sets were to used to generate DORT reference solutions, ranging from a $(1, 1)$ to a $(4, 9)$ quadrature. The calculation with the $(4, 9)$ set serves as a reference to which the other calculations were compared, as shown in the table below.

Table 11: CISE Reference Calculation Comparison

Quadrature	$(1, 1)$	$(1, 3)$	$(2, 5)$	$(3, 7)$
Eigenvalue Difference	0.368%	0.239%	0.000%	0.000%
Average FR Difference	3.163%	1.774%	0.010%	0.005%
Maximum FR Difference	-9.448%	-4.923%	0.039%	0.010%

Calculations with very low order quadrature sets were performed in order to demonstrate that the transport effects in this problem have a substantial impact on the results. The

most efficient set is the $(2, 5)$ quadrature, which was used for all subsequent calculations. The details of the final reference calculation are shown in the table below.

Table 12: CISE $(2, 5)$ Reference Calculation

Eigenvalue	0.952678
Total Inner / Outer Iterations	294 / 33
Actual Flux / k Convergence	1.9E-5 / 1.9E-6
Computational Time (sec)	240.3

It is worth noting that the eigenvalue, as calculated by the QUANDRY nodal code using a 8×8 non-uniform spatial fine-mesh per coarse-mesh, was reported to be 0.95240 (Smith, 1980).

5.4.2 Coarse Mesh Results

Forward and adjoint mode response functions were computed for each of the six coarse-mesh types with the parameters shown in Table 13. Coarse-mesh types W and X do not contain any fissionable material, so the k grid is irrelevant. The uncontrolled coarse-mesh types have quarter symmetry, whereas the controlled coarse-meshes have only diagonal symmetry. As a result, twice the number of response functions have to be computed for the controlled coarse-meshes.

Table 13: CISE Response Function Parameters

Maximum Spatial Order	2^{nd}
Maximum Azimuthal Order	2^{nd}
Maximum Polar Order	1^{st}
k Grid	0.9, 1.0
Total Response Functions	864
Total Computational Time (sec)	934.0

An inner iteration limit study was performed, as with the modified Henry-Worley problem, using a (0,0,0) expansion. A much larger number of inner iterations was found to be optimal for the CISE problem. For the **NV** method, a limit of 20 inner iterations per outer

iteration was found to be the most efficient, while a limit of 35 iterations was best for the **RQ** method. These limits were used in all coarse-mesh calculations for this problem.

A thorough study of the coarse-mesh results versus expansion order and method was conducted, in the same fashion as the Henry-Worley problem. The complete comparison of the coarse-mesh and reference fine-mesh results is shown in Figure 19 in Appendix B.

5.4.3 Discussion

To examine the impact of varying the maximum expansion order in an individual dimension an average was calculated of the differences associated with all of the calculations shown in Figure 19 having a given maximum expansion order in a given dimension. The results are shown in Tables 14 and 15.

Table 14: CISE Coarse Mesh Results Summary I

		NV Method		
Dimension	Max. Order	k Diff.	Avg. FD	Max. FD
Spatial	0	1.47%	1.57%	4.34%
	1	0.30%	3.61%	8.99%
	2	0.44%	1.48%	4.37%
Azimuthal	0	0.89%	3.61%	9.27%
	1	0.70%	1.61%	4.57%
	2	0.62%	1.44%	3.42%
Polar	0	0.79%	2.25%	6.12%
	1	0.68%	2.19%	5.69%

As with the modified Henry-Worley problem, the eigenvalue errors are significant with a 0^{th} order spatial expansion, on the average. The azimuthal and polar orders do not have a large impact on the eigenvalue in this problem. The **RQ** method is successful at achieving large increases in eigenvalue accuracy for all expansion orders.

The fission rate accuracy is strongly affected by the azimuthal expansion order. On the average, the 0^{th} order expansion leads to large maximum fission rate errors, which can be recovered by increasing the azimuthal order. Surprisingly, the 1^{st} order spatial expansion

Table 15: CISE Coarse Mesh Results Summary II

		RQ Method			**V** Method	
Dimension	Max. Order	k Diff.	Avg. FD	Max. FD	Avg. FD	Max. FD
Spatial	0	0.63%	1.51%	4.67%	1.15%	3.38%
	1	0.03%	3.76%	9.67%	3.06%	6.90%
	2	0.09%	1.76%	5.70%	-	-
Azimuthal	0	0.26%	3.78%	10.73%	2.62%	6.36%
	1	0.26%	1.73%	5.10%	1.84%	3.75%
	2	0.24%	1.53%	4.21%	0.61%	1.27%
Polar	0	0.27%	2.41%	6.99%	2.19%	5.13%
	1	0.24%	2.28%	6.37%	1.88%	4.35%

also leads to large fission rate errors – larger than either the 0^{th} or 2^{nd} order expansions. One exception is the $(1, 2, 1)$ calculation, which leads to an average and maximum fission rate error of 1.96% and -4.14%, respectively. The remainder the 1^{st} order spatial calculations lead to larger fission rate errors. The worst is the $(1, 0, 0)$ calculation, which has a maximum error of -14.92%. The detailed results show a sensitive spatial-angular interaction for the 1^{st} and 2^{nd} order spatial expansions, that is not present with the 0^{th} order spatial expansion. Unfortunately, the consequence is that increasing the spatial order only leads to increased fission rate accuracy if either 1^{st} or 2^{nd} order angular expansions are used.

The numerical difficulties associated with the **V** method are prevalent in the CISE problem. Only 4 of 18 cases converged to the correct solution; the others diverged toward obviously incorrect solutions characterized by enormous positive and negative fluxes. In addition, the four cases were only able to be converged by deactivating the finite element treatment for the W (water) and X (void) coarse-meshes in a sort of hybrid variational/non-variational inner iteration technique. For the cases that did converge, the **V** method results are as expected – the fission rate errors are substatially improved compared to the **NV** or **RQ** methods.

Figure 6 shows the average and maximum edit region fission rate errors within each

coarse-mesh (as arranged in Figure 14) for the $(0, 0, 0)$ and $(2, 2, 1)$ **NV** method calculations. The normalized reference fission rates are also shown. The shaded blocks represent the controlled assemblies. The $(0, 0, 0)$ calculation exhibits a significant tilt in the average fission rate difference, which is negative at the center of the core, and positive at the periphery. The same tilt is present for the $(2, 2, 1)$ calculation, but with a much smaller magnitude.

					0.641 3.416% 0.179%		
				0.691 1.374% 0.040%	**0.782** 3.621% 0.087%	**0.615** 5.377% 0.287%	
			0.901 -1.221% -0.253%	**0.733** 0.223% -0.000%	**0.869** 2.033% 0.076%	**0.846** 3.268% 0.224%	
		0.943 -2.542% -0.358%	**1.095** -1.146% -0.318%	**1.281** 0.006% -0.086%	**1.096** 0.713% 0.418%	**1.040** 2.527% 0.607%	**0.730** 3.210% 0.445%
	0.941 -3.786% -0.759%	**0.843** -3.251% -0.416%	**1.283** -1.702% -0.470%	**1.214** -0.702% -0.011%	**1.393** -0.096% 0.361%	**1.067** 1.112% 0.583%	**0.852** 2.526% 0.520%
0.940[a] -4.202%[b] -0.834%[c]	**1.084** -3.265% -0.977%	**1.262** -2.748% -0.827%	**0.866** -2.845% -0.407%	**1.040** -1.468% -0.047%	**1.232** -0.339% 0.235%	**1.302** 0.732% 0.437%	**0.946** 1.704% 0.568%

[a] normalized reference fission rate
[b] (0,0,0) calculation: Avg. FD
[c] (2,2,1) calculation: Avg. FD

Figure 6: CISE Coarse-Mesh Results

5.5 HAFAS Benchmark

The HAFAS BWR benchmark problem developed by (Smith, 1980) is another large quarter-core problem, which contains nine coarse-mesh types. Each coarse-mesh contains

five material regions, and a total of fifteen materials with two-group cross sections are used in the problem. The coarse-mesh model and core configuration are illustrated in Figures 15 and 16 in Appendix A. This benchmark was converted to a transport problem in the same way as the modified Henry-Worley and CISE problems discussed previously.

This benchmark is of a similar nature to the CISE problem studied in the previous section. However, the HAFAS benchmark is far more heterogeneous. The core contains not only controlled and uncontrolled coarse-meshes, but also assemblies with voided coolant. In addition, each coarse-mesh contains three different fuel materials, and the control blades are substantially thicker (0.8cm) than in the CISE problem (0.5cm).

5.5.1 Reference Solution

A non-uniform spatial mesh was used in this problem. The fine-mesh widths in each dimension were chosen as $\{2\times 0.2\text{cm}, 3\times 0.32333\text{cm}, 32\times 0.4075\text{cm}, 3\times 0.3\text{cm}\}$, so that each coarse-mesh contains a non-uniform 40×40 spatial fine mesh. Sixteen edit regions were assigned to each coarse-mesh, corresponding to the sixteen fuel regions shown in Figure 15. The overall core problem is a 10×10 array of coarse-meshes, and a 400×400 array of fine-meshes. A total of 1,232 edit regions, each with a dimension of 3.26cm×3.26cm, are modeled in the core.

As with the CISE problem, five quadrature sets were to used to generate DORT reference solutions, ranging from a $(1, 1)$ to a $(4, 9)$ quadrature. The calculation with the $(4, 9)$ set serves as a reference to which the other calculations were compared, as shown in the table below.

Table 16: HAFAS Reference Calculation Comparison

Quadrature	$(1,1)$	$(1,3)$	$(2,5)$	$(3,7)$
Eigenvalue Difference	0.268%	0.158%	0.002%	0.000%
Average FR Difference	2.801%	1.808%	0.027%	0.031%
Maximum FR Difference	-10.212%	4.947%	-0.091%	-0.062%

Calculations with very low order quadrature sets were performed in order to demonstrate that the transport effects in this problem have a substantial impact on the results, as with the CISE problem. The most efficient set is the $(2, 5)$ quadrature, which was used for all subsequent calculations. The details of the final reference calculation are shown in the table below.

Table 17: HAFAS $(2, 5)$ Reference Calculation

Eigenvalue	1.042766
Total Inner / Outer Iterations	879 / 125
Actual Flux / k Convergence	-1.3E-4/ 3.4E-7
Computational Time (min)	19.71

The DORT calculation did not converge before reaching the outer iteration limit of 125 iterations. It was determined that the diamond difference approximation was the culprit, since a weighted difference calculation converged well before reaching the limit. Diamond difference scalar flux solutions at 50 and 100 outer iterations were compared, and it was determined that the low-magnitude fluxes in the north-eastern corner of the problem (*i.e.*, in the reflector near the vacuum boundary) did not agree within the convergence criterion. It is likely that negative angular fluxes that were observed in that region cause oscillations in the scalar fluxes at, or very near, the boundary. Within the core, where the edit regions are present, the two solutions agreed to within the expected convergence value. Consequently, the reference solution was deemed acceptable.

It is worth noting that the eigenvalue, as calculated by the QUANDRY nodal code using a 7×7 non-uniform spatial fine-mesh per coarse-mesh, was reported to be 1.04420 (Smith, 1980).

5.5.2 Coarse Mesh Results

Forward and adjoint mode response functions were computed for each of the nine coarse-mesh types with the parameters shown in Table 18. Coarse-mesh type W does not contain

any fissionable material, so the k grid is irrelevant. Due to the selected fine-mesh arrangements, all coarse-meshes types have only diagonal symmetry.

Table 18: HAFAS Response Function Parameters

Maximum Spatial Order	4^{th}
Maximum Azimuthal Order	3^{rd}
Maximum Polar Order	1^{st}
k Grid	1.0, 1.1
Total Response Functions	5,440
Total Computational Time (min)	106.12

An inner iteration limit study was performed, as with the modified Henry-Worley and CISE problems, using a (0,0,0) expansion. A much larger number of inner iterations was found to be optimal than for the CISE problem. For the **NV** method, a limit of 40 inner iterations per outer iteration was found to be the most efficient, while a limit of 145 iterations was best for the **RQ** method. These limits were used in all coarse-mesh calculations for this problem.

A thorough study of the coarse-mesh results versus expansion order and method was conducted, in the same fashion as the Henry-Worley and CISE problems. The complete comparison of the coarse-mesh and reference fine-mesh results is shown in Figure 20 in Appendix B.

5.5.3 Discussion

To examine the impact of varying the maximum expansion order in an individual dimension an average was calculated of the differences associated with all of the calculations shown in Figure 20 having a given maximum expansion order in a given dimension. The results are shown in Tables 19 and 20.

It is immediately obvious that the maximum fission rate errors are much larger than in previous problems. This is most likely a result of the fact that the edit regions are much

Table 19: HAFAS Coarse Mesh Results Summary I

		NV Method		
Dimension	Max. Order	k Diff.	Avg. FD	Max. FD
Spatial	0	1.68%	4.88%	30.16%
	1	0.15%	5.11%	13.37%
	2	0.25%	2.65%	10.12%
Azimuthal	0	0.76%	5.68%	21.71%
	1	0.67%	3.55%	16.48%
	2	0.66%	3.41%	15.47%
Polar	0	0.71%	4.30%	18.73%
	1	0.67%	4.13%	17.04%

Table 20: HAFAS Coarse Mesh Results Summary II

		RQ Method		
Dimension	Max. Order	k Diff.	Avg. FD	Max. FD
Spatial	0	0.79%	5.98%	28.55%
	1	0.03%	5.40%	13.75%
	2	0.03%	3.32%	10.69%
Azimuthal	0	0.28%	6.68%	21.83%
	1	0.28%	4.16%	16.03%
	2	0.28%	3.86%	15.13%
Polar	0	0.28%	5.12%	18.54%
	1	0.28%	4.68%	16.78%

smaller than those previously considered. Consequently, the effect of fortuitous error cancellations is minimized. On the average, increasing the expansion order in any dimension has a positive effect on the results. Of the expansion orders used in the previous problems, only the $(2, 2, 1)$ calculation achieves a maximum fission rate error of less than 5%. Calculations with even higher order expansions were performed, as shown in Figure 20. The $(3, 3, 1)$ and $(4, 3, 1)$ calculations provide highly accurate results, but require many more response functions than were used in previous problems. The $(4, 3, 1)$ calculation achieved an average and maximum fission rate difference of 0.80% and -2.23%, respectively. However, the computational costs associated with this magnitude of expansion are quite large.

Figure 7 and 8 shows the average and maximum edit region fission rate errors, respectively, within each coarse-mesh (as arranged in Figure 16) for the $(0, 0, 0)$ and $(4, 3, 1)$ **NV** method calculations. The normalized reference fission rates are also shown. The shaded blocks represent the controlled assemblies.

						1.104	**0.698**	**0.402**
						3.256%	4.833%	12.674%
						1.528%	1.572%	1.490%
					1.490	**1.214**	**1.005**	**0.518**
					3.921%	2.359%	2.061%	6.936%
					1.183%	1.391%	1.484%	1.400%
				1.000	**1.285**	**1.380**	**0.985**	**0.647**
				6.579%	4.342%	3.070%	1.844%	5.727%
				0.393%	0.717%	1.140%	1.248%	1.253%
			1.119	**0.889**	**1.274**	**1.107**	**1.025**	**0.577**
			4.528%	6.452%	4.706%	3.706%	1.951%	5.363%
			0.955%	0.757%	0.235%	0.584%	0.878%	0.908%
		1.575	**1.493**	**1.381**	**0.813**	**0.769**	**0.802**	**0.593**
		2.955%	1.367%	2.712%	6.470%	6.142%	1.982%	5.743%
		0.423%	0.512%	0.582%	0.822%	0.478%	0.338%	0.532%
	1.581	**1.413**	**1.662**	**1.234**	**0.857**	**0.652**	**0.844**	**0.515**
	8.972%	5.545%	2.155%	1.940%	6.056%	5.856%	2.044%	5.458%
	0.482%	0.489%	0.579%	0.798%	1.212%	0.930%	0.159%	0.154%
1.343[a]	**1.174**	**1.245**	**1.039**	**0.941**	**1.024**	**1.052**	**0.811**	**0.572**
13.037%[b]	11.268%	7.090%	5.281%	5.520%	3.384%	3.196%	2.160%	5.276%
0.513%[c]	0.527%	0.695%	1.220%	1.375%	0.905%	0.531%	0.192%	0.076%

[a] normalized reference fission rate
[b] (0,0,0) calculation: Avg. FD
[c] (4,3,1) calculation: Avg. FD

Figure 7: HAFAS Coarse-Mesh Results I

						1.104	**0.698**	**0.402**
						8.823%	14.499%	32.551%
						1.653%	1.621%	1.622%
					1.490	**1.214**	**1.005**	**0.518**
					6.992%	6.882%	6.148%	16.099%
					1.397%	1.511%	1.574%	1.475%
				1.000	**1.285**	**1.380**	**0.985**	**0.647**
				14.521%	7.454%	7.427%	-6.236%	14.200%
				1.013%	1.081%	1.337%	1.361%	1.408%
			1.119	**0.889**	**1.274**	**1.107**	**1.025**	**0.577**
			15.268%	16.666%	10.602%	8.813%	9.132%	12.414%
			1.788%	1.800%	0.604%	0.948%	1.081%	1.119%
		1.575	**1.493**	**1.381**	**0.813**	**0.769**	**0.802**	**0.593**
		4.735%	3.223%	7.949%	15.322%	16.953%	9.305%	12.363%
		0.483%	0.783%	0.871%	1.853%	1.322%	0.606%	0.794%
	1.581	**1.413**	**1.662**	**1.234**	**0.857**	**0.652**	**0.844**	**0.515**
	12.798%	9.287%	4.947%	6.367%	15.988%	15.915%	8.618%	12.202%
	0.572%	0.617%	0.977%	1.060%	2.027%	1.957%	0.438%	0.381%
1.343[a]	**1.174**	**1.245**	**1.039**	**0.941**	**1.024**	**1.052**	**0.811**	**0.572**
15.454%[b]	14.736%	9.399%	20.450%	17.399%	9.881%	7.336%	7.919%	11.932%
0.565%[c]	0.574%	1.064%	2.104%	2.223%	1.252%	0.954%	0.330%	0.147%

[a] normalized reference fission rate
[b] (0,0,0) calculation: Max. FD
[c] (4,3,1) calculation: Max. FD

Figure 8: HAFAS Coarse-Mesh Results II

CHAPTER VI

CONCLUSIONS

6.1 Overview

It seems very likely that the next generation of reactor analysis methods will be based largely on neutron transport theory, at both the assembly and core levels. Significant progress has been made in recent years toward the goal of developing a transport method that is applicable to large, heterogeneous coarse-meshes. Unfortunately, the major obstacle hindering a more widespread application of transport theory to large-scale calculations is still the computational cost.

In this dissertation, a variational heterogeneous coarse-mesh transport method has been extended from one to two-dimensional Cartesian geometry in a practical fashion. A generalization of the angular flux expansion within a coarse-mesh was developed. This allows a far more efficient class of response functions (or basis functions) to be employed within the framework of the original variational principle. New finite element equations were derived that can be used to compute the expansion coefficients for an individual coarse-mesh given the incident fluxes on the boundary. In addition, the non-variational method previously used to converge the expansion coefficients was developed in a new and more thorough manner by considering the implications of the fission source treatment imposed by the response expansion.

The new coarse-mesh method was implemented for both one and two-dimensional problems in the finite-difference, multigroup, discrete ordinates approximation. An efficient set of response functions was generated using orthogonal boundary conditions constructed from the discrete Legendre polynomials. Several one and two-dimensional heterogeneous light water reactor benchmark problems were studied. Relatively low-order response expansions were used to generate highly accurate results for each problem using both the variational

and non-variational coarse-mesh methods. The expansion order was found to have a far more significant impact on the accuracy of the results than the type of method used. The variational techniques provide better accuracy, but at substantially higher computational costs. The non-variational method is extremely robust and was shown to achieve accurate results in the two-dimensional problems, as long as the expansion order was not extremely low.

6.2 Recommendations for Future Work

The discrete Legendre polynomials that were used in the response function boundary conditions are derived as an orthogonal (discrete) function set on uniform intervals. However, non-uniform spatial intervals are more computationally efficient to use in detailed problems than a very small, uniform meshes. Consequently, an interesting study would be to identify and implement an alternative set of orthogonal functions that are less sensitive to the uniformity of the spatial mesh, which would lead to a more efficient discrete ordinates response function expansion.

The implemented coarse-mesh method's capabilities (*e.g.*, cross section treatment, geometry modelling, *etc.*) are fundamentally determined by the fine-mesh method used to compute response functions. Consequently, an extension to other fine-mesh transport methods (*e.g.*, Monte Carlo) could lead to a more flexible overall coarse-mesh method.

Finally, an extension of the method to three-dimensional problems is conceptually straightforward. However, additional (perhaps evolutionary) techniques must be developed to make a three-dimensional method practical.

APPENDIX A

BENCHMARK PROBLEMS

A specification of the one and two-dimensional benchmark problems solved in Chapter 5 is provided in this appendix. Note that for all materials $\sigma_s^{2\to1} = 0$, and for all fissionable materials: $\chi_1 = 1$, $\chi_2 = 0$, and $\nu_{1,2} = 2.5$.

Table 21: One-Dimensional Benchmark Cross Sections

	σ_{tr}^1	σ_{tr}^2	$\sigma_s^{1\to1}$	$\sigma_s^{1\to2}$	$\sigma_s^{2\to2}$	$\nu\sigma_f^1$	$\nu\sigma_f^2$
Water	0.1890	1.4633	0.1507	0.0380	1.4536		
Fuel I	0.2263	1.0119	0.2006	0.0161	0.9355	0.0067	0.1241
Fuel II	0.2252	0.9915	0.1995	0.0156	0.9014	0.0078	0.1542
Fuel II + Gd	0.2173	1.0606	0.1902	0.0136	0.5733	0.0056	0.0187

Table 22: One-Dimensional Benchmark Material Map

	Region I	Region II	Region III
CM A	Water	Fuel I	Fuel II
CM B	Water	Fuel I	Fuel I
CM C	Water	Fuel I	Fuel II + Gd
CM D	Water	Fuel II + Gd	Fuel II + Gd

Table 23: MHW Benchmark Cross Sections

	σ_{tr}^1	σ_{tr}^2	$\sigma_s^{1\to1}$	$\sigma_s^{1\to2}$	$\sigma_s^{2\to2}$	$\nu\sigma_f^1$	$\nu\sigma_f^2$
Water	0.21575	1.06633	0.18693	0.02838	1.05759		
Fuel	0.23213	0.86177	0.20566	0.01596	0.75997	0.007293	0.15310
Blade	0.30525	0.95048	0.27340	0.	0.54838		

Table 24: MHW Benchmark Material Map

	Fuel Region	Blade Region
CM A	Fuel	Blade
CM B	Fuel	Water
CM W	Water	Water

Table 25: CISE Benchmark Cross Sections

	σ_{tr}^1	σ_{tr}^2	$\sigma_s^{1\to1}$	$\sigma_s^{1\to2}$	$\sigma_s^{2\to2}$	$\nu\sigma_f^1$	$\nu\sigma_f^2$
Water	0.16667	1.11111	0.12667	0.04	1.10111		
Fuel I	0.18519	0.60606	0.16519	0.012	0.52106	0.006	0.11
Fuel II	0.18519	0.60606	0.16519	0.012	0.52106	0.005	0.10
Blade	0.11111	2.22222	0.03111	0.	1.22222		

Table 26: One-Dimensional Benchmark Material Map

	Fuel Region	Channel Region	Blade Region
CM A	Fuel I	Water	Water
CM A^+	Fuel I	Water	Blade
CM B	Fuel II	Water	Water
CM B^+	Fuel II	Water	Blade
CM W	Water	Water	Water

Table 27: HAFAS Benchmark Cross Sections

	σ_{tr}^1	σ_{tr}^2	$\sigma_s^{1\to1}$	$\sigma_s^{1\to2}$	$\sigma_s^{2\to2}$	$\nu\sigma_f^1$	$\nu\sigma_f^2$
Water	0.16667	1.11111	0.12667	0.04	1.10111		
Blade	0.3003	1.8018	0.2128	0.00375	0.8518		
Chnl	0.21786	1.12994	0.18636	0.031	1.12094		
Fuel I	0.2381	0.88889	0.2131	0.016	0.80889	0.0065	0.122
Fuel II	0.2381	0.88889	0.2121	0.017	0.81889	0.0057	0.1
Fuel III	0.2381	0.88889	0.2111	0.018	0.82889	0.0051	0.08
Fuel IV	0.2381	0.88889	0.2111	0.018	0.83889	0.0051	0.07
Fuel I^{40}	0.19841	0.62893	0.18041	0.01	0.55193	0.0063	0.118
Fuel II^{40}	0.19841	0.62893	0.17941	0.0105	0.56193	0.0055	0.096
Fuel III^{40}	0.19841	0.62893	0.17841	0.011	0.57193	0.0049	0.078
Fuel IV^{40}	0.19841	0.62893	0.17841	0.011	0.58193	0.0049	0.068
Fuel I^{70}	0.16667	0.41667	0.15367	0.0052	0.34367	0.0061	0.114
Fuel II^{70}	0.16667	0.41667	0.15317	0.0053	0.35367	0.0053	0.092
Fuel III^{70}	0.16667	0.41667	0.15267	0.0054	0.36367	0.0047	0.072
Fuel IV^{70}	0.16667	0.41667	0.15267	0.0054	0.37367	0.0047	0.062

Table 28: HAFAS Benchmark Material Map

	Fuel Reg. I	Fuel Reg. II	Fuel Reg. III	Channel Reg.	Blade Reg.
CM A	Fuel I	Fuel II	Fuel III	Chnl	Chnl
CM A^{40}	Fuel I^{40}	Fuel II^{40}	Fuel III^{40}	Chnl	Chnl
CM A^{70}	Fuel I^{70}	Fuel II^{70}	Fuel III^{70}	Chnl	Chnl
CM A^+	Fuel I	Fuel II	Fuel III	Chnl	Blade
CM B	Fuel II	Fuel III	Fuel IV	Chnl	Chnl
CM B^{40}	Fuel II^{40}	Fuel III^{40}	Fuel IV^{40}	Chnl	Chnl
CM B^{70}	Fuel II^{70}	Fuel III^{70}	Fuel IV^{70}	Chnl	Chnl
CM B^+	Fuel II	Fuel III	Fuel IV	Chnl	Blade
CM W	Water	Water	Water	Water	Water

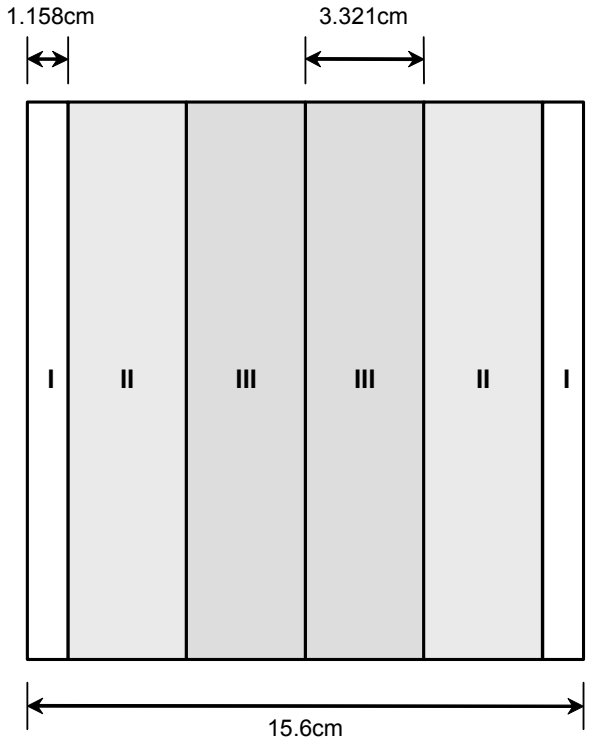

Figure 9: One-Dimensional Benchmark Coarse-Mesh Model

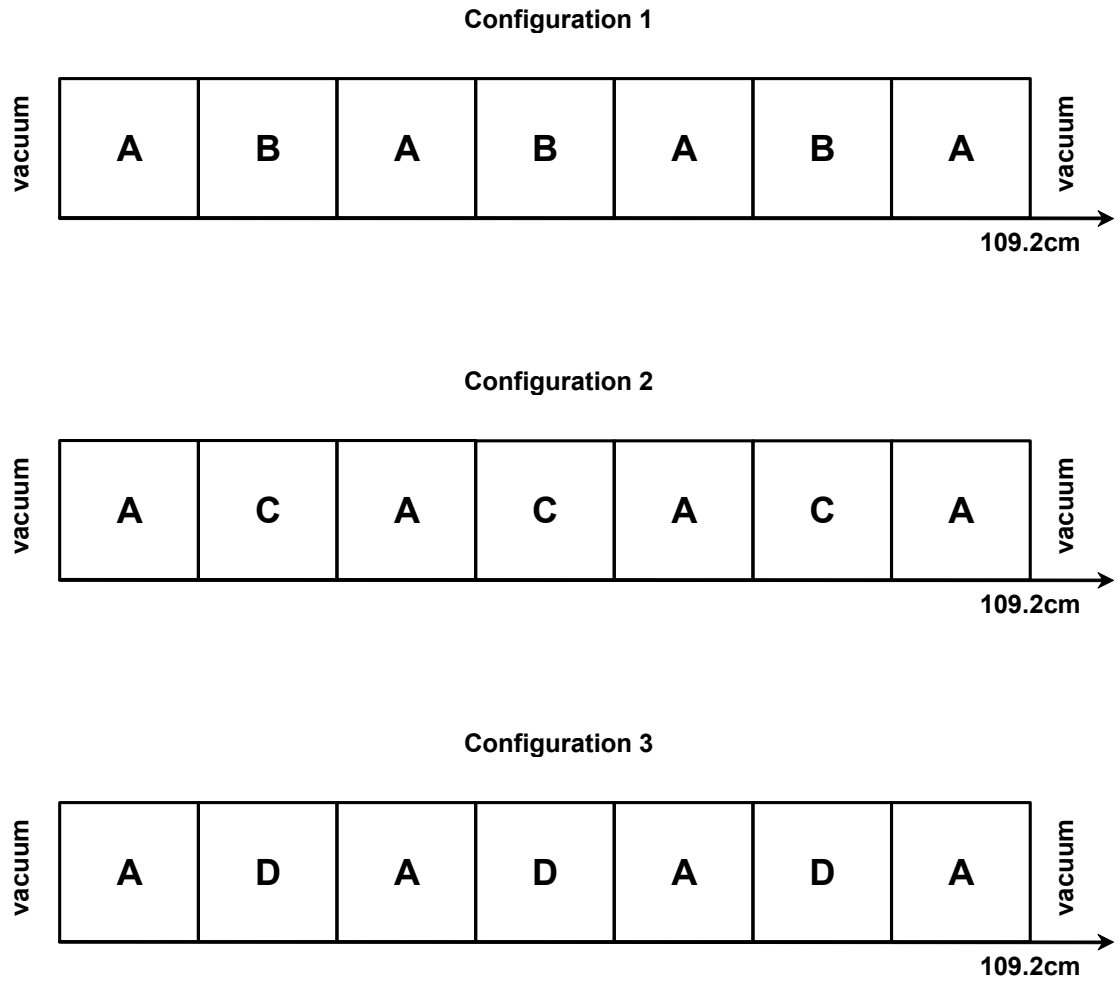

Figure 10: One-Dimensional Benchmark Core Configurations

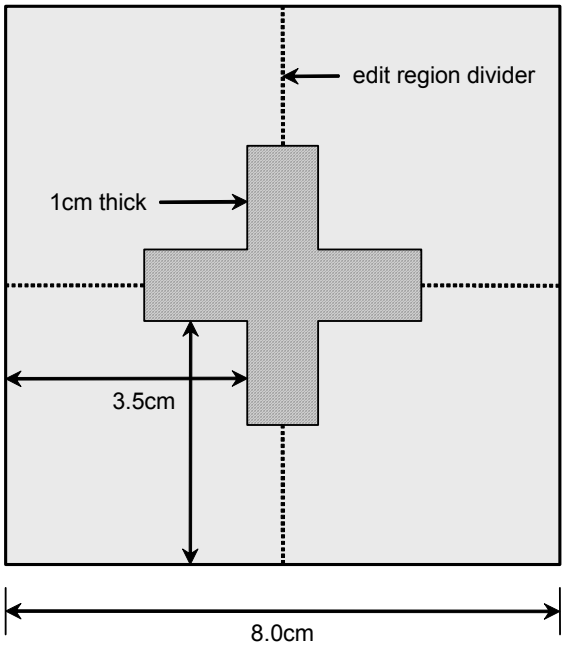

Figure 11: MHW Coarse-Mesh Model

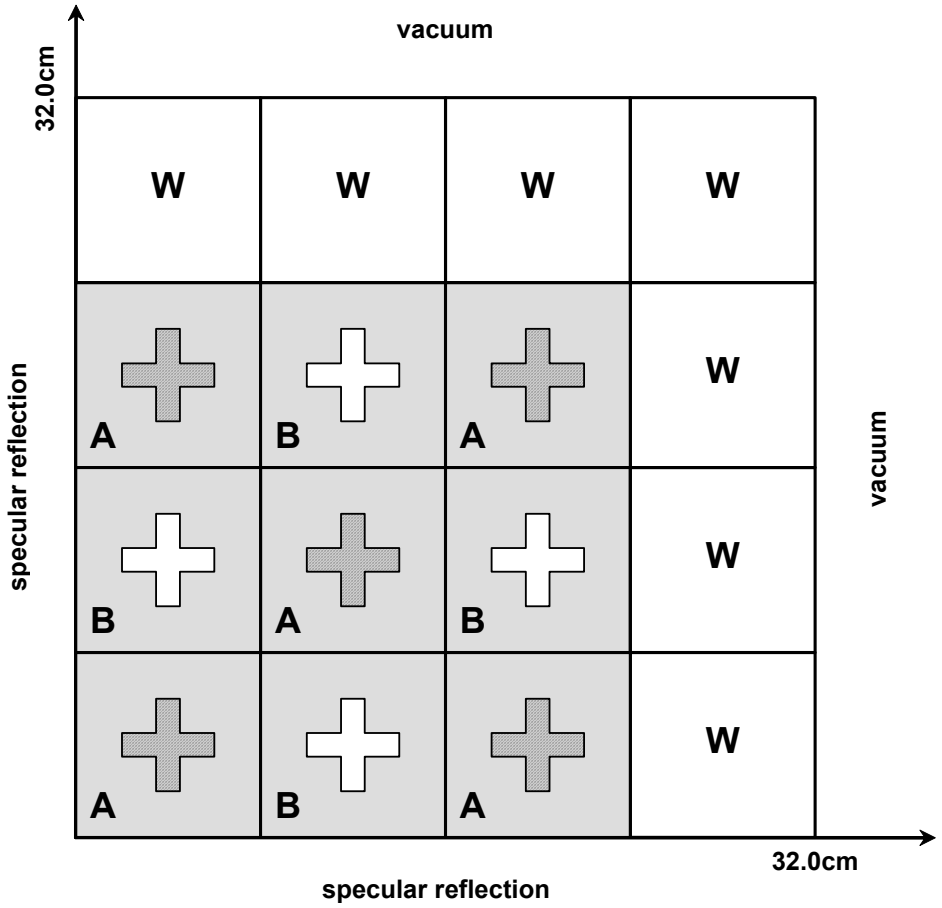

Figure 12: MHW Core Configuration

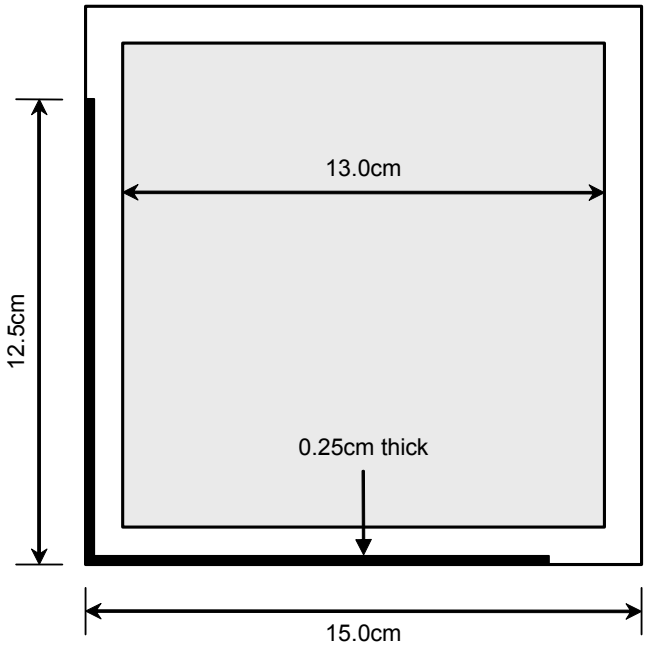

Figure 13: CISE Coarse-Mesh Model

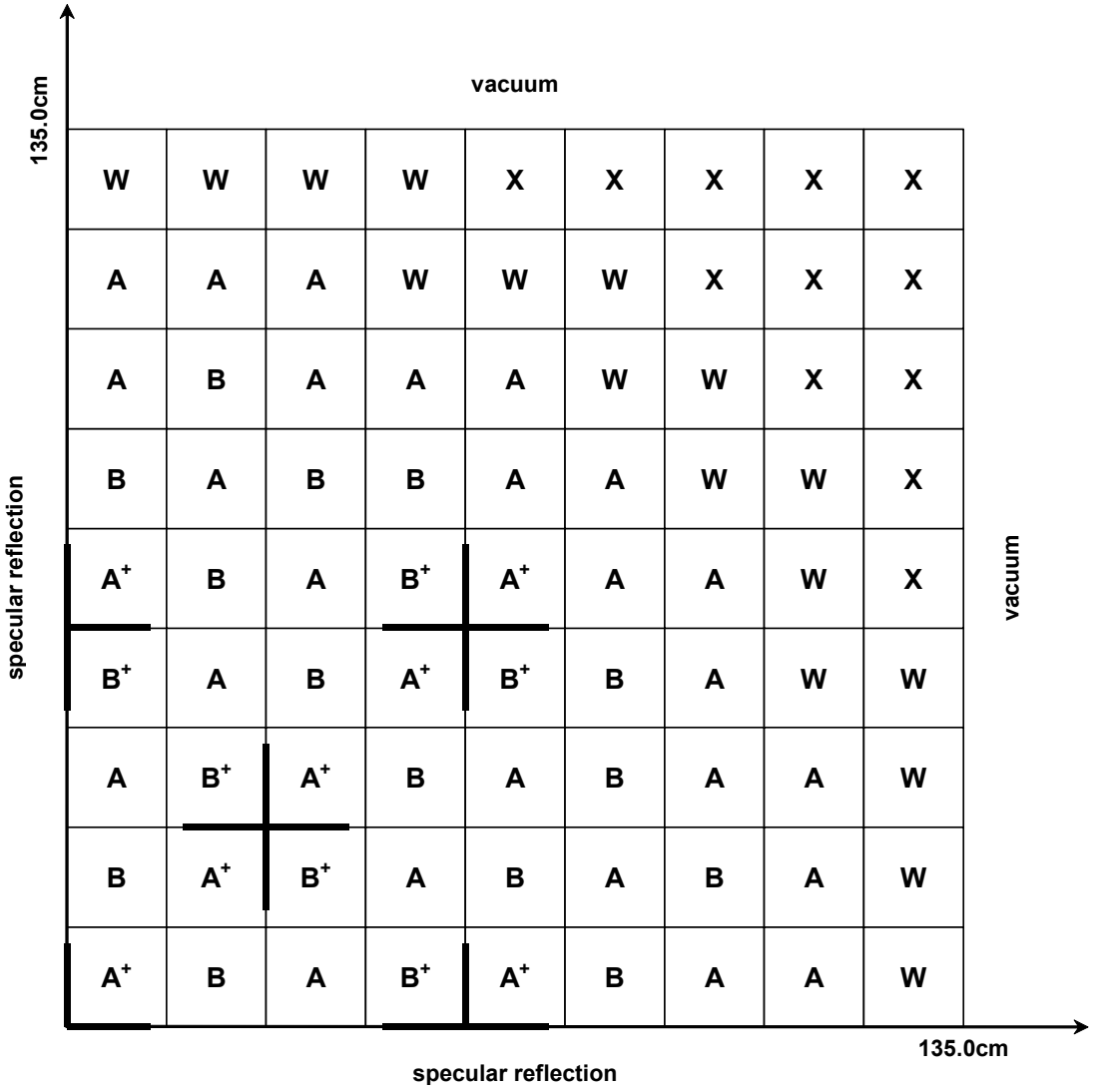

Figure 14: CISE Core Configuration

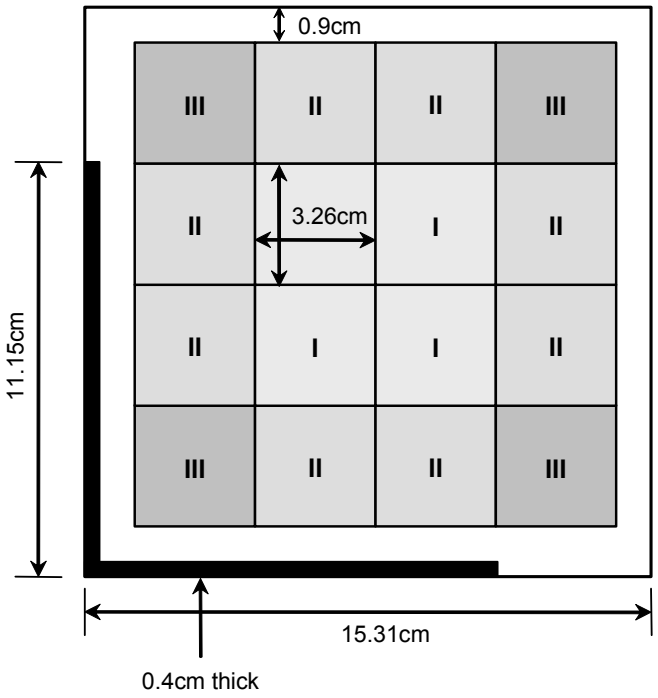

Figure 15: HAFAS Coarse-Mesh Model

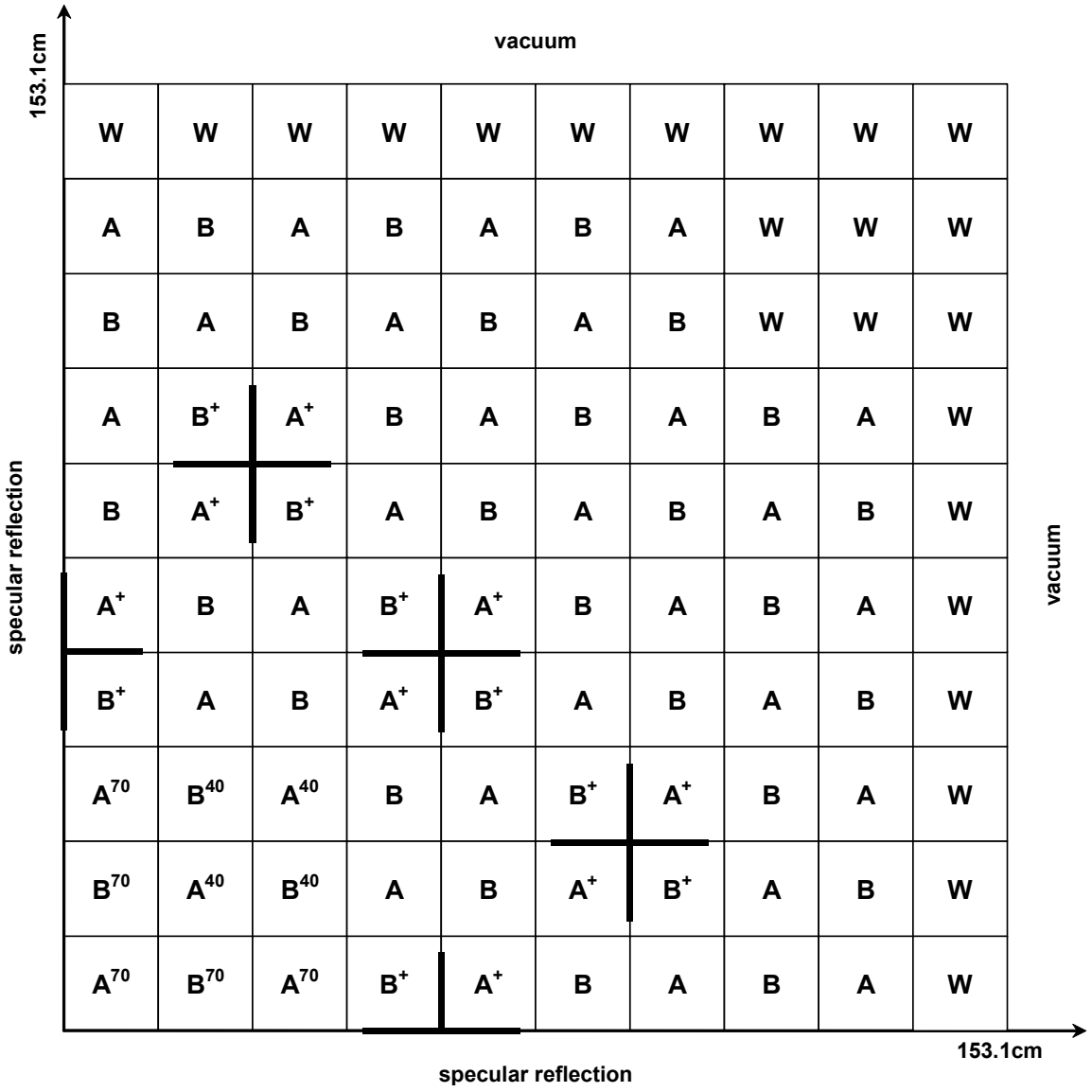

Figure 16: HAFAS Core Configuration

APPENDIX B

COMPLETE COARSE MESH RESULTS

The complete set of coarse-mesh results that were generated for each benchmark problem are presented in this appendix.

Core 1, Two-Group, S-32 Calculation

	NV Method			Time	RQ Method			Time	V Method		Time	Inner	Inverse Condition #	
Order	k Diff	Avg FD	Max FD	(sec)	k Diff	Avg FD	Max FD	(sec)	Avg FD	Max FD	(sec)	Conv	A	B
0	0.113%	0.610%	-1.843%	0.08	0.001%	0.648%	-1.861%	0.12	0.357%	-1.296%	0.17	9.60E-07	3.36E-01	3.40E-01
1	-0.004%	0.072%	-0.221%	0.11	0.000%	0.070%	-0.215%	0.22	0.113%	0.271%	0.36	3.20E-06	2.57E-03	2.52E-03
2	-0.011%	0.091%	-0.242%	0.16	0.000%	0.087%	-0.226%	0.30	0.018%	-0.024%	0.39	1.67E-04	4.17E-04	4.22E-04
3	-0.007%	0.061%	-0.181%	0.17	0.000%	0.057%	-0.172%	0.38	0.011%	-0.026%	0.56	5.72E-03	7.16E-06	6.70E-06
4	-0.006%	0.059%	-0.173%	0.25	0.000%	0.056%	-0.165%	0.53	0.008%	-0.024%	0.78	1.21E-01	8.58E-07	8.94E-07
5	-0.006%	0.059%	-0.173%	0.28	0.000%	0.056%	-0.165%	0.69	0.009%	-0.041%	1.11	1.22E+02	2.20E-08	2.45E-08

Core 2, Two-Group, S-32 Calculation

	NV Method			Time	RQ Method			Time	V Method		Time	Inner	Inverse Condition #	
Order	k Diff	Avg FD	Max FD	(sec)	k Diff	Avg FD	Max FD	(sec)	Avg FD	Max FD	(sec)	Conv	A	C
0	0.247%	1.071%	-2.499%	0.08	-0.004%	1.142%	-2.529%	0.12	0.458%	-1.091%	0.16	9.92E-07	2.88E-01	3.67E-01
1	0.007%	0.062%	-0.144%	0.09	0.000%	0.065%	-0.150%	0.16	0.138%	-0.436%	0.25	5.67E-07	2.04E-03	3.98E-03
2	-0.019%	0.095%	-0.155%	0.12	0.000%	0.090%	-0.138%	0.20	0.022%	0.063%	0.31	1.66E-04	3.40E-04	4.35E-04
3	-0.001%	0.041%	-0.112%	0.16	0.000%	0.040%	-0.110%	0.28	0.010%	-0.020%	0.45	5.31E-03	6.00E-06	3.61E-06
4	0.000%	0.038%	-0.100%	0.22	0.000%	0.037%	-0.099%	0.36	0.005%	-0.018%	0.64	1.21E-01	7.18E-07	3.90E-06
5	0.000%	0.038%	-0.100%	0.27	0.000%	0.038%	-0.100%	0.48	0.005%	-0.017%	0.88	1.63E+01	1.91E-08	1.61E-08

Core 3, Two-Group, S-32 Calculation

	NV Method			Time	RQ Method			Time	V Method		Time	Inner	Inverse Condition #	
Order	k Diff	Avg FD	Max FD	(sec)	k Diff	Avg FD	Max FD	(sec)	Avg FD	Max FD	(sec)	Conv	A	D
0	0.422%	1.807%	-3.872%	0.12	-0.019%	2.134%	-4.187%	0.16	0.796%	-2.129%	0.17	7.80E-07	2.14E-01	5.24E-01
1	0.071%	0.127%	-0.460%	0.19	-0.001%	0.180%	-0.541%	0.22	0.247%	0.884%	0.36	3.56E-06	1.33E-03	8.10E-03
2	0.028%	0.075%	0.231%	0.23	0.000%	0.083%	-0.254%	0.28	0.040%	-0.193%	0.38	2.04E-04	2.37E-04	1.79E-04
3	0.034%	0.103%	-0.271%	0.30	0.000%	0.131%	-0.341%	0.41	0.014%	-0.028%	0.55	3.80E-03	4.27E-06	1.85E-05
4	0.034%	0.105%	-0.269%	0.44	0.000%	0.133%	-0.340%	0.52	0.008%	-0.033%	0.77	8.14E-01	5.11E-07	7.35E-07
5	0.034%	0.105%	-0.269%	0.53	0.000%	0.134%	-0.341%	0.67	0.018%	-0.051%	1.06	7.63E+01	1.38E-08	6.71E-09

Figure 17: Complete 1-D Benchmark Results

Modified Henry-Worley, 10% k, Max 4(NV), 10(RQ), 50(V) Inner Iterations

max expansion order				NV Method			Time	RQ Method			Time	V Method		Time
spatial ≤ 2	azi ≤ 2	polar ≤ 1	orders	k Diff	Avg FD	Max FD	(sec)	k Diff	Avg FD	Max FD	(sec)	Avg FD	Max FD	(sec)
0	0	0	1	-0.83%	1.88%	-5.33%	0.11	-0.40%	1.92%	-5.48%	1.34	0.95%	-3.82%	3.33
0	0	1	2	-0.87%	1.83%	-5.17%	0.14	-0.43%	1.86%	-5.31%	2.50	0.72%	3.15%	11.14
0	1	0	2	-2.77%	1.52%	-4.11%	0.12	-0.62%	1.67%	-4.81%	2.44	1.15%	-3.74%	8.14
1	0	0	2	3.64%	1.00%	-4.19%	0.11	0.10%	0.95%	-3.67%	3.16	0.47%	1.15%	8.16
0	2	0	3	-2.92%	1.50%	-3.88%	0.11	-0.72%	1.61%	-4.61%	3.22			
2	0	0	3	3.55%	1.49%	-5.29%	0.14	0.15%	1.39%	-4.81%	4.41	0.47%	-1.41%	15.38
0	1	1	4	-3.35%	1.42%	3.45%	0.16	-0.68%	1.49%	-4.24%	4.62	1.14%	-3.59%	29.81
1	0	1	4	3.44%	0.98%	-4.09%	0.16	0.10%	0.92%	-3.61%	5.84	0.42%	1.28%	29.89
1	1	0	4	1.35%	0.39%	-1.20%	0.16	0.00%	0.28%	-0.99%	5.70			
0	2	1	6	-3.57%	1.42%	3.69%	0.17	-0.80%	1.44%	-3.94%	6.61			
1	2	0	6	1.10%	0.32%	-0.97%	0.19	0.02%	0.30%	-0.71%	8.44	0.35%	-1.13%	54.28
2	0	1	6	3.34%	1.45%	-5.08%	0.19	0.15%	1.35%	-4.64%	8.38	0.89%	3.78%	56.45
2	1	0	6	1.31%	0.75%	-2.38%	0.22	-0.03%	0.58%	-2.22%	8.45	0.13%	-0.33%	56.55
1	1	1	8	0.58%	0.36%	-1.08%	0.22	0.00%	0.33%	-0.92%	11.20			
2	2	0	9	1.05%	0.48%	-1.53%	0.23	0.00%	0.36%	-1.41%	12.38	0.04%	-0.12%	112.95
1	2	1	12	0.22%	0.60%	1.45%	0.28	0.00%	0.62%	1.52%	16.67			
2	1	1	12	0.54%	0.43%	-1.17%	0.28	-0.02%	0.35%	-1.08%	16.55			
2	2	1	18	0.15%	0.17%	-0.30%	0.42	-0.01%	0.17%	-0.31%	24.64			

Figure 18: Complete MHW Coarse-Mesh Results

CISE, 10% k, Max 20(NV), 35(RQ), 50(V) Inner Iterations

max expansion order				NV Method			Time	RQ Method			Time	V Method		Time
spatial ≤ 2	azi ≤ 2	polar ≤ 1	orders	k Diff	Avg FD	Max FD	(sec)	k Diff	Avg FD	Max FD	(sec)	Avg FD	Max FD	(sec)
0	0	0	1	-1.23%	2.04%	5.38%	0.92	-0.58%	1.61%	4.47%	58.12	1.15%	-3.38%	124.75
0	0	1	2	-1.23%	1.71%	5.23%	1.12	-0.59%	1.28%	4.33%	110.73			
0	1	0	2	-1.55%	1.06%	4.07%	1.11	-0.64%	1.03%	3.06%	110.89			
1	0	0	2	0.71%	5.81%	-14.92%	1.11	-0.08%	6.23%	-16.73%	171.31	3.57%	8.25%	307.44
0	2	0	3	-1.52%	1.31%	3.17%	1.28	-0.66%	1.43%	4.61%	163.06			
2	0	0	3	0.91%	2.92%	-8.64%	1.34	-0.17%	3.57%	-11.43%	208.77			
0	1	1	4	-1.63%	1.48%	4.00%	1.47	-0.66%	1.60%	4.90%	216.62			
1	0	1	4	0.57%	5.73%	-14.49%	1.55	-0.05%	6.06%	-15.91%	276.06	3.15%	7.43%	1098.06
1	1	0	4	0.26%	3.11%	-8.08%	1.55	-0.04%	3.27%	-8.78%	216.59	1.84%	-3.75%	715.16
0	2	1	6	-1.63%	1.84%	4.21%	1.88	-0.68%	2.10%	6.65%	323.58			
1	2	0	6	0.12%	2.57%	-6.17%	1.98	-0.01%	2.63%	-6.46%	324.41			
2	0	1	6	0.67%	3.48%	-9.66%	2.03	-0.06%	3.91%	-11.49%	413.66			
2	1	0	6	0.53%	0.84%	-2.79%	2.08	-0.17%	1.14%	-4.66%	412.39			
1	1	1	8	0.03%	2.49%	-6.17%	2.47	-0.01%	2.51%	-6.24%	428.45			
2	2	0	9	0.28%	0.61%	-1.86%	2.81	-0.05%	0.75%	-2.72%	613.80			
1	2	1	12	-0.12%	1.96%	-4.14%	3.59	-0.02%	1.89%	-3.88%	644.23	0.61%	-1.27%	4924.31
2	1	1	12	0.20%	0.66%	-2.30%	3.69	-0.06%	0.81%	-2.98%	820.48			
2	2	1	18	-0.05%	0.37%	-0.98%	5.78	-0.03%	0.36%	-0.93%	961.61			

Figure 19: Complete CISE Coarse-Mesh Results

HAFAS, 10% k, Max 40(NV) and 145(RQ) Inner Iterations

max expansion order				NV Method			Time	RQ Method			Time
spatial ≤ 2	azi ≤ 2	polar ≤ 1	orders	k Diff	Avg FD	Max FD	(sec)	k Diff	Avg FD	Max FD	(sec)
0	0	0	1	-1.55%	4.78%	32.57%	4.48	-0.76%	5.63%	30.68%	123.47
0	0	1	2	-1.57%	4.71%	32.22%	5.11	-0.77%	5.58%	30.36%	236.02
0	1	0	2	-1.71%	4.92%	29.64%	5.09	-0.80%	6.12%	27.81%	236.09
1	0	0	2	0.33%	7.63%	-18.24%	5.34	-0.04%	8.66%	19.38%	364.94
0	2	0	3	-1.72%	4.84%	29.26%	5.55	-0.81%	6.04%	27.47%	349.33
2	0	0	3	0.51%	4.54%	-15.94%	5.88	-0.05%	6.05%	-17.21%	541.77
0	1	1	4	-1.76%	5.04%	28.88%	6.12	-0.81%	6.28%	27.12%	462.36
1	0	1	4	0.23%	7.59%	17.70%	6.66	-0.04%	8.32%	18.90%	718.11
1	1	0	4	0.09%	4.41%	-12.31%	6.52	-0.02%	4.65%	-12.53%	590.52
0	2	1	6	-1.78%	4.99%	28.40%	7.39	-0.82%	6.23%	27.92%	688.31
1	2	0	6	0.01%	3.99%	11.03%	7.98	-0.01%	4.03%	11.10%	880.16
2	0	1	6	0.35%	4.85%	-13.60%	8.23	-0.03%	5.86%	-14.48%	1070.44
2	1	0	6	0.30%	1.80%	-10.56%	8.08	-0.04%	2.62%	-11.25%	880.17
1	1	1	8	-0.08%	3.73%	10.64%	9.53	-0.01%	3.63%	10.44%	1176.44
2	2	0	9	0.20%	1.79%	-9.05%	10.33	-0.02%	2.33%	-9.49%	1319.16
1	2	1	12	-0.17%	3.32%	10.33%	13.58	-0.02%	3.11%	-10.12%	1715.39
2	1	1	12	0.08%	1.42%	-6.83%	13.52	-0.02%	1.65%	-7.05%	1709.45
2	2	1	18	-0.06%	1.53%	-4.73%	20.83	-0.02%	1.44%	-4.65%	2448.67
2	3	1	24	-0.09%	0.93%	-3.90%	29.48				
3	2	1	24	-0.05%	1.58%	-4.10%	29.73				
3	3	1	32	-0.08%	0.97%	-3.19%	44.12				
4	3	1	40	-0.08%	0.80%	-2.23%	62.53				

Figure 20: Complete HAFAS Coarse-Mesh Results

REFERENCES

Abu-Shumays, I.K. (1977), "Compatible Product Angular Quadrature for Neutron Transport in x-y Geometry," *Nuclear Science and Engineering*, **64**, 299-316.

Abu-Shumays, I.K. (2001), "Angular Quadratures for Improved Transport Computations," *Transport Theory and Statistical Physics*, **30**, 169-204.

Azmy, Y.Y. (2003), *Private Communication.*

Carlson, B.G. and Lathrop, K.D. (1968), "Transport Theory – The Method of Discrete Ordinates," in Computing Methods in Reactor Physics, Greenspan, H. Kelber, C.N., and Okrent, D., Eds., Gordon and Breach, New York.

Case, K.M. and Zweifel, P.F. (1967), Linear Transport Theory, Ch. 1 and Sec. 2.6, Addison-Wesley, Reading, Massachusetts.

Dilber, I. and Lewis, E.E. (1985), "Variational Nodal Methods for Neutron Transport," *Nuclear Science and Engineering*, **91**, 132-142.

Duderstadt, J.J. and Hamilton, L.J. (1976), Nuclear Reactor Analysis, Sec. 4.IV, Wiley & Sons, New York.

Engle, W.W., Jr. (1967), "A Users Manual for ANISN: A One Dimensional Discrete Ordinates Transport Code with Anisotropic Scattering," Report K-1693, Oak Ridge National Laboratory.

Ilas, D. (2001), "Coarse Mesh Transport Theory Model for Heterogeneous Systems," Ph.D. Thesis, Georgia Institute of Technology.

Ilas, D. and Rahnema, F. (2003), "A Heterogeneous Coarse Mesh Transport Method," *Transport Theory and Statistical Physics*, **32**, 441-467.

Koebke, K. and Hetzelt, L. (1985), "On the Reconstruction of Local Homogeneous Neutron Flux and Current Distributions of Light Water Reactors from Nodal Schemes," *Nuclear Science and Engineering*, **91**, 123-131.

Larsen, E.W. (1975), "Neutron Transport and Diffusion in Inhomogeneous Media. I," *Journal of Mathematical Physics*, **16**, 1421-1427.

Larsen, E.W. (1976), "Neutron Transport and Diffusion in Inhomogeneous Media. II," *Nuclear Science and Engineering*, **60**, 357-368.

Lawrence, R.D. (1986), "Progress in Nodal Methods for the Solution of the Neutron Diffusion and Transport Equations," *Progress in Nuclear Energy*, **17**, 271-301.

Lewis, E.E. and Miller, W.F., Jr. (1984), Computational Methods of Neutron Transport, American Nuclear Society, La Grange Park, Illinois.

Lewis, E.E., Palmiotti, G., and Taiwo, T.A. (1999), "Space-Angle Approximation in the Variational Nodal Method," *Proceedings of the International Conference on Mathematics and Computation, Reactor Physics and Environmental Analysis of Nuclear Systems*, Madrid, Spain, September 27-30.

Mosher, S.W. and Rahnema, F. (2003), "An Intra-Nodal Flux Expansion for a Heterogeneous Coarse Mesh Discrete Ordinates Method," *Proceedings of the Conference on Nuclear Mathematical and Computational Sciences (M&C 2003),* Gatlinburg, Tennessee, April 6-10.

Neuman, C.P. and Schonbach, D.I. (1974), "Discrete (Legendre) Orthogonal Polynomials - A Survey," *International Journal of Numerical Methods in Engineering*, **8**, 743-770.

Nichita, E.M. and Rahnema, F. (2003), "A Heterogeneous Finite Element Method in Diffusion Theory," *Annals of Nuclear Energy*, **30**, 317-347.

Radiation Safety Information Computational Center (1998), Code Package CCC-650, Oak Ridge National Laboratory, http://www-rsicc.ornl.gov/rsicc.html.

Rahnema, F. and Nichita, E.M. (1997), "Leakage Corrected Spatial (Assembly) Homogenization Technique," *Annals of Nuclear Energy*, **24**, 477-488.

Rathkopf, J.A. and Martin, W.R. (1986), "The Finite Element Response Matrix Method for the Solution of the Neutron Transport Equation," *Progress in Nuclear Energy*, **18**, 237-250.

Rhoades, W.A. and Childs, R.L. (1988), "The DORT Two-Dimensional Discrete Ordinates Transport Code," *Nuclear Science and Engineering*, **99**, 88-89.

Rhoades, W.A. and Emmett, M.B. (1982), "DOS: The Discrete Ordinates System," ORNL/TM-8362, Oak Ridge National Laboratory.

Sanchez, R. and McCormick, N.J. (1972), "A Review of Neutron Transport Approximations," Sec. II.C.3, *Nuclear Science and Engineering*, **80**, 481-535.

Smith, K.S. (1980), "Spatial Homogenization Methods for Light Water Reactor Analysis," Ph.D. Thesis, Massachusetts Institute of Technology.

Smith, K.S. (1986), "Assembly Homogenization Techniques for Light Water Reactor Analysis," *Progress in Nuclear Energy*, **17**, 303-335.

Smith, M.A., Tsoulfanidis, N., Lewis, E.E., Palmiotti, G., and Taiwo, T.A. (2000), "Whole-Core Neutron Transport Calculations without Fuel-Coolant Homogenization," *Proceedings of the International Meeting on Advances in Reactor Physics and Mathematics and Computation into the Next Millennium*, Pittsburgh, May 7-11.

Spanier, J. and Gelbard, E. M. (1969), Monte Carlo Principles and Neutron Transport Problems, Addison-Wesley, Reading, Massachusetts.

Stamm'ler, R.J.J. and Abbate, M.J. (1983), Methods of Steady-State Reactor Physics in Nuclear Design, Ch. IV, Academic Press, London.

Villarino, E.A. and Stamm'ler, R.J.J. (1984), "The Heterogeneous Response Method in Slab Geometry," *Annals of Nuclear Energy*, **11**, 429-440.

Volterra, V. (1959), Theory of Functionals and of Integral and Integro-Differential Equations, Dover Publications, New York.

Zhang, H., Rizwan-uddin, and Dorning, J.J. (1995), "Systematic Homogenization and Self-Consistent Flux and Pin Power Reconstruction for Nodal Diffusion Methods - I: Diffusion Equation-Based Theory," *Nuclear Science and Engineering*, **121**, 226-244.

Zhang, H., Rizwan-uddin, and Dorning, J.J. (1997), "Systematic Homogenization and Self-Consistent Flux and Pin Power Reconstruction for Nodal Diffusion Methods. Part II: Transport Equation Based Theory," *Transport Theory and Statistical Physics*, **26**, 433-468.

VITA

Scott William Mosher was born in St. Petersburg, Florida on May 17^{th}, 1974 to David and Carol Mosher. Two months later, Scott, his older brother Greg, and his parents relocated to Marietta, Georgia and have lived there ever since. Scott attended George Walton High School and graduated in 1992. He received a Bachelors degree in Nuclear Engineering from Georgia Tech in 1997. As a co-operative work plan student, Scott worked for the Georgia Power Company at the Vogtle Electric Generating Plant in Waynesboro (20 miles south of Augusta). In 2001, he received a Masters degree in Nuclear Engineering with a thesis entitled, "Implementation of an Adaptive Importance Sampling Technique for Monoenergetic Slab Problems." Scott began work on his doctoral dissertation immediately afterward.